Thesis for the degree
Doctor of Philosophy

Submitted to the Scientific Council of the
Weizmann Institute of Science
Rehovot, Israel

עבודת גמר (תזה) לתואר
דוקטור לפילוסופיה

מוגשת למועצה המדעית של
מכון ויצמן למדע
רחובות, ישראל

By
Assaf Carmi

מאת
אסף כרמי

זיהומים קוונטיים במערכות עם קורלציה
Quantum Impurities in Correlated Systems

Advisors:
Prof. Yuval Oreg
Prof. Micha Berkooz

מנחים:
פרופסור יובל אורג
פרופסור מיכה ברכוז

July 2012

אב תשע"ב

Contents

Abstract

The subject of this work are quantum-dot-based impurities in correlated systems. Modern nano-technology allows advanced experiments, where engineered quantum impurities are placed inside a correlated host, allowing a controlled way of studying their physics. A commonly engineered quantum impurity is the quantum dot, a small droplet of electron liquid confined in a small region of space. In this thesis we study structures of quantum dots that are attached to electronic leads as concrete realizations of various types of quantum impurities.

We suggest a new realization of Kondo impurities which allows a spin-resolved measurements, and can be generalized to the more complex $SU(N)$-Kondo impurities. We focus on the realization of $SU(2)$ and $SU(3)$ Kondo and study the transmission through these impurities. We find in the unitary limit a $3/4$ quantum conductance in the $SU(3)$ case.

We study the coherence properties of transmission through Kondo impurities, by considering an open Aharonov-Bohm ring with an embedded quantum dot. We develop a novel many-body scattering theory which enables us to calculate the conductance through the dot, the transmission phase shift, and the normalized visibility. We find, for the non-Fermi liquid fixed point of the two-channel Kondo, that the transmission phase is $\pi/2$ despite the fact that a scattering phase shift is not defined. The normalized visibility at zero temperature is found to be $1/2$, indicating that exactly half of the conductance is carried by coherent single-particle processes.

Also, we present a model of two interacting levels that are attached to two electronic leads, where one of the levels is attached very weakly to the leads. We analyze, using rate equations, the average current and the noise of electrons transmitted through the two levels. We show that the shot noise is enhanced by the interactions, and that the Fano factor depends on the properties of the couplings between the levels and the leads. We study both sequential tunneling and cotunneling processes and show that there is a range of parameters in which the cotunneling processes affect the noise significantly, even though most of the current is carried by sequential tunneling.

Most of the results that are presented here were already published; the discussion of the $SU(N)$-Kondo appears in **PRL 106, 10640**. The shot noise and Fano factor of two-level systems are analyzed in **PRB 85, 045325**. The work that discusses the transmission through Kondo impurities was submitted for publication in **PRB**, and a preprint can be found on the Arxiv.

תקציר

עבודה זו עוסקת בזיהומים קוונטיים מבוססי נקודות-קוונטיות (Quantum dots) בתוך תווך המורכב מחלקיקים עם קורלציות ביניהם. כיום, התקדמותה של הננו-טכנולוגיה מאפשרת את ביצועם של ניסויים מתקדמים בהם זיהומים קוונטיים מלאכותיים מיוצרים ומשולבים בתוך מערכות עם קורלציה. ניסויים כאלה מאפשרים ללמוד בצורה מבוקרת את הפיסיקה של מערכות אלו. זיהום מלאכותי נפוץ היא הנקודה הקוונטית, התקן אלקטרוני מזערי בו אלקטרונים מאולצים להיות באזור מצומצם למדי במרחב. בעבודה זו, אנו חוקרים מימושים של זיהומים קוונטיים שונים בעזרת התקנים בהם נקודות קוונטיות מצומדות לאלקטרודות חיצוניות.

ראשית, אנו מציעים דרך חדשה לממש זיהומים מסוג קונדו (Kondo), המאפשרת מדידה נפרדת לכל ספין. את המימוש המוצע אפשר להכליל עבור זיהומי קונדו מורכבים יותר בהם הסימטריה SU(2) הקשורה לספין, מוכללת לסימטריה SU(N). אנו מתמקדים במימושים של SU(2) ו SU(3) וחוקרים את הולכת האלקטרונים דרכם. אנו מוצאים כי במקרה של SU(3) המוליכות בטמפרטורה אפס היא ¾ מהמוליכות הקוונטית.

לאחר מכן, אנו חוקרים את תכונות הקוהרנטיות של מעבר אלקטרונים דרך זיהומי קונדו. המערכת הקונקרטית בעזרתה אנו לומדים על תכונות אלה היא נקודה קוונטית המשולבת בתוך טבעת אהרונוב-בוהם. אנו מפתחים תיאורית פיזור חדשנית המאפשרת לנו לחשב את המוליכות דרך הנקודה הקוונטית, את הפאזה שאלקטרונים צוברים כשהם עוברים דרכה ואת הנראות (visibility) המנורמלת. לזיהומים מסוג קונדו דו-נתיבי, ישנה נקודת שבת של תהליך הנרמול-מחדש, שאינה מסוג נוזל פרמי. בנקודת שבת זו, אנו מראים כי הפאזה הנצברת על-ידי אלקטרון העובר דרך הזיהום היא $\pi/2$ וזאת למרות שפאזת פיזור לא מוגדרת עבור מקרה זה. הנראות בנקודת שבת זו היא בדיוק ½, סימן לכך שבדיוק חצי מהמוליכות קשורה לתהליכים קוהרנטיים.

בנוסף, אנו מציגים מודל של שתי רמות אנרגיה עם אינטראקציות ביניהן, המצומדות לשתי אלקטרודות חיצוניות, כאשר אחת הרמות מצומדת חלש בהרבה מהשניה. אנו מנתחים, בעזרת משוואות קצב, את הזרם הממוצע ואת הרעש המתקבלים ממעבר אלקטרונים דרך שתי הרמות. אנו מראים כי האינטראקציות מגבירות את הרעש ושמקדם פאנו (Fano) תלוי בפרטי הצימוד בין הרמות לבין האלקטרודות החיצוניות. אנו לוקחים בחשבון גם מנהור מסדר ראשון (sequential tunneling) וגם מנהור מסדר שני (cotunneling) ומראים כי קיים תחום במרחב הפרמטרים שבו תהליכי המנהור מסדר שני משפיעים על הרעש באופן ניכר וזאת למרות שרובו המכריע של הזרם הוא תוצר של תהליכי מנהור מסדר ראשון.

Acknowledgments

It has been a long journey, and there are many people who helped me along the way, or simply made it more fun to go through. It is my pleasure to be able to thank all these friends, family and colleagues.

First and foremost I would like to thank my wife Lia, for her endless patience and support. For her understanding and willing to settle in a student salary for such a long time... I want to thank my three wonderful children, Dror, Hadar and Noa, for giving me such a great happiness and putting everything in the right perspective.

I want to thank my two advisors Prof. Yuval Oreg and Prof. Micha Berkooz for many hours of discussions about physics, physicists, and life. I couldn't ask for better advisors and I deeply acknowledge their guidance. I learned a lot from them, and I'm glad that I had the opportunity to work with them.

I've made many friends during the last years, and it would be impossible to list them all. Especially, I want to thank my office-mates: Ariel Amir, Zohar Ringel, Natalie Lezmy, Omer Sidis, and Arbel Haim. We spent so many hours together, discussing physics and all the other non-important things that make life so great. I also want to thank Oded Zilberberg for hours of physics and more, it was really fun doing science with him.

I want to thank the department of Condensed Matter Physics at the Weizmann Institute of Science for the hospitality. I've been here almost seven years, and it feels like my second home.

At last, I want to thank my parents Haim and Sara Carmi, for encouraging me to ask questions and seeking knowledge. I dedicate this thesis to them.

Chapter 1

Introduction

The problems of correlated electrons systems are among the most difficult and interesting problems of physics. Particles in correlated electrons systems influence each other and therefore, in principle, one needs to consider complex many-body states in order to describe these systems. When describing electrons in a metal, the huge number of interacting particles makes this task effectively impossible. Fortunately, in most cases, the simple Fermi liquid picture describes well the physics of electrons in metal. In the Fermi liquid theory, the interacting electrons are replaced by renormalized weakly interacting quasi-fermions with the same charge and spin as the original electrons [1, 2, 3]. The Fermi liquid description is so successful, that the rare cases where it fails are usually referred to as 'non-Fermi-liquids'.

This work deals with quantum impurities that are embedded into a correlated electrons host. The interactions between the electrons and the impurity can change dramatically the behavior of the system, resulting in a completely different theoretical description for the correlated hosting particles. A canonical example of a quantum impurity in a metallic host is the Kondo impurity model [4, 5] that describes a magnetic impurity in a non-magnetic metal. The Kondo model was established in order to explain a non-monotonic behavior of the electrical resistance in various metals as a function of the temperature. The dominant mechanism for the resistivity in metals is electrons scattering by vibrating nuclei. Since these vibrations increase with temperature, the resistivity increases monotonically with temperature in most metals. However, in 1934, a resistance minimum was measured in gold, indicating that another scattering mechanism exists [6]. Kondo showed in 1964, that electrons scattering off magnetic impurities gives a $\ln(T)$ contribution to the resistivity, which can explain the observed minimum in the resistance.

In the simple Kondo model, free electrons, ψ_s, interact with a local magnetic impurity, $\vec{S}$. This situation is described by the Hamiltonian

$$H_{\text{Kondo}} = \sum_{k,s} \epsilon_k \psi^\dagger_{ks} \psi_{ks} + J \sum_{k,s} \sum_{k's'} \psi^\dagger_{ks} \vec{\sigma}_{ss'} \psi_{k's'} \cdot \vec{S} \,, \tag{1.1}$$

where J is the Kondo interaction strength, and $\vec{\sigma}$ are the three Pauli matrices. At relatively high temperatures, the interactions are small and J can be treated perturbatively. When the temperature is reduced, J becomes larger, and as the temperature goes below a characteristic energy scale- the Kondo temperature T_K- the spins of the electrons screen the impurity and

J cannot be treated perturbatively anymore. In the two extremes, the high temperatures ($T \gg T_K$) and the very low temperatures ($T \ll T_K$), the system is close to renormalization group (RG) fixed points, both of which are described by Fermi liquid theories: At $T \gg T_K$ a free electrons fixed point, and at $T \ll T_K$, the Kondo fixed point, in which the impurity is screened by the spins of the surrounding electrons.

There are two natural ways to generalize the Kondo physics: the multi-channel-Kondo, and the $SU(N)$-Kondo. In the multi-channel-Kondo (MCK), a few disconnected channels screen the impurity [7]:

$$H_{\mathrm{MCK}} = \sum_{i=1}^{\mathrm{k}} \sum_{k,s} \epsilon_k \psi^\dagger_{kis} \psi_{kis} + \sum_{i=1}^{\mathrm{k}} J_i \sum_{k,s} \sum_{k's'} \psi^\dagger_{kis} \vec{\sigma}_{ss'} \psi_{k'is'} \cdot \vec{S} \,. \tag{1.2}$$

If the strengths of the couplings of the different channels, J_i, are identical, then the system flows to a non-Fermi liquid fixed point at zero temperature. In this case, the spin $SU(2)$-level 1 symmetry is generalized to a $SU(2)$ symmetry at level k.

In the $SU(N)$-Kondo case, the system is generalized to have N flavors instead of spin up and spin down [8, 9, 10]:

$$H_{SU(N)} = \sum_{f=1}^{N} \sum_{k} \epsilon_k \psi^\dagger_{kf} \psi_{kf} + J \sum_{\alpha=1}^{N^2-1} \sum_{k,f} \sum_{k'f'} \psi^\dagger_{kf} T^\alpha_{ff'} \psi_{k'f'} S^\alpha \,. \tag{1.3}$$

The three 2×2 Pauli matrices are generalized to the N^2-1 $N\times N$ generators of the $SU(N)$ group. There are therefore N species of spin-less-like electrons in the leads, which are rotated into each other by $SU(N)$ transformations. This model flows to one of N possible RG fixed points, depending on the details of the impurity. All these fixed points are described by Fermi-liquid theories.

Modern technology allows the fabrication of nano-scale devices, which are small enough to manifest the laws of quantum mechanics. The nano-scale system which we are interested in is the quantum dot. A quantum dot device [11, 12, 13] is a small droplet of electron liquid confined in a small region of space. The droplet can be attached by tunneling processes to external leads, allowing electronic transport across the system. Another electrode, the gate, is capacitively coupled to the dot, and by varying the potential on the gate-electrode one can control the number of electrons in the dot. Quantum dot devices are not only important in themselves, but they can also be used as a very powerful experimental tool. The possibility to control the strength of the dot-to-environment coupling, the number of electrons in the dot, and the fact that it is possible to integrate it with

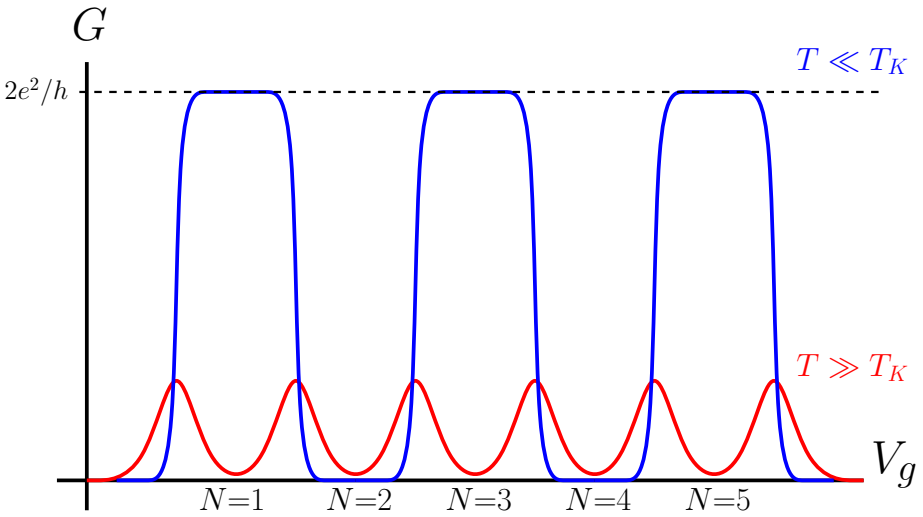

Figure 1.1: Schematic picture of the conductance through a quantum dot at temperatures much below the charging energy of the dot. N is the number of electrons in the dot. The red line is the conductance at temperatures much above the Kondo temperature, $T \gg T_K$, and the blue line is the conductance at the Kondo regime, $T \ll T_K$. The conductance at the odd valleys (odd number of electrons in the dot) is enhanced because of the Kondo effect.

other electronic systems, allow us to realize many physical concepts using quantum dots. In the context of impurities, one can think of a dot as a tunable impurity; the dot serves as impurity, with the attached electrodes being the hosting environment.

When the ground state of a quantum dot is tuned by a gate voltage to carry a fixed number of electrons, decreasing the temperature to below the charging energy of the dot, reduces the conductance through the dot, because of Coulomb blockade [11, 12, 13, 14]. Hence, when the conductance through the dot is measured as the function of the gate voltage, the conductance at values of the gate potential, with a well defined charge in the dot is reduced. Similarly, the conductance peaks whenever there is a degeneracy between two states with different number of electrons in the dot (see Fig. 1.1).

When the temperature is lowered even further, then whenever the ground state of the dot is tuned to carry an odd number of electrons, the conductance through the dot is enhanced, until it reaches (for a symmetrically coupled dot) $2e^2/h$ at zero temperature [15, 16, 17]. The enhancement of the conductance is due to the single-channel Kondo (1CK) effect [4, 5]- the dot acts as a magnetic impurity that interacts with the spins of the electrons in the surrounding leads. At low temperatures, below the characteristic Kondo

temperature, T_K, a spin resonance is formed, and the conductance through the resonance is perfect and equals e^2/h per spin (see Fig. 1.1).

In the following parts of the introduction we provide a background material which is important for the main subjects of this work. In Sec. 1.1, we discuss the transport though quantum dots in the Coulomb blockade regime, the sequential tunneling, and the cotunneling processes. In Sec. 1.2, we hint the relations between the Anderson model and the Kondo model. In Sec. 1.3, we shortly discuss existing realizations of various Kondo impurities with quantum dots and their limitations. In Sec. 1.4, we bring the background material and highlight important questions about the coherence properties of transmission through Kondo impurities. In Sec. 1.5, we discuss the shot noise, the Fano factor, and what can we learn by measuring them. This part gives necessary background material both for high-temperature description of the $SU(N)$-Kondo systems, and for the the two-level model analysis.

1.1 Low-temperature transport through quantum dots

We describe the transport through a quantum dot using the Anderson model [18]. We consider a quantum dot with discrete spinful levels which is attached to two leads, left and right (see Fig. 1.2). This system is described by the Hamiltonian [19, 20]:

$$H_n = \sum_{a=L,R} \sum_{k,s} \epsilon_k c^\dagger_{aks} c_{aks} + \sum_{n,s} \epsilon_n d^\dagger_{ns} d_{ns} + E_c (N - C_g V_g/e)^2 - E_s \vec{\Sigma}^2 + \left(\sum_{a,n} t^a_n \sum_k c^\dagger_{aks} d_{ns} + \text{H.C.} \right) , \tag{1.4}$$

where the operator c_{aks} annihilates an electron with momentum k and spin s in lead a, the operator d_s annihilates an electron in the dot at energy level n with spin s, $N = \sum_{n,s} d^\dagger_{ns} d_{ns}$, and $\vec{\Sigma} = \sum_{n,s,s'} d^\dagger_{ns} \frac{\vec{\sigma}_{ss'}}{2} d_{ns'}$. C_g is the capacitance between the dot and the gate, V_g is the gate voltage, E_c is the charging energy of the dot, and E_s is the total spin energy of the dot.

The conductance through the dot is carried by electron tunneling between the dot and the leads. At the lowest order in the tunneling coefficients, t^a_n, electrons can tunnel from one of the leads into an empty level in the dot, or from an occupied level into the leads. Such tunneling events are called *sequential tunneling*, and they are allowed whenever an empty level (occupied

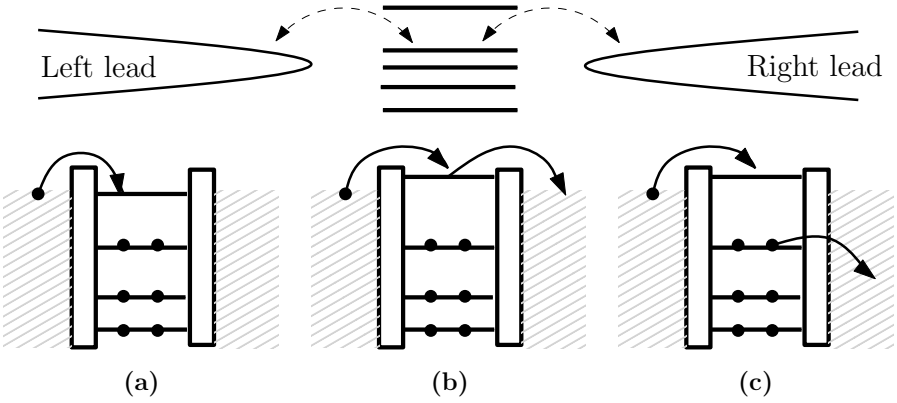

Figure 1.2: Schematic picture of a multi-level quantum dot attached to two leads. **(a)** Example of a sequential tunneling process. **(b)** Example of an elastic cotunneling process. **(c)** Example of an inelastic cotunneling process.

level) is aligned with available electron (hole) in the leads (see Fig. 1.2). The next leading order tunneling processes are the so-called *cotunneling processes* in which an electron or a hole tunnels between two leads through a virtual state in the dot (see Fig. 1.2). There are two types of cotunneling processes: elastic cotunneling- where the state of the dot is not changed by the tunneling process, and inelastic cotunneling- where the state of the dot is changed (either its spin, or its energy) by the cotunneling process.

1.2 Transport through quantum dots in the Kondo regime

In this section, we shortly present the relation between the Anderson model and the Kondo model. We consider a single level dot that is coupled to two leads, left and right. The Anderson model Hamiltonian of this system can be written as

$$H_1 = \sum_{a=L,R}\sum_{k,s}\epsilon_k c^\dagger_{aks}c_{aks} + \epsilon_g\sum_s d^\dagger_s d_s + U d^\dagger_\uparrow d_\uparrow d^\dagger_\downarrow d_\downarrow + \left(\sum_a t_a \sum_k c^\dagger_{aks} d_s + \text{H.C.}\right) , \tag{1.5}$$

where the energy of the single level (tuned by a gate voltage) is casted into ϵ_g. Double occupation of the level requires an additional charging energy U.

The Anderson model Hamiltonian (1.5) is related to the Kondo Hamiltonian (1.1) via the Schrieffer-Wolff transformation [21]. In order to get the

Kondo Hamiltonian, we first perform the following rotation of the two leads:

$$\begin{pmatrix} \psi \\ \xi \end{pmatrix} = \begin{pmatrix} \cos(\alpha) & \sin(\alpha) \\ -\sin(\alpha) & \cos(\alpha) \end{pmatrix} \begin{pmatrix} c_L \\ c_R \end{pmatrix} , \tag{1.6}$$

with the angle $\alpha = \tan^{-1}(t_R/t_L)$. In the new basis, only one linear combination of the two leads, ψ, is coupled to the dot, and the orthogonal linear combination, ξ is decoupled from the other parts of the system. The second step is to perform a unitary transformation of the Hamiltonian (1.5): $\tilde{H} = e^A H e^{-A}$, where $A^\dagger = -A$. The dot is tuned to a Coulomb valley, where sequential tunneling is not allowed. By choosing the operator A properly, one can eliminate the first order in tunneling part of the Hamiltonian and bring it to the form

$$\tilde{H}_1 = \sum_{k,s} \epsilon_k \xi^\dagger_{ks} \xi_{ks} + \sum_{k,s} \epsilon_k \psi^\dagger_{ks} \psi_{ks} - U \left[\frac{|t_L|^2 + |t_R|^2}{\epsilon_g(U+\epsilon_g)} \right] \sum_{k,s} \sum_{k's'} \psi^\dagger_{ks} \vec{\sigma}_{ss'} \psi_{k's'} \cdot \vec{\Sigma} , \tag{1.7}$$

which is equivalent to the Kondo Hamiltonian (1.1) with an additional free fermion-field, ξ (higher order terms are neglected). The total spin of the dot replaces the magnetic impurity, and the Kondo coupling strength is

$$J = \left(|t_L|^2 + |t_R|^2\right) \left(\frac{1}{U+\epsilon_g} - \frac{1}{\epsilon_g} \right) . \tag{1.8}$$

1.3 Realizations of two-channel and $SU(N)$ Kondo

Realizations of 2CK

As already mentioned, the 1CK physics can be generalized to more complex models, known as the multi-channel Kondo models, where a few independent channels compete to screen the impurity [7]. In the 2CK case, when the couplings of the two channels to the impurity are identical the system flows to a non-Fermi liquid fixed point at zero temperature. The 2CK system was first discussed as a purely theoretical problem [7], but it was soon invoked as a candidate explanation for remarkable low-energy properties of some heavy fermion materials [22, 23, 24, 25] and glassy metals [26, 27, 28, 29, 30] and more recently in graphene [31, 32, 33]. In the past decade, a few single-impurity realizations of the 2CK system were proposed [34, 35, 36, 37, 38], offering the hope of microscopically manipulating system parameters, and one of the proposals [37], that suggested a realization with quantum dots,

was built and measured [39]. The conductance through a 2CK impurity, within one of the two channels, at the non-Fermi liquid fixed point is $e^2/2h$ per spin, assuming equal coupling to the two leads in that channel [40].

Realizations of SU(N) Kondo

Physical systems that exhibit $SU(N > 2)$ Kondo are quite rare, and usually complex. In practice, they are limited to $N = 4$, where the spin and another degree of freedom are exploited to form a four-fold degeneracy. Examples of such systems are: double-quantum-dot systems [41, 42, 43, 44], triangular triple-quantum-dot systems [45] and carbon nanotubes [46, 47, 48].

In one of our works [49], we suggest a new way to realize Kondo impurities with quantum dots that can be easily generalized into $SU(N > 2)$ Kondo, by using a structure of N quantum dots. For concreteness, we focus on the case $N = 3$ as it is relatively easy to construct, yet rich enough to exhibit most of the features of the larger N cases. In addition to the realization of $SU(N)$-Kondo, our system allows spin-resolved measurements, giving access to physical quantities that are not accessible from other existing realizations of Kondo impurities. Recently, such a device with $N = 2$ was built, and spin-resolved spectroscopy of the Kondo effect was made [50].

1.4 Coherent transmission through Kondo impurities

The Fermi liquid nature of the 1CK fixed point states that the system can be described using exclusively single-particle excitations. It means that at zero temperature, when a single particle hits the impurity, it can only be scattered into a single-particle. In the original Kondo problem (1.1), the outgoing single particles and the incoming single particles are connected by a $\pi/2$ scattering phase shift [51]. Thus, in the configuration of a quantum dot coupled to two leads, in the scattering $\psi - \xi$ basis (1.6), incoming single particle states in the ψ-lead are scattered off the dot into outgoing single particle states in the ψ-lead, with a $\pi/2$ scattering phase shift. In the left-right basis it has been shown [52] that at zero temperature, incoming electrons from one of the leads, always scatter coherently through the dot into the other lead. The phase that these electrons accumulate while they cross the dot was found to be identical to the scattering phase shift, $\pi/2$ [52].

At the non-Fermi liquid fixed point of the 2CK, the simple picture of elastic scattering of single particles is no longer valid. At zero temperature, a single particle that interacts with a 2CK impurity, can be scattered only

into a many-body state [40, 53]. Thus, there is no elastic single-particle scattering off a 2CK impurity at the non-Fermi liquid fixed point. Given that there are no elastic single-particle scattering events off the impurity, one might imagine that the transport through a 2CK impurity has no coherent part. Nevertheless, we showed [54] that at this fixed point exactly half of the conductance is carried by coherent processes. This result is in agreement with the relation between the inelastic scattering cross section and the total cross section that was found in Refs. [55, 56]. The conductance through a 2CK impurity has a coherent part because the electrons that interact with the effective spin of the dot are described by the ψ linear combination of the two leads (1.6) . The other linear combination of electron operators in the two leads, ξ, is decoupled from the dot. While there are no elastic single ψ-particle scattering events, coherent transport via ξ-particles is possible.

The coherent properties of the transport through an impurity can be measured in a two-path experiment, in which electrons are sent from a source lead through two possible paths into a drain lead (see Fig. 1.3). We assume that the propagations along the different paths are independent of each other, namely, changes in the properties of one path do not affect the propagation along the other path. One of the paths contains the impurity of interest, and the two paths encircle a magnetic flux ϕ. The interference between the two paths depends on ϕ through the Aharonov-Bohm (AB) effect. Hence, the conductance of the setup contains two parts: a flux-independent part, which is related to the separate conductances of the two paths, and a flux-dependent part, which is related to the interference of the two paths.

Two measurable quantities can be extracted from a two-path experiment: the transmission phase shift of the flux-dependent conductance, and the ratio between the amplitude of the flux-dependent part and the flux-independent part of the conductance. We cast [54] the source-to-drain conductance of the two-path device into the form

$$G_{\rm sd} = G_{\rm d} + G_{\rm ref} + 2\sqrt{\eta}\sqrt{G_{\rm d}G_{\rm ref}}\cos\left(\frac{e\phi}{\hbar c} + \varphi_t\right), \tag{1.9}$$

where $G_{\rm d}$ is the conductance through the path with the impurity when the reference path is switched off, and $G_{\rm ref}$ is the conductance through the reference path when the impurity's conduction is switched off. The impurity will generally be realized as one or more quantum dots, so we will interchangeably refer to "impurity" and "dot" depending on context. We assume that the paths are independent: manipulations of the dot (for example, with gate potential) do not influence the conductance of the reference path, and vice versa. The *transmission phase*, φ_t, is related to the relative phase between

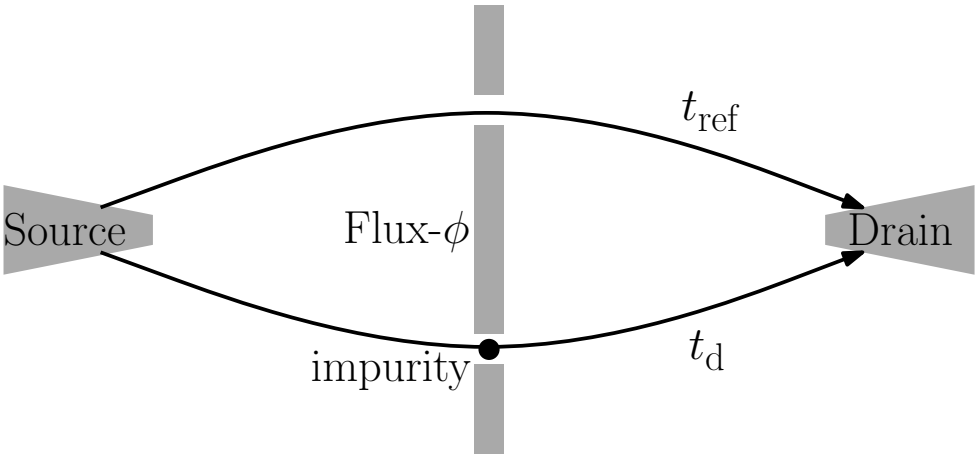

Figure 1.3: Schematic picture of a two-path setup. Electrons are sent from the source lead toward the drain lead through two paths, whose partial waves interfere with each other. The transmission amplitudes of the two paths are t_{d} and t_{ref}, and they encircle a magnetic flux ϕ. The coherent transport through the impurity can be studied by embedding it into one of the paths.

the two paths, and the *normalized visibility* η is related to the size of the coherent part of the conductance compared to the total conductance. Note: the phase of the reference path is arbitrary, determined by path length, potential landscape, etc. So is the phase of the path with the impurity, excluding the transmission phase of the impurity itself. Below we assume for simplicity that each of these phases is 0 mod 2π, so that φ_t is purely the transmission phase of the impurity itself. The definition of η, implicit in Eq. (1.9), is such that for Fermi liquids, at zero temperature and without spin, $\eta = 1$. This can be easily checked by applying the Landauer formalism [57, 58, 59, 60] for the two-path experiment setup.

The normalized visibility η can be reduced to below one by four mechanisms: First, if the transmitted electrons accumulate an energy-dependent phase when they are scattered through the impurity, or just along either path, then at nonzero temperature η is reduced because of the thermal averaging. Second, if the phase depends on the spin, the spin summation can also reduce η. Third, if part of the conductance is carried by incoherent scattering processes, where single electrons are scattered into many-body states, the interference and therefore η are reduced. Fourth, electrons that are subjected to external dephasing lose their coherence, so external dephasing also decreases the interference and η. External dephasing depends on the specific model and the details of the setup. Hence in this dissertation, we focus mainly on the first three mechanisms, and only qualitatively explore

the effect of external dephasing on η.

Since $G_{\rm d}$ and $G_{\rm ref}$ can be measured directly, the normalized visibility can be experimentally determined. This requires two measurements: the conductance through one of the paths, and the two-path conductance. Measuring the transmission phase of a 1CK impurity in a two-path setup was already suggested before [52], and the predicted $\varphi_t = \pi/2$ was measured [61], demonstrating coherent electron transmission through a many-body state. Yet, no special attention was given to the amplitude of the flux-dependent part of the conductance. In particular, non-Fermi liquid cases, where η can give information on the underlying physics (and also φ_t is different from that in the 1CK case), were not treated.

1.5 Shot noise, Fano factor and Coulomb interactions

In this thesis, we also present a work we did on the shot noise in asymmetric interacting two level systems [62]. The motivation for this work goes back to my MSc thesis [63], where we analyzed the asymmetry-dependence of the Fano factor in two-level quantum dots, in order to explain the experimental results reported in Ref. [64]. In the current work, we fully analyze how the shot noise and the Fano factor depend on the asymmetry, we study how the temperature affects this dependence and in addition, we extensively study the effect of cotunneling processes (next leading order perturbation). Surprisingly, we find that the latter play an important role in this system, and there is a range of parameters where the noise is governed by the rare cotunneling processes even though most of the average current is carried by sequential tunneling processes.

Let us first present some necessary background on shot noise, Fano factor, and the effects that Coulomb interactions impose on them. Fluctuations in electrical current, which we simply call *noise* provide additional information about the charge transport that is not accessible from average current measurements (for a review see Ref. [65]). Among the various noise sources we focus on the shot noise. The discreteness of the transferred charge causes fluctuations in the current. These fluctuations, named *shot noise*, depend on the charge of the conducting particles and therefore measurements of shot noise provide information on the discrete nature of the conducting particles and their correlations. The shot noise of a Poisson process of uncorrelated current pulses of charge e is $S_{\rm Shot} = 2e\langle I\rangle$, where $\langle I\rangle$ is the time averaged current. The noise is proportional to the average current since in a Pois-

son distribution the mean equals the variance, therefore the mean number of current pulses equals its variance. The Fano factor, $F = \frac{S_{\rm shot}}{2e\langle I\rangle}$, is a dimensionless parameter that characterizes the granularity of the current. When driving a current through a single spinless electronic level, the correlations that are imposed by the Pauli exclusion principle reduce the Fano factor; the Fano factor varies between half and one depending on the symmetry of the couplings between the level and the external leads [66, 67, 68].

Correlations can also be imposed by Coulomb interactions [69]. In most cases, the effect of Coulomb repulsion on the noise of a mesoscopic system is similar to the effect of the Pauli exclusion principle. Both impose a time delay between consecutive current pulses and therefore we expect negative correlations between them that suppress the shot noise [70]. However, several theoretical works on various systems have showed that Coulomb interactions might also lead to a super-Poisson shot noise with a Fano factor $F > 1$. Examples of such systems are: quantum dots that are coupled to ferromagnetic leads [71, 72, 73, 74], multi-levels quantum dots [75, 76], multi-dots structures [77, 78, 79, 80, 81, 82], and also three terminal quantum dots [83, 84, 85]. There are also experimental works [86, 87, 88, 89, 64] in which a super-Poisson noise was measured in quantum dots, rather than the sub-Poisson noise, which is expected from the single level model of the quantum dots.

A simple mechanism that might explain the enhancement of the Fano factor in such systems is tunneling through two levels that are coupled to the leads, where one of the levels is coupled much stronger than the other level. The two levels are interacting, namely, there is a Coulomb repulsion between electrons that occupy the two levels. In this case, the electrons that cross the system tunnel mainly through the level that is strongly coupled to the leads. However, once in a while an electron can tunnel into the weakly coupled level and then, because of the Coulomb interactions, the tunneling of other electrons through the strongly coupled level is prevented, and the current is blocked. The current resumes only after the electron tunnels out of the weakly coupled level. Therefore the intuitive picture is a current that is blocked occasionally and therefore the noise is enhanced. The idea of two interacting levels as a possible source of super-Poisson noise was discussed in the context of quantum dots that are coupled to ferromagnetic leads [71, 72] and also in the context of double quantum dots structures [77].

In this thesis, we present a detailed analysis of the two levels model with Coulomb interactions, this analysis is based on the work which we report in Ref. [62]. In particular, we study how the shot noise and the Fano factor depend on the left-right asymmetry, namely, the asymmetry between the couplings to the two external leads. The fact that the enhancement of the

shot noise depends on the left-right asymmetry of the coupling to the leads emerges from previous works (*e.g.*, the results of Refs. [74] and [77]), and also from my MSc thesis [63]. Nevertheless, a complete theoretical analysis of this dependence was missing. The two levels mechanism for noise enhancement can be found in many physical realizations such as single level with spin dependant coupling and double quantum dots, or two levels in a quantum dot, in a strong magnetic field. Although the quantitative details of each system are different, the qualitative behavior of the noise enhancement is the same.

This thesis covers three main projects, which deal with different aspects of the subject of quantum-dot-based impurities in correlated electron systems: realization of $SU(N)$-Kondo impurities, transmission properties of Kondo impurities, and shot noise in asymmetric two-level systems. In Chapter 2, we present the techniques that we used in our research. Some parts of this Chapter are relevant only to parts of these projects, and therefore, the context of the presented material is emphasized when it is needed. In Chapter 3, we present the main results of our study. We divide this chapter into three parts, each of them corresponds to one of the main projects. In Chapter 4, we summarize this work as a whole and provide an outlook for possible further study. In the four Appendices, we give additional material which is not essential for the understanding of the main ideas this thesis expresses, and yet can enlighten parts of this work.

Chapter 2

Methods

In this part, we present the techniques that we used in order to derive the results that we later report on Chapter 3. Some of the techniques are relevant for more than one project that included in this dissertation, but part of them are relevant for only one project, or even part of it. Hence, on each section in this chapter, we refer to the relevant works and emphasize the context of the presented material.

2.1 Realization of $SU(N)$-Kondo using quantum dots and edge states

2.1.1 The basic building blocks

We suggest [49] a new realization of the Kondo effect and its generalization to $SU(N)$, using edge states of the quantum Hall effect that interact with quantum dots (see Fig. 2.1). The basic building block that we use is a quantum dot coupled to the edge state of an integer quantum Hall liquid. The Hamiltonian of a single building block is therefore

$$H_1 = \sum_k \epsilon_k \psi_k^\dagger \psi_k + \epsilon_g d^\dagger d + \left(W \sum_k \psi_k^\dagger d + \text{H.C.} \right) . \tag{2.1}$$

The edge state is described by a chiral spinless fermion, ψ. The operator $d^\dagger$ populates the dot, which is assumed to have a single energy level ϵ_g that is controlled by an outer gate. W is the tunneling coefficient, we use the notation W (rather than the previous-t notation) in order to emphasize that there is only one edge state (and not two leads).

Consider now N such building blocks as drawn in Figs. 2.1(a) and 2.1(c) for $N = 2, 3$. We suggest using quantum dots with strong Coulomb interactions between them but very small tunneling between different dots (smaller than T_K). Double-dot systems fulfilling even stricter conditions already exist [90, 91, 92, 93] with good control over the couplings to the leads, the gate voltages, and with practically zero tunneling between the dots. The implementation of Kondo effect due to the Coulomb interactions in those systems was demonstrated [90, 92, 93]. Promising triple-dots systems are also experimentally available [94, 95] making the current proposed realization of

$SU(3)$-Kondo reasonably possible. We want to stress that obtaining the $SU(N)$-Kondo physics at low energies (IR) does not require a high accuracy of the symmetry between the N different blocks. As long as the deviations from the symmetry are not relevant under RG, the system exhibits Kondo physics in the IR.

The Hamiltonian that describes a system with N building blocks is

$$H_N = \sum_{\alpha=1\ldots N} \sum_k \epsilon_k \psi^\dagger_{k\alpha}\psi_{k\alpha} + \epsilon_g \sum_\alpha d^\dagger_\alpha d_\alpha + \left(W \sum_\alpha \sum_k \psi^\dagger_{k\alpha} d_\alpha + h.c. \right) + \sum_{\alpha<\beta} U_{\alpha\beta} d^\dagger_\alpha d_\alpha d^\dagger_\beta d_\beta. \tag{2.2}$$

The indices α, β label the different building blocks and $U_{\alpha\beta}$ is the charging energy between the dots α and β. We have made the assumption of identical sub-systems (that is ϵ_k ,W and ϵ_g are flavor-independent), and we assumed that there is no tunneling between the dots. These assumptions are not crucial. Small differences between the energies of the dots and small changes in the tunneling coefficients have an effect similar to a small magnetic field and a small exchange field in the familiar $SU(2)$ Kondo effect. We therefore only require that the differences are small compared to the Kondo temperature: $\Delta\epsilon_g \ll T_K$ and $|\Delta W|^2/\epsilon_g \ll T_K$. Jumping ahead, these deviations from the symmetry will at most change the IR behavior by marginal operators and the conductance through flavor i would be given by $\frac{e^2}{h}\sin^2(\pi n_i)$ (n_i is the average occupation of the ith dot). Small tunneling terms between the dots ($t_{\alpha\beta} d^\dagger_\alpha d_\beta + h.c.$) can be mapped to small differences in the energies of the dots by simply rotating the basis of the dots, we only require that $|t_{\alpha\beta}| \ll T_K$.

In the $N = 2$ case, the Hamiltonian (2.2) can be mapped to the spinful dot Hamiltonian (1.5) after the rotation to the $\psi - \xi$ basis (1.6) (not including the trivial part of the free ξ lead). The two blocks act as up and down pseudo-spins and the system realizes the $SU(2)$-Kondo physics. By using N building blocks, we obtain the $SU(N)$-Kondo. For concreteness, we later focus on the case $N = 3$ as it is relatively easy to construct, yet rich enough to exhibit most of the features of the larger N cases.

Besides the ability to realize $SU(N)$ Kondo, the systems that we suggest have more advantages: First, as our realization is based on edge states it can be easily integrated into an electronic Mach-Zehnder interferometer, allowing accurate phase shift measurements. Second, our realization allows measurements of a single pseudo-spin (or generally a single flavor) transport. Third, we can break the $SU(N)$ symmetry, potentially allowing a non Fermi liquid behavior such as in the two impurity Kondo model and its generalizations [8].

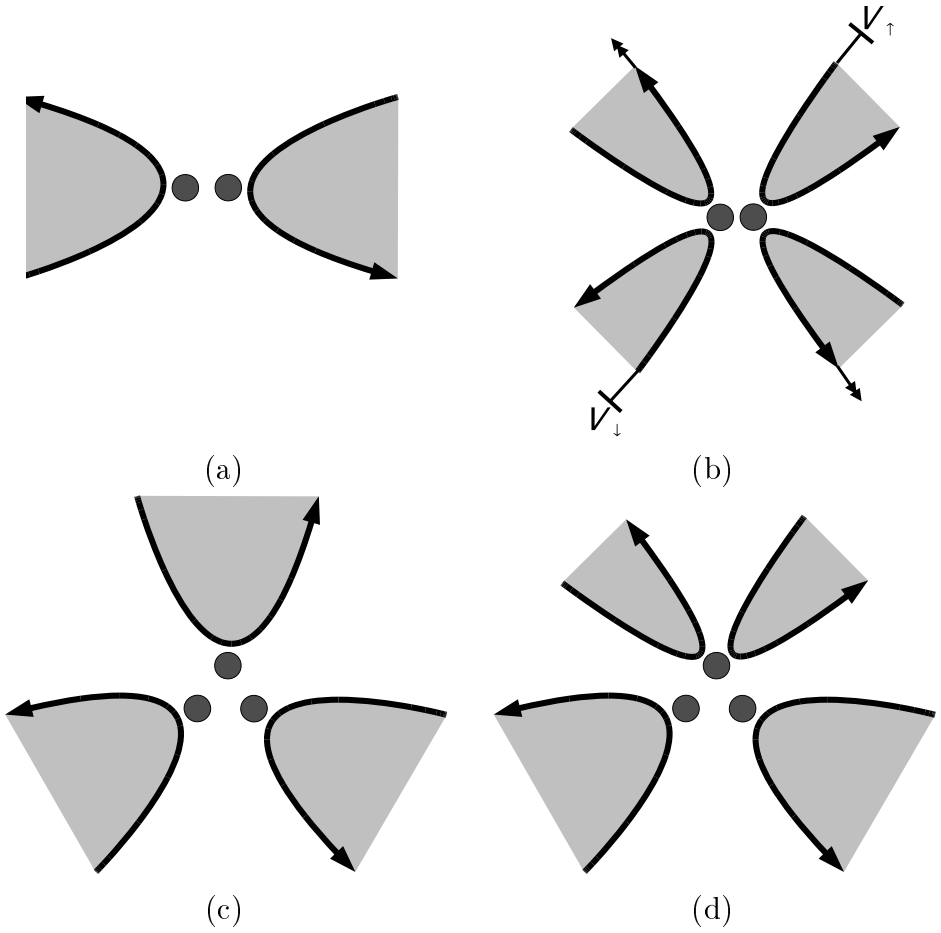

Figure 2.1: **(a)** Realizing $SU(2)$ Kondo using two edge states and two quantum dots. Electrons can tunnel from each edge state to its nearest dot. There is a strong coulomb interaction between the dots. The left/right subsystems act as different pseudo spins. This realization *allows phase shift measurements*. **(b)** Realizing $SU(2)$ Kondo using four edge states and two quantum dots. The edge states are split to *allow an independent transport measurement* of each pseudo-spin. **(c)** Realizing $SU(3)$ Kondo using three edge states and three quantum dots with strong coulomb interaction between them. Electrons can tunnel from edge state to the nearest dot only. The three sub-systems act as different flavors. **(d)** Realizing $SU(3)$ Kondo using four edge states and three quantum dots. Here, we split the upper edge state to *allow transport measurements* between the two new upper edge states.

Fourth, it paves the way to possible generalizations to fractional quantum Hall edges, which may show a richer structure.

2.1.2 Realization of $SU(N)$-Kondo

Let us assume temporarily identical charging energies, $U_{\alpha\beta} = U$. In this case the Hamiltonian (2.2) possesses a $SU(N)$ symmetry acting on the states of the dots by $S^i = \sum_{\alpha,\beta} d^\dagger_\alpha T^i_{\alpha\beta} d_\beta$, where T^i are the $N \times N$ generators of $SU(N)$. Having m electrons in the dots amounts to an impurity in a representation of $SU(N)$ with m anti symmetrized indices, each in the fundamental representation [9, 8]. We will discuss below to what extent different m's can be realized, but for now we consider a general m. In this case, after a Schrieffer-Wolff transformation the Hamiltonian (2.2) is:

$$H_K = \sum_\alpha \sum_k \epsilon_k \psi^\dagger_{k\alpha} \psi_{k\alpha} + J \sum_i \sum_{\alpha,\beta} \sum_{k,k'} \psi^\dagger_{k\alpha} T^i_{\alpha\beta} \psi_{k'\beta} S^i,$$

where $J \sim W^2/U$ and the index i runs over the $N^2 - 1$ $SU(N)$ generators. Conformal field theories with $SU(N)$ Kac-Moody level 1, which is the case here, have N gaussian invariant boundary states that correspond to N possible Fermi liquid fixed points of the RG. The natural conjecture, supported by the Friedel sum rule, is that populating the array of dots by $0 \leq m < N$ electrons leads to a flow to each of these boundary states, characterized by boundary conditions $\psi_i(x = 0^+) = e^{2i\frac{m\pi}{N}} \psi_i(x = 0^-)$.

We now discuss the feasibility of the $SU(N)$ picture. We make a distinction between two cases: $N = 2, 3$, where the situation $U_{\alpha\beta} = U$ (or close to it) can be achieved, and $SU(N \geq 4)$, where there is no way to achieve identical charging energies.

SU(N $\leq$ 3) Kondo: We arrange the dots on the vertices of a triangle, such that the distances between pairs of dots are roughly the same. We do not require that the triangle be exactly equilateral. However, it is convenient to start from this idealized case, and then verify that the dynamics of the system does not change significantly in the non strictly equilateral physical case. In the exactly equilateral case $U_{\alpha\beta} = U$, the Hamiltonian:

$$\begin{aligned} H_N = & \sum_{\alpha=1\ldots N} \sum_k \epsilon_k \psi^\dagger_{k\alpha} \psi_{k\alpha} + \epsilon_g \sum_\alpha d^\dagger_\alpha d_\alpha \\ & + \left(W \sum_\alpha \sum_k \psi^\dagger_{k\alpha} d_\alpha + h.c. \right) + \sum_{\alpha<\beta} U_{\alpha\beta} d^\dagger_\alpha d_\alpha d^\dagger_\beta d_\beta, \end{aligned}$$

is $SU(N) \times U(1)$ symmetric and the system therefore flows to a $SU(N)$ symmetric fixed point at zero temperature. The $SU(N)$ symmetry breaking

operators are marginal at most: $\sum_{\alpha\beta}\lambda_{\alpha\beta}\psi^\dagger_\alpha\psi_\beta$ with $\lambda_{\alpha\beta}\sim\epsilon_g/U_{\alpha\beta}$, hence, small deviations from the point $U_{\alpha\beta}=U$ can then be analyzed using the IR theory where they are at most marginal.

SU($\mathbf{N\geq 4}$) Kondo: Unlike the $N\leq 3$ case, we can no longer assume $U_{\alpha\beta}=U$ because the distances between the various pairs of dots, adjacent and non adjacent, cannot be made approximately equal. We can however arrange the dots on a two dimensional regular polygon, then $U_{\alpha\beta}=U_{\alpha-\beta}$. In this case, the system has a Z_N symmetry (rotation by $2\pi/N$) and a $U(1)^N$ symmetry associated with charge conservation of each flavor. In the next paragraph we show that the $Z_N\times U(1)^N$ symmetry ensures that the $SU(N)$ symmetric single occupation fixed point ($m=1$ or $m=N-1$) is attractive. In the physical case, the Z_N symmetry is not exact, nevertheless analyzing the IR fixed point shows that symmetry breaking operators are marginal at most.

The stability of the fixed point in the $Z_N\times U(1)^N$ symmetric case proceeds as follows: The general marginal operator near the IR is of the form $\sum_{\alpha\beta}\lambda_{\alpha\beta}\psi^\dagger_\alpha\psi_\beta$. The $U(1)$ symmetry on each of the edges, i.e. charge conservation in each subsystem, implies invariance under independent multiplication of each ψ_α by a phase. Hence the matric $\lambda_{\alpha\beta}=\lambda_\alpha\delta_{\alpha\beta}$. The Z_N symmetry then enforces that all the λ_α are equal. The only remaining permissible operator, $\lambda\sum_\alpha\psi^\dagger_\alpha\psi_\alpha$, does not break the $SU(N)$ symmetry. Since the $SU(N)$ fixed point is attractive, there is a finite range of UV couplings in which the theory flows to this IR fixed point. In the physical case the $Z_N\times U(1)^N$ symmetry is approximate and the only exact symmetry is total charge conservation which is the sum of the N different $U(1)$s. This symmetry in enough to exclude all the relevant operators in the theory (ψ and $\psi^\dagger$). The allowed operators $\psi^\dagger_\alpha\psi_\beta$ are marginal at most. Notice that if the system is tuned to have $1<m<N-1$ electrons in the dots then without further tuning the ground states do not form a representation of $SU(N)$ and therefore the theory is not $SU(N)\times U(1)$ symmetric.

This picture explains the experimental results in [44] and [47] where indications of $SU(4)$ Kondo were obtained starting from UV systems which lack the exact symmetry. The picture is further supported by a perturbative scaling analysis and by NRG computations for $N=4$ [41], suggesting a large basin of attraction for this flow.

2.2 Two-path experiments, transmission phase, visibility, and normalized visibility

In this section, we discuss two-path setups and define the transmission phase φ_t and the normalized visibility η. These quantities are essential for studying the coherent properties of transmission through impurities, and we later calculate them for various Kondo impurities (see Sec. 3.2).

The prototype of two-path experiments is the double-slit experiment. In a double-slit experiment particles are launched toward the double slit, where they split into partial waves which interfere with each other. In the electronic version of the double-slit experiment, schematically drawn in Fig. 1.3, a coherent electron beam is emitted from a source lead toward a drain lead, via a beam splitter that allows electron flow along two different paths that encircle a magnetic flux ϕ. The source-to-drain conductance is given by

$$G_{\rm sd} = \frac{e}{h} \sum_s \int d\epsilon \left(-\frac{\partial f}{\partial \epsilon} \right) T_s(\epsilon), \tag{2.3}$$

where $T_s(\epsilon)$ is the probability for an incoming electron with energy ϵ and spin s to be transmitted through the double slit, and $f(\epsilon)$ is the Fermi-Dirac distribution function. If all the electrons that pass through the double slit do so elastically and coherently, the probability $T_s(\epsilon)$ is given by [57]

$$T_s = |t_{{\rm d},s}|^2 + |t_{{\rm ref},s}|^2 + 2\,|t_{{\rm d},s} t_{{\rm ref},s}| \cos\left(\frac{e\phi}{\hbar c} + \theta_s \right), \tag{2.4}$$

where $t_{{\rm d},s}$ and $t_{{\rm ref},s}$ are the transmission amplitudes of the two slits. The transmission amplitudes are complex quantities with a phase difference, $\frac{e\phi}{\hbar c} + \theta_s$, between them. The phase difference contains a contribution θ_s determined by the details of the transmission through the double-slit setup, and a magnetic-flux-dependent part $\frac{e\phi}{\hbar c}$ coming from the AB effect.

Equation (2.4) is valid only if all the electrons are coherently transferred through the double slit [96]. If some of the electrons are transferred incoherently through one of the slits, then, since these electrons do not interfere, the flux-dependent term of T_s is reduced. If we embed into one of the paths a quantum dot (as in the lower path in Fig. 1.3), we can examine the dot's coherence properties by measuring the conductance. In such a device, the phase that electrons accumulate as they cross the dot is encoded in the relative phase between the two paths θ_s.

In experiments, the measured source to drain conductance is typically cast in the form

$$G_{\rm sd} = G_0 + G_\phi \cos\left(\frac{e\phi}{\hbar c} + \varphi_t \right). \tag{2.5}$$

G_0 is the part of the conductance which is independent of the magnetic flux, and is related to the independent conductances of the two paths, and G_ϕ is the amplitude of the flux-dependent part of the conductance. In the general case, φ_t is different from θ_s, but if $t_{\mathrm{d},s}$, $t_{\mathrm{ref},s}$, and θ_s are independent of spin and energy, then $\varphi_t = \theta_\uparrow = \theta_\downarrow$. In standard two-path experiments, the ratio G_ϕ/G_0, is called "visibility", and it measures the strength of the flux-dependent conductance oscillation compared to the average conductance.

The ratio G_ϕ/G_0 can be reduced by several mechanisms. Trivially, a mismatch between the transmission amplitudes, $|t_{\mathrm{d}}| \neq |t_{\mathrm{ref}}|$, decreases the ratio $|t_{\mathrm{d}} t_{\mathrm{ref}}|/(|t_{\mathrm{d}}|^2 + |t_{\mathrm{ref}}|^2)$, and therefore reduces G_ϕ/G_0. In addition to the trivial transmission amplitude mismatch, four other mechanisms noted earlier (see Sec. 1.4) can reduce G_ϕ/G_0: thermal averaging, spin averaging, inelastic scattering, and externally-induced dephasing.

There is a conceptual difference between transmission amplitude mismatch of the two paths, and the other three mechanisms for G_ϕ/G_0 reduction (we assume for the moment that there is no external dephasing). Unlike the transmission amplitude mismatch, these other mechanisms cannot be probed by simple single-path conductance measurements of the system. To isolate the transmission mismatch from elastic versus inelastic scattering and energy or spin dependent phase, we decompose the conductance (2.5) into the form of Eq. (1.9):

$$G_{\mathrm{d}} + G_{\mathrm{ref}} + 2\sqrt{\eta}\sqrt{G_{\mathrm{d}} G_{\mathrm{ref}}} \cos\left(\frac{e\phi}{\hbar c} + \varphi_t\right) \ .$$

G_{d} and G_{ref} are the independent conductances through the two paths, which can be measured directly by closing off one and then the other path. Equation (1.9) defines a new quantity, the *normalized visibility* η. If all the electrons transmit coherently through the two paths, and accumulate the same phase, then $\eta = 1$, independent of possible transmission amplitudes mismatch.

We want to make a comment about the feasibility of interference measurements in two-path experiments: In real experiments, there is a typical coherence length, l_{coh}, along which the propagating electrons preserve their coherence. This length depends on the details of the realization of the two-path setup, and we assume that it is much larger than the lengths of the two paths $l_{\mathrm{ref}}, l_d \ll l_{\mathrm{coh}}$. However, this assumption is not enough: Electrons with different energies propagate along the two paths, accumulating an energy-dependent phase difference $\theta_s = \epsilon(l_{\mathrm{ref}} - l_d)/v_F$, where v_F is the Fermi velocity. As a result, the thermal averaging introduces a new lengthscale, the

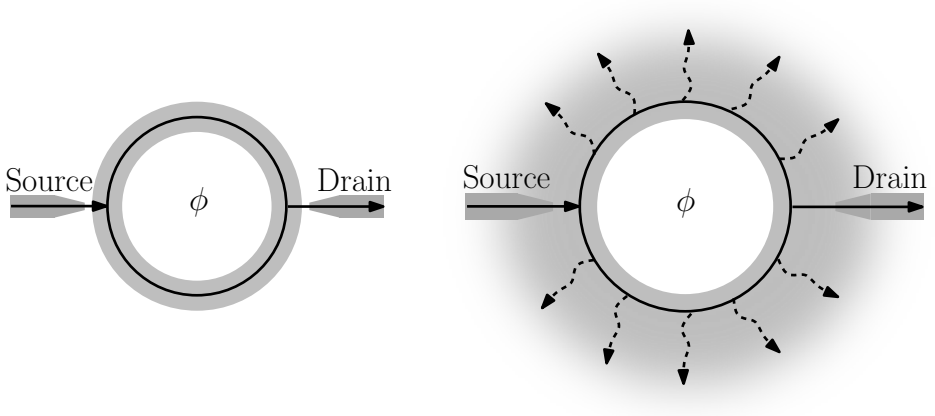

(a) Closed AB ring (b) Open AB ring

Figure 2.2: **(a)** Closed AB ring: electrons that are emitted from the source tunnel to the drain through the ring either clockwise or counter-clockwise. The two interfering paths encircle a penetrating flux, ϕ. Time reversal symmetry constrains the conductance: $G(\phi) = G(-\phi)$. **(b)** Open AB ring: electrons that propagate along the ring may leak out to side leads that are attached to the ring. The restriction $G(\phi) = (-\phi)$ ceases to be valid.

thermal length [97] $l_T = v_F/\pi K_B T$:

$$\int d\epsilon \left(-\frac{\partial f}{\partial \epsilon}\right) 2\left|t_{\mathrm{d},s} t_{\mathrm{ref},s}\right| \cos\left[\frac{e\phi}{\hbar c} + \theta_s(\epsilon)\right]$$
$$= 2\left|t_{\mathrm{d},s} t_{\mathrm{ref},s}\right| \cos\left[\frac{e\phi}{\hbar c}\right] \frac{l_{\mathrm{ref}} - l_d}{l_T} \frac{1}{\sinh[(l_{\mathrm{ref}} - l_d)/l_T]} \,. \tag{2.6}$$

Hence we also require that the difference in length between the two paths is much shorter than the thermal length [98] $|l_{\mathrm{ref}} - l_d| \ll l_T$. In this case, the difference in length introduces a second-order correction to the amplitude of the oscillations: $\frac{l_{\mathrm{ref}} - l_d}{l_T} \frac{1}{\sinh[(l_{\mathrm{ref}} - l_d)/l_T]} \approx 1 - \frac{1}{6}\left(\frac{l_{\mathrm{ref}} - l_d}{l_T}\right)^2 \sim 1 - T^2$.

Open Vs. Closed Aharonov-Bohm ring

Although we will not need or discuss all its details, it is useful to have in mind a concrete physical system that realizes a two paths experiment, the AB ring. In an AB ring setup with closed geometry, as schematically drawn in Fig. 2.2(a), electrons tunnel between two leads through a conducting ring which encircles a magnetic flux. Electrons can propagate through each of the two arms of the ring, and as the two possible ways interfere, the conductance

depends on the magnetic flux. Yet, there is a major difference between the closed AB ring setup and the double-slit experiment. In a naive electronic double-slit experiment picture, the phase of the interference depends continuously on the flux-tuned relative phase between the two paths. In the closed AB ring, however, Onsager relations impose the restriction $G(\phi) = G(-\phi)$, which yields [99, 59] $\varphi_t = \pm\pi$. This phase rigidity has been measured [100], and although it is an interesting phenomenon by itself, it prevents a direct measurement of the phase difference between the two arms of the ring.

We can overcome this by using an open-AB-ring setup, as schematically depicted in Fig. 2.2(b). In such an experimental setup, that was used by Schuster *et al.* [101] and later on by others [102, 103, 104, 61], electrons that propagate along the ring can leak out of the ring into side leads. The loss of electrons during the propagation through the ring relaxes the two-terminal Onsager restriction [60] $G(\phi) = G(-\phi)$. Although the open geometry solves the phase rigidity problem, the intuitive double-slit picture is not assured. In a double-slit setup, the transmissions through the two slits are independent of each other, and particles traverse the two slits only once. Therefore, we require that in the open AB ring setup, the propagation of particles along each path is independent of the details of the other path, and that there are no multiple traversals of the ring. We rely on the same features when defining the procedure for measuring η. An example of a model for an open AB ring with a detailed analysis of the conditions required for the realization of a double-slit setup appears in Ref. [105].

Another difference between the AB ring and the ideal double-slit experiment is the effect that the penetrating magnetic flux has on the propagation along the two paths. In the ideal double-slit experiment, magnetic flux tunes only the relative phase of the paths. In contrast, in a real AB ring with an embedded dot, the Kondo temperature of the dot, and the conductance through the dot, may depend on the magnetic flux. These effects of the magnetic flux on AB rings, were studied before and appear in the literature [106, 107, 108, 109, 110, 111, 112]. But these effects can be made small, particularly for open AB rings [110]. From now on, we thus assume an open geometry that realizes a double-slit experiment.

2.3 Single-particle transmission properties and the $\mathcal{T}$-matrix

In this section, we present a general discussion on the relation between scattering of electrons off the impurity and the conductance of the system. We

relate the three measurable quantities, G_d, φ_t, and η, that were defined in Eq. (1.9), to the scattering matrix and the $\mathcal{T}$-matrix of the ψ-particles.

We develop a novel many-body scattering theory [54] which enables us to derive the mathematical expressions for φ_t and η. We also show, that if one measures only the total conductance of the two spins together, then at $T \ll T_K$ the phase φ_t is always equal to $\pi/2$, and it has no perturbative corrections up to order $\mathcal{O}(T/T_K)^2$ for the Fermi liquid fixed points and $\mathcal{O}(T/T_K)^{\frac{2}{2+k}}$ for the non-Fermi liquid fixed points of the k-channel Kondo systems. The theoretical part that appears in this section is essential for the derivation of the results that we present in Sec. 3.2.

We consider an open AB geometry that realizes a two-path setup, and we zoom in on the path that contains the impurity. We make a distinction between the external leads (the source and the drain), and the internal leads through which the electrons propagate toward the impurity. We refer to the latter as left and right leads (see, for example, Fig. A.1). Electrons from the source can be transmitted into the left lead, then they propagate toward the impurity. After the electrons are scattered off the impurity they can propagate along the right lead and then be transmitted out into the drain. A specific model that describes this situation is proposed and presented in Appendix A. While the source and the drain are coupled very weakly to the internal leads (because of the losses needed to ensure each electron traverses the ring only once), the electrons in the internal leads can, in principle, interact very strongly with the impurity. Hence, in general, the left and the right leads are described by complex many-body states. A general state in the two leads can be characterized by two numbers, n_L and n_R, measures of charge carried in each lead. There are, of course, many possible states with charges en_L and en_R, since states with the same charges in the two leads can differ by multiple particle-hole excitations. We use the notation $|n_L, n_R, i\rangle$ for these states, where the index i labels the possible states with charges en_L and en_R in the two leads. Note: in the k-channel Kondo case, if there is no charge transfer between the different channels, n_L and n_R are the charges in one of the channels, and states with the same values of n_L and n_R can also differ by excitations in the other $\mathrm{k}-1$ channels.

The scattering matrix, $\mathcal{S}$, connects incoming and outgoing states in the leads

$$|n'_L, n'_R, j\rangle_{\text{out}} = \mathcal{S}^{n'_L,n'_R,j}_{n_L,n_R,i} |n_L, n_R, i\rangle_{\text{in}} \ . \tag{2.7}$$

Charge conservation imposes $n'_L + n'_R = n_L + n_R = m$, so $\mathcal{S}$ is a block-diagonal matrix, as sectors with different integer value m, are not mixed. Since the source and the drain are coupled very weakly to the internal leads, in the limit of zero source-drain bias voltage at low temperature, we assume

that only one particle at a time is launched from the external leads toward the impurity. Hence, we focus only on the block $m = 1$ of the $\mathcal{S}$-matrix. When a single electron is sent from the source, through the left lead, into the impurity, there are three possible options:

- The electron is reflected back to the left lead,
- The electron is transmitted to the right lead,
- A complex many-body state is produced, where a total charge ne is transmitted to the right lead and a charge $(1-n)e$ is reflected to the left lead ($n = 0, \pm 1, \pm 2...$) .

We want to distinguish between the elastic single-particle scattering processes and the scattering processes that involve many-body states. We therefore use the following notation: we denote by $|L\rangle$ the incoming or outgoing single-electron states in the left lead, and similarly $|R\rangle$ in the right lead. In the notation $|n_L, n_R, i\rangle$,

$$|L\rangle = |1,0,0\rangle \ , \qquad |R\rangle = |0,1,0\rangle \ , \tag{2.8}$$

where we arbitrarily choose $i = 0$ for the single-particle states with total charge one. The many-body states (also with total charge one) are denoted by $|\chi_n^i\rangle$, where

$$|\chi_n^i\rangle = |1-n, n, i\rangle \ . \tag{2.9}$$

We use the following notation for the $\mathcal{S}$-matrix elements that connect incoming single-particle states with outgoing single-particle states:

$$\mathcal{S}^{1,0,0}_{1,0,0} = r \ , \ \ \mathcal{S}^{1,0,0}_{0,1,0} = t \ , \ \ \mathcal{S}^{0,1,0}_{0,1,0} = r' \ , \ \ \mathcal{S}^{0,1,0}_{1,0,0} = t' \ . \tag{2.10}$$

The matrix elements that connect single-particle states with many-body states are:

$$\mathcal{S}^{1-n,n,i}_{1,0,0} = B_L^{ni} \ , \qquad \mathcal{S}^{1-n,n,i}_{0,1,0} = B_R^{ni} \ , \tag{2.11}$$

$$\mathcal{S}^{1,0,0}_{1-n,n,i} = \left(A_L^{ni}\right)^* \ , \ \ \mathcal{S}^{0,1,0}_{1-n,n,i} = \left(A_R^{ni}\right)^* \ . \tag{2.12}$$

Schematically, the $n_L + n_R = 1$ block of the $\mathcal{S}$-matrix is

$$\begin{pmatrix} |L\rangle_{\rm out} \\ |R\rangle_{\rm out} \\ |\boldsymbol{\chi}\rangle_{\rm out} \end{pmatrix} = \begin{pmatrix} r & t' & \boldsymbol{A_L}^\dagger \\ t & r' & \boldsymbol{A_R}^\dagger \\ \boldsymbol{B_L} & \boldsymbol{B_R} & \boldsymbol{C} \end{pmatrix} \begin{pmatrix} |L\rangle_{\rm in} \\ |R\rangle_{\rm in} \\ |\boldsymbol{\chi}\rangle_{\rm in} \end{pmatrix} \ , \tag{2.13}$$

where the matrix $\boldsymbol{C}$ denotes the matrix elements of $\mathcal{S}$ that connect incoming many-body states with outgoing many-body states. Here we don't include spin, but generalization of what follows to spinful electrons is straightforward.

Since the $\mathcal{S}$-matrix is unitary and block diagonal, its $n_L + n_R = 1$ block is also unitary. This leads to the following relations:

$$|r|^2 + |t|^2 + \sum_{n,i} \left|B_L^{ni}\right|^2 = 1 \,, \tag{2.14}$$

$$|r'|^2 + |t'|^2 + \sum_{n,i} \left|B_R^{ni}\right|^2 = 1 \,, \tag{2.15}$$

$$|r|^2 + |t'|^2 + \sum_{n,i} \left|A_L^{ni}\right|^2 = 1 \,, \tag{2.16}$$

$$|r'|^2 + |t|^2 + \sum_{n,i} \left|A_R^{ni}\right|^2 = 1 \,. \tag{2.17}$$

Consider now the average current at the right lead. The current is carried either by transmitted charge (from the left), or by reflected charge

$$\begin{aligned} I &= \frac{e}{h} \int d\epsilon \left[f_l(\epsilon) \left(|t|^2 + \sum_{n,i} n \left|B_L^{ni}\right|^2 \right) + f_r(\epsilon) \left(|r'|^2 + \sum_{n,i} n \left|B_R^{ni}\right|^2 - 1 \right) \right] \\ &= \frac{e}{h} \int d\epsilon \left[f_l(\epsilon) \left(|t|^2 + \sum_{n,i} n \left|B_L^{ni}\right|^2 \right) - f_r(\epsilon) \left(|t'|^2 + \sum_{n,i} (1-n) \left|B_R^{ni}\right|^2 \right) \right] . \end{aligned} \tag{2.18}$$

At equilibrium, the current is zero, therefore

$$|t|^2 + \sum_{n,i} n \left|B_L^{ni}\right|^2 = |t'|^2 + \sum_{n,i} (1-n) \left|B_R^{ni}\right|^2 \,, \tag{2.19}$$

and the current becomes

$$I = \frac{e}{h} \int d\epsilon \left[f_l(\epsilon) - f_r(\epsilon) \right] \left(|t|^2 + \sum_{n,i} n \left|B_L^{ni}\right|^2 \right) . \tag{2.20}$$

Thus, the conductance is

$$G_{\mathrm{d}} = \frac{e^2}{h} \int d\epsilon \left(-\frac{\partial f}{\partial \epsilon} \right) \left(|t|^2 + \sum_{n,i} n \left|B_L^{ni}\right|^2 \right) . \tag{2.21}$$

The coherent part of the conductance is obtained directly from Eq. (2.21)

$$G_{\mathrm{coh}} = \frac{e^2}{h} \int d\epsilon \left(-\frac{\partial f}{\partial \epsilon} \right) |t|^2 \,. \tag{2.22}$$

The contribution of the incoherent processes, where the single particles are scattered into many-body states, is

$$G_{\text{incoh}} = \frac{e^2}{h} \int d\epsilon \left(-\frac{\partial f}{\partial \epsilon}\right) \sum_{n,i} n \left|B_L^{ni}\right|^2 \ . \tag{2.23}$$

Suppose now, that there is a unitary transformation that mixes the two leads and block-diagonals the $n_L + n_R = 1$ block of the $\mathcal{S}$-matrix. Physically, it means that there is a linear combination of the two leads, $\xi = -\sin(\alpha)L + \cos(\alpha)R$, which is decoupled both from the impurity and from the orthogonal combination of the leads, $\psi = \cos(\alpha)L + \sin(\alpha)R$. This is the case, for example, in the Anderson model for a single level quantum dot that is coupled to two leads. The fact that ξ is a free decoupled field simplifies the above expressions as it imposes the following restrictions on the $\mathcal{S}$-matrix in the $\psi - \xi$ basis: $\mathcal{S}_{\xi x} = \mathcal{S}_{x\xi} = 0$ $(x = \psi, \vec{\chi}_n)$, and $\mathcal{S}_{\xi\xi} = 1$. In particular, the restriction $\mathcal{S}_{\psi\xi} = \mathcal{S}_{\xi\psi} = 0$ requires $t' = t$ which, together with Eq. (2.19), yields the relation

$$\sum_{n,i} n \left|B_L^{ni}\right|^2 = \sum_{n,i} (1-n) \left|B_R^{ni}\right|^2 \ . \tag{2.24}$$

Moreover, we can relate B_L^{ni} and B_R^{ni}. Since (omitting the in and out subscripts)

$$B_L^{ni} = \langle \chi_n^i | L \rangle = \cos(\alpha) \langle \chi_n^i | \psi \rangle - \sin(\alpha) \langle \chi_n^i | \xi \rangle, \tag{2.25}$$

$$B_R^{ni} = \langle \chi_n^i | R \rangle = \sin(\alpha) \langle \chi_n^i | \psi \rangle + \cos(\alpha) \langle \chi_n^i | \xi \rangle, \tag{2.26}$$

and as $\langle \chi_n^i | \xi \rangle = 0$ we get

$$B_L^{ni} = \cos(\alpha) \langle \chi_n^i | \psi \rangle \ , \tag{2.27}$$

$$B_R^{ni} = \sin(\alpha) \langle \chi_n^i | \psi \rangle \ . \tag{2.28}$$

We obtain the relation

$$B_R^{ni} = \tan(\alpha) B_L^{ni} \ . \tag{2.29}$$

Plugging this relation into Eq. (2.24) gives

$$[1 + \tan^2(\alpha)] \sum_{n,i} n \left|B_L^{ni}\right|^2 = \tan^2(\alpha) \sum_{n,i} \left|B_L^{ni}\right|^2 . \tag{2.30}$$

Thus, we get the important equalities

$$\sum_{n,i} n \left|B_L^{ni}\right|^2 = \sin^2(\alpha) \sum_{n,i} \left|B_L^{ni}\right|^2 , \tag{2.31}$$

$$\sum_{n,i} n \left|B_R^{ni}\right|^2 = \sin^2(\alpha) \sum_{n,i} \left|B_R^{ni}\right|^2 . \tag{2.32}$$

Together with Eqs. (2.14) and (2.15), the sum rules (2.31) and (2.32), tell us that the incoherent part of the conductance, which is carried by single-particle to many-particles scattering processes, can also be determined by the coherent single-particle part of the $\mathcal{S}$-matrix.

Notice also that $\sum_{n,i}\langle\psi|\chi_n^i\rangle\langle\chi_n^i|\psi\rangle = \sum_{ni}|\langle\psi|\chi_n^i\rangle|^2$ is the sum of probabilities to find outgoing states if the incoming state is $|\psi\rangle$. Since we sum over all possible outgoing states besides $|\psi\rangle$ and $|\xi\rangle$, and as $\langle\xi|\psi\rangle = 0$ we find that

$$\sum_{n,i}\langle\psi|\chi_n^i\rangle\langle\chi_n^i|\psi\rangle = 1 - |{}_{\text{out}}\langle\psi|\psi\rangle_{\text{in}}|^2 = 1 - |\mathcal{S}_{\psi\psi}|^2, \tag{2.33}$$

so

$$\sum_{n,i}\left|B_L^{ni}\right|^2 = \cos^2(\alpha)(1 - |\mathcal{S}_{\psi\psi}|^2)\ , \tag{2.34}$$

$$\sum_{n,i}\left|B_R^{ni}\right|^2 = \sin^2(\alpha)(1 - |\mathcal{S}_{\psi\psi}|^2)\ . \tag{2.35}$$

The conductance (2.21) can be written as

$$G_{\text{d}} = -\frac{e^2}{h}\int d\epsilon\frac{\partial f}{\partial\epsilon}\left[|t|^2 + \sin^2(\alpha)\cos^2(\alpha)(1 - |\mathcal{S}_{\psi\psi}|^2)\right]\ , \tag{2.36}$$

and the contribution of the single-particle processes to the conductance, out of the total conductance is

$$G_{\text{coh}}/G_{\text{d}} = \frac{\int d\epsilon\frac{\partial f}{\partial\epsilon}|t|^2}{\int d\epsilon\frac{\partial f}{\partial\epsilon}\left(|t|^2 + \sin^2(\alpha)\cos^2(\alpha)(1 - |\mathcal{S}_{\psi\psi}|^2)\right)}\ . \tag{2.37}$$

The fact that there is a linear combination of L and R which is decoupled both from the impurity and from the orthogonal linear combination imposes restrictions on the values of r, t, r', t' (since $\mathcal{S}_{\psi\xi} = \mathcal{S}_{\xi\psi} = 0$ and $\mathcal{S}_{\xi\xi} = 1$). By applying the unitary transformation on the $\mathcal{S}$-matrix one finds that

$$\mathcal{S}_{\psi\psi} = 1 + \frac{t}{\cos(\alpha)\sin(\alpha)}\ . \tag{2.38}$$

Plugging (2.38) into (2.36) and (2.37) gives

$$G_{\text{d}} = -\frac{e^2}{h}\frac{\sin^2(2\alpha)}{4}\int d\epsilon\frac{\partial f}{\partial\epsilon}\left(|\mathcal{S}_{\psi\psi} - 1|^2 + \left[1 - |\mathcal{S}_{\psi\psi}|^2\right]\right), \tag{2.39}$$

$$G_{\text{coh}}/G_{\text{d}} = \frac{\int d\epsilon\frac{\partial f}{\partial\epsilon}|\mathcal{S}_{\psi\psi} - 1|^2}{\int d\epsilon\frac{\partial f}{\partial\epsilon}\left(|\mathcal{S}_{\psi\psi} - 1|^2 + [1 - |\mathcal{S}_{\psi\psi}|^2]\right)}\ . \tag{2.40}$$

At this point we can already see two important features: First, $G_{\rm coh}/G_{\rm d}$ depends only on $\mathcal{S}_{\psi\psi}$ and in particular does not depend directly on α. Second, if $|\mathcal{S}_{\psi\psi}| = 1$ (but $\mathcal{S}_{\psi\psi} \neq 1$) then $G_{\rm coh}/G_{\rm d} = 1$, and if $\mathcal{S}_{\psi\psi} = 0$ then $G_{\rm coh}/G_{\rm d} = 1/2$. In other words, for a zero temperature Fermi liquid theory $\eta = 1$, and for a theory where ψ has no single-particle to single-particle scattering processes (like in the 2CK case at zero temperature) $\eta = 1/2$.

Using the definition $\mathcal{S} = 1 + i\mathcal{T}$ for the $\mathcal{T}$-matrix, we get the known result [113, 114, 115] for the conductance through the impurity

$$G_{\rm d} = \frac{e^2}{h}\frac{\sin^2(2\alpha)}{4}\int d\epsilon \left(-\frac{\partial f}{\partial \epsilon}\right) 2Im\left\{\mathcal{T}_{\psi\psi}\right\} \ . \tag{2.41}$$

The ratio of the coherent part to the total conductance is

$$G_{\rm coh}/G_{\rm d} = \frac{\int d\epsilon \left(-\frac{\partial f}{\partial \epsilon}\right) |\mathcal{T}_{\psi\psi}|^2}{\int d\epsilon \left(-\frac{\partial f}{\partial \epsilon}\right) 2Im\left\{\mathcal{T}_{\psi\psi}\right\}} \ . \tag{2.42}$$

2.3.1 Normalized visibility

There is no way to measure directly the contribution of the single-particle processes to the conductance. Namely, there is no direct measurement of $G_{\rm coh}/G_{\rm d}$. However, a two-path experiment gives access to the transmission amplitude, t. If in addition to the impurity, the two leads are connected via an independent free reference arm, then the flux-dependent part of the conductance is $G_{\rm flux} = \int d\epsilon \left(-\frac{\partial f}{\partial \epsilon}\right) 2Re\left\{t_{\rm ref} t e^{i\frac{e\phi}{\hbar c}}\right\}$. Since $|t_{\rm ref}|$ can be extracted from the conductance of the reference arm when the other arm closed off, t is accessible from the flux-dependent conductance.

While $G_{\rm coh}$ is proportional to the thermally-averaged value of the transmission squared [see Eq. (2.22)], $G_{\rm flux}$ is proportional to the thermally-averaged value of the transmission, $\int d\epsilon \left(-\frac{\partial f}{\partial \epsilon}\right) t(\epsilon)$. The normalized visibility that we have defined in Eq. (1.9) is therefore slightly different from $G_{\rm coh}/G_{\rm d}$

$$\eta = \frac{\left|\int d\epsilon \left(-\frac{\partial f}{\partial \epsilon}\right) \mathcal{T}_{\psi\psi}\right|^2}{\int d\epsilon \left(-\frac{\partial f}{\partial \epsilon}\right) 2Im\left\{\mathcal{T}_{\psi\psi}\right\}} \ . \tag{2.43}$$

Although $G_{\rm coh}/G_{\rm d}$ is closely related to the measurable quantity η, they are identical only at zero temperature, or where $\mathcal{T}_{\psi\psi}$ is independent of the energy.

2.3.2 Transmission phase

The phases of t and $\mathcal{T}_{\psi\psi}$ are related to the phase shift of the scattering theory of the ψ-particles. If we write $\mathcal{S}_{\psi\psi} = |\mathcal{S}_{\psi\psi}|e^{2i\delta_\psi}$, then

$$\arg(\mathcal{T}_{\psi\psi}) = \arctan\left(\frac{1-|\mathcal{S}_{\psi\psi}|\cos(2\delta_\psi)}{|\mathcal{S}_{\psi\psi}|\sin(2\delta_\psi)}\right). \tag{2.44}$$

The phase $\arg(\mathcal{T}_{\psi\psi})$ yields the value δ_ψ for $|\mathcal{S}_{\psi\psi}| \to 1$ and $\pi/2$ in the limit $|\mathcal{S}_{\psi\psi}| \to 0$. The transmission phase is the phase of the thermally averaged $\mathcal{T}$-matrix

$$\varphi_t = \arg\left\{\int d\epsilon\left(-\frac{\partial f}{\partial\epsilon}\right)\mathcal{T}_{\psi\psi}(\epsilon)\right\}. \tag{2.45}$$

2.3.3 The $\pi/2$ phase-lock of the transmission through Kondo impurities at $T \ll T_K$

The flux-dependent part of the conductance, G_{flux}, depends on the average value of $\mathcal{T}_{\psi\psi}$. Until now, the averaging was over different incoming energies (thermal averaging). When we add the spin degree of freedom, we average $\mathcal{T}_{\psi\psi}$ also over spin. This is because in G_{flux}, we sum over the two spins

$$\begin{aligned} G_{\text{flux}} &= -\sum_s \int d\epsilon \frac{\partial f}{\partial\epsilon} 2Re\left\{t_{\text{ref}} t_s e^{i\frac{e\phi}{\hbar c}}\right\} \\ &= -\sum_s \int d\epsilon \frac{\partial f}{\partial\epsilon} 2Re\left\{i\cos(\alpha)\sin(\alpha) t_{\text{ref}} \mathcal{T}_{s,\psi\psi} e^{i\frac{e\phi}{\hbar c}}\right\}. \end{aligned} \tag{2.46}$$

We have assumed that t_{ref} is independent of the spin. If the system is spin-symmetric, $\mathcal{T}_{\uparrow,\psi\psi} = \mathcal{T}_{\downarrow,\psi\psi} \equiv \mathcal{T}_{\psi\psi}$ can be extracted from G_{flux}. The normalized visibility in this case is

$$\eta = \frac{\left|\int d\epsilon\left(-\frac{\partial f}{\partial\epsilon}\right)\mathcal{T}_{\psi\psi}\right|^2}{\int d\epsilon\left(-\frac{\partial f}{\partial\epsilon}\right) 2Im\left\{\mathcal{T}_{\psi\psi}\right\}}, \tag{2.47}$$

and the transmission phase is

$$\varphi_t = \arg\left\{\int d\epsilon\left(-\frac{\partial f}{\partial\epsilon}\right)\mathcal{T}_{\psi\psi}(\epsilon)\right\}. \tag{2.48}$$

In the absence of spin-symmetry, G_{flux} does not necessarily give us access to $\mathcal{T}_{s,\psi\psi}$. To see this, consider the simple case where all the particles are scattered into single particles, namely, $|\mathcal{S}_{\psi\psi}| = 1$ for both spins. This situation

describes, for example, the Fermi-liquid fixed points of 1CK or 2CK with an applied magnetic field. In this case, $\mathcal{T}_{s,\psi\psi} = i(1 - e^{2i\delta_{\psi s}}) = 2\sin(\delta_{\psi s})e^{i\delta_{\psi s}}$. In the Kondo case, the system has the following particle-hole symmetry [see, for example, the Hamiltonian in Eq. (1.1)]

$$\psi_{ks} \to \psi^{\dagger}_{-k,-s} \ , \tag{2.49}$$

that enforces [51, 116] $\delta_{\psi\uparrow}(\epsilon) = -\delta_{\psi\downarrow}(-\epsilon)$. The transmission phase at zero temperature is

$$\varphi_t = \arg\left[\sin(\delta_{\psi\uparrow})(e^{i\delta_{\psi\uparrow}} - e^{-i\delta_{\psi\uparrow}})\right] = \frac{\pi}{2} \ , \tag{2.50}$$

and the normalized visibility at zero temperature

$$\eta = \frac{\left|\sin(\delta_{\psi\uparrow})(e^{i\delta_{\psi\uparrow}} - e^{-i\delta_{\psi\uparrow}})\right|^2}{2Im\left\{\sin(\delta_{\psi\uparrow})(e^{i\delta_{\psi\uparrow}} - e^{-i\delta_{\psi\uparrow}})\right\}} = \sin^2(\delta_{\psi\uparrow}) \ . \tag{2.51}$$

We see that the transmission phase is locked at $\pi/2$, independent of the phases of $\mathcal{T}_{s,\psi\psi}$. We also see that the normalized visibility can be smaller than one, even though all the scattering processes are single-particle to single-particle scattering. Interestingly, information about the phases of $\mathcal{T}_{s,\psi\psi}$ (the phase shifts of the scattering theory), is now encoded in η . There are two ways to extract $\mathcal{T}_{\psi\psi}$ despite the $\pi/2$ phase-lock of Kondo impurities: either to use the normalized visibility to extract the phase shift, or to measure the transmission of each spin separately.

2.4 Rate equations method

In this section, we present the rate equations technique for transport calculations, which we used for obtaining the results in two different systems: The UV conductance of the $SU(N)$-Kondo systems (see Sec. 3.1), and for the extensive study of the transport properties in the interacting two level system (see Sec. 3.3).

We shortly review the technique that was developed in Ref. [117] and the generalization of it to include cotunneling processes that was developed in Ref. [118]. Consider a small system with n possible states, $|1\rangle, |2\rangle, \ldots, |n\rangle$, which is weakly tunnel-coupled to external leads. The system can be in one of its n states, and its dynamics is driven by tunneling processes. For example, in the triple-dot structure of the $SU(3)$-Kondo, the system has eight states: empty dots, single electron in one of the dots (three states), two electrons in the dots (three states), and full occupation of the three dots. Generally, there

are many tunneling processes that change the state of the system from $|i\rangle$ to $|f\rangle$ which we denote their rates by $\omega_{i,f}^{\alpha}$ where α labels the different possible tunneling processes. The rate $\omega_{i,f} = \sum_{\alpha} \omega_{i,f}^{\alpha}$ is the total transition rate from the state $|i\rangle$ to the state $|f\rangle$. The dynamics of the system is described by the rate equations

$$\frac{\partial}{\partial t} P(f,t/i) = \sum_{k \in S} \left[P(k,t/i)\omega_{k,f} - P(f,t/k)\omega_{f,k} \right], \tag{2.52}$$

where $P(f,t/i)$ is the probability of the system to be in the state $|f\rangle$ at time t if it was in the state $|i\rangle$ at $t = 0$, so the initial condition is $P(f,t=0/i) = \delta_{i,f}$. Eq. (2.52) neglects coherence superpositions of different states [the terms $P(f,t/i)$ are the diagonal matrix elements of the density matrix]. Neglecting the coherent superpositions of the states is justified when the coherence time is much shorter than the delay time between consecutive tunneling events. Alternatively, if there is a quantum number that distinguishes the two states (*e.g.*, spin), if at some point in time the density matrix that describes the system is diagonal, then coherent superpositions are zero at all later times.

It appears to be useful to write the rate equations in a matrix form. We define the vector (there are four such vectors)

$$\mathbf{P}_i(t) \equiv [P(1,t/i), P(2,t/i), \ldots, P(n,t/i)], \tag{2.53}$$

and the matrix

$$M = \begin{pmatrix} -\sum_{k \neq 1} \omega_{1,k} & \omega_{2,1} & \omega_{3,1} & \cdots \\ \omega_{1,2} & -\sum_{k \neq 2} \omega_{2,k} & \omega_{3,2} & \cdots \\ \omega_{1,3} & \omega_{2,3} & -\sum_{k \neq 3} \omega_{3,k} & \cdots \\ \vdots & \vdots & \vdots & \ddots \end{pmatrix}. \tag{2.54}$$

The rate equations become $\frac{\partial}{\partial t}\mathbf{P}_i(t) = M\mathbf{P}_i(t)$, with the initial condition $\mathbf{P}_i(t=0) = (0,\ldots,0,1,0,\ldots,0) \equiv \widehat{e}_i$. The solution of Eq. (2.52) is readily found to be $\mathbf{P}_i(t) = e^{Mt}\widehat{e}_i$. Let P^{st} be the stationary solution, namely, $MP^{st} = 0$ and (since it is a probabilities vector) $\sum_n P_n^{st} = 1$.

current. We define the quantity $s_{i,f}^{a\alpha}$, the total number of electrons that tunnel through the tunnel-junction a to the right during the process α that changes the system's state from $|i\rangle$ to $|f\rangle$. The junction α connects the system to one of the external leads. For example, the junction between the two level system to the left lead or the right lead. If $s_{i,f}^{a\alpha}$ has a negative sign, it

corresponds to electrons that are moving to the left. The stationary current through the junction a can be written as

$$\langle I_a \rangle = e \sum_{i,f \in S} \sum_{\alpha} s_{i,f}^{a\alpha} P_i^{st} \omega_{i,f}^{\alpha}. \tag{2.55}$$

Zero frequency noise. The noise is related to the auto-correlation function via Wiener-Khinchin theorem

$$S_{ab}(\omega) = 2 \int_{-\infty}^{\infty} d\tau e^{i\omega\tau} [\langle I_a(t+\tau) I_b(t) \rangle - \langle I \rangle^2], \tag{2.56}$$

where we are interested in the zero frequency limit. We write here a compact expression for the noise, details of the derivation can be found in Ref. [118]. The zero frequency noise can be written as

$$S_{ab}(\omega \to 0) = 2e^2 \{ tr \mathbf{U}_{ab} - \mathbf{W}_b \cdot M^{-1} \bar{\mathbf{Y}}_a - \mathbf{W}_a \cdot M^{-1} \bar{\mathbf{Y}}_b \}, \tag{2.57}$$

with the following vectors:

$$(\mathbf{U}_{ab})_i \equiv \sum_{f \in S} \sum_{\alpha} s_{i,f}^{a\alpha} s_{i,f}^{b\alpha} P_i^{st} \omega_{i,f}^{\alpha}, \tag{2.58}$$

$$(\bar{\mathbf{Y}}_a)_j \equiv \sum_{i \in S} \sum_{\alpha} s_{i,j}^{a\alpha} P_i^{st} \omega_{i,j}^{\alpha} - \frac{\langle I_a \rangle}{e} P_j^{st}, \tag{2.59}$$

$$(\mathbf{W}_b)_k \equiv \sum_{f \in S} \sum_{\alpha} s_{k,f}^{b\alpha} \omega_{k,f}^{\alpha}. \tag{2.60}$$

We have used the trace of a vector to denote the sum of its elements. Although the matrix M is not invertible, there is only one traceless vector $\mathbf{V}_a$ (*i.e.* the sum of all its elements is zero) that satisfies $M\mathbf{V}_a = \bar{\mathbf{Y}}_a$ [118] and we use this vector as $M^{-1}\bar{\mathbf{Y}}_a$.

2.5 Two interacting levels

In this section we describe two models that we used in the analysis of the transport through asymmetric interacting two-level systems, which is presented in Sec. 3.3. We start with the Anderson model, with two interacting levels that are attached to two leads (see Fig. 2.3). For simplicity, we discuss a spinless problem, adding the spin degree of freedom does not change the qualitative behavior of the system and not important for the understanding of the underlying physics. One of the levels (level 2 in Fig. 2.3) is attached

very weakly (compared to the other level) to the leads. A simultaneous occupation of the two levels is possible, however this situation is not likely to happen as it requires an additional charging energy, U, because of the Coulomb interaction. This model describes, for example, an interacting two level quantum dot in a strong magnetic field. The Hamiltonian that describes the system is

$$H = H_{\text{leads}} + H_{\text{2levels}} + H_{\text{t}}, \tag{2.61}$$

where

$$\begin{aligned} H_{\text{leads}} &= \sum_k \epsilon_k^L L_k^\dagger L_k + \sum_k \epsilon_k^R R_k^\dagger R_k, \\ H_{\text{2levels}} &= E_1 d_1^\dagger d_1 + E_2 d_2^\dagger d_2 + U d_1^\dagger d_1 d_2^\dagger d_2, \\ H_{\text{t}} &= \sum_{i,k} \left(t_i^L L_k^\dagger d_i + t_i^R R_k^\dagger d_i \right) + \text{H.C.} \quad . \end{aligned}$$

Here, L_k (R_k) are left (right) lead annihilation operators, d_i is the ith level annihilation operator, and we have assumed that the tunneling coefficients ($t_i^{L,R}$) are independent of the energy. We also assume that all the tunneling coefficients have the same sign.

We calculate the average current and the zero-frequency noise using rate equations method in which we assume that the two levels are weakly coupled to the leads. By weakly coupled we mean that the widths of the levels are much smaller than the temperature, or alternatively, at low temperatures it means that the bias voltage (see Fig. 2.3) is much larger than the levels' widths

$$\gamma_i = \pi\nu \left(\left| t_i^L \right|^2 + \left| t_i^R \right|^2 \right) \ll \left| \mu^{R,L} - E_i \right|, \tag{2.62}$$

where $\mu^{R,L}$ are the electro-chemical potentials of the leads and we have assumed for simplicity the same density of states, ν, in the two leads.

2.5.1 Qualitative simplified model

Before we continue with the analysis of the Anderson model using rate equations, we want to present a simplified intuitive model, which we suggested in Ref. [62]. This simplified model captures, at least qualitatively, most of the results that we later achieve through a more rigorous analysis. The advantage of this model is that it helps us to establish a simple physical picture that we can use to interpret the results that we get through the rate equations formalism.

Consider the two level system which is depicted in Fig. 2.3 and assume strong interactions, *i.e.*, a large U. At this point, we also assume, for simplicity, zero temperature. As a function of E_1, there are two regions where

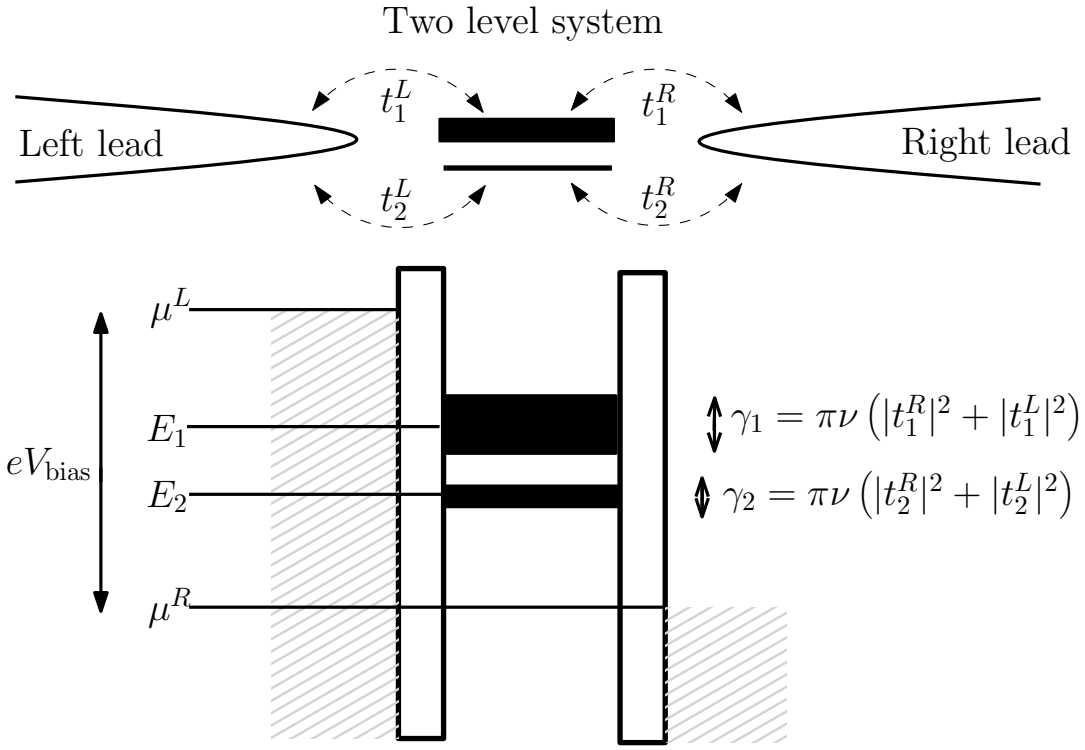

Figure 2.3: A schematic picture of the model. The energies of the two levels are E_1 and E_2. The bias voltage is the difference between the two chemical potentials: $eV_{\rm bias} = \mu^L - \mu^R$. Here the width of level 2 is much smaller than the width of level 1 which is assumed to be much smaller than the bias voltages: $\gamma_2 \ll \gamma_1 \ll |\mu^{R,L} - E_{1,2}|$. We assume that the tunneling coefficients are independent of the energy and we also assume for simplicity that they all have the same sign, and that the two ratios between the left tunneling coefficients and the right tunneling coefficients are identical, $t_1^L/t_1^R = t_2^L/t_2^R$.

we expect to have current: at $\mu^R < E_1 < \mu^L$ where the two levels are between the chemical potentials (assuming that $|E_1 - E_2| \ll V_{\text{bias}}$), and at $\mu^R < E_1 + U < \mu^L$ where one of the levels is occupied and effectively, because of the Coulomb interaction, the other level is shifted up and placed between the chemical potentials. We choose to focus at this point on the later: $\mu^R < E_1 + U < \mu^L$. Since level 2 is coupled weaker than level 1 to the leads, most of the time the current flows through level 1 (*i.e.* level 2 is occupied and electrons enter and leave level 1). However, after a while, the electron in level 2 can tunnel out to the right lead and by that, because of the Coulomb interaction, it reduces the effective energy of level 1 (from $E_1 + U$ to E_1) making the tunneling out of level 1 impossible. The current is therefore blocked. The current resumes only after a new electron from the left lead tunnels into level 2. Hence, the picture is a current (through level 1) that is stopped occasionally (by tunneling out of level 2). This situation is schematically drawn in Fig. 2.4.

Shot noise on top of a telegraph noise

The current, as drawn in Fig. 2.4, fluctuates between two modes: A zero-current mode where the current is dramatically suppressed, and a nonzero mode where the current is carried by pulses of charge (electrons) that tunnel through level 1. We therefore suggest the following simplified model: the current $I(t)$ is a multiplication of two signals

$$I(t) = I_{\text{shot}}(t) \times C_{\text{telegraph}}(t), \tag{2.63}$$

where $I_{\text{shot}}(t)$ is the current through level 1 and $C_{\text{telegraph}}(t)$ is a random telegraph signal that fluctuates between two values, zero and one, according to the occupation of level 2. In this simplified model, the current flows only through level 1 and only when level 2 is occupied. We neglect the effects that the Pauli principle imposes on the current $I_{\text{shot}}(t)$ and treat it as a sequence of current pulses of charge e with a Poissonian statistics characterized by a rate Γ_1. The changes in the value of $C_{\text{telegraph}}$ are Poissonian events with the rates $1/\tau_1$ and $1/\tau_0$ for the events of changing the value of $C_{\text{telegraph}}$ from one to zero and zero to one, respectively. The fluctuations in the current $I_{\text{shot}}(t)$ are known as shot noise, and the fluctuations in the signal $C_{\text{telegraph}}(t)$ are known as telegraph noise [119].

Assuming that I_{shot} and $C_{\text{telegraph}}$ are uncorrelated, the average current is

$$\langle I \rangle = \langle I_{\text{shot}} \rangle \langle C_{\text{telegraph}} \rangle = e\Gamma_1 \frac{\tau_1}{\tau_1 + \tau_0}. \tag{2.64}$$

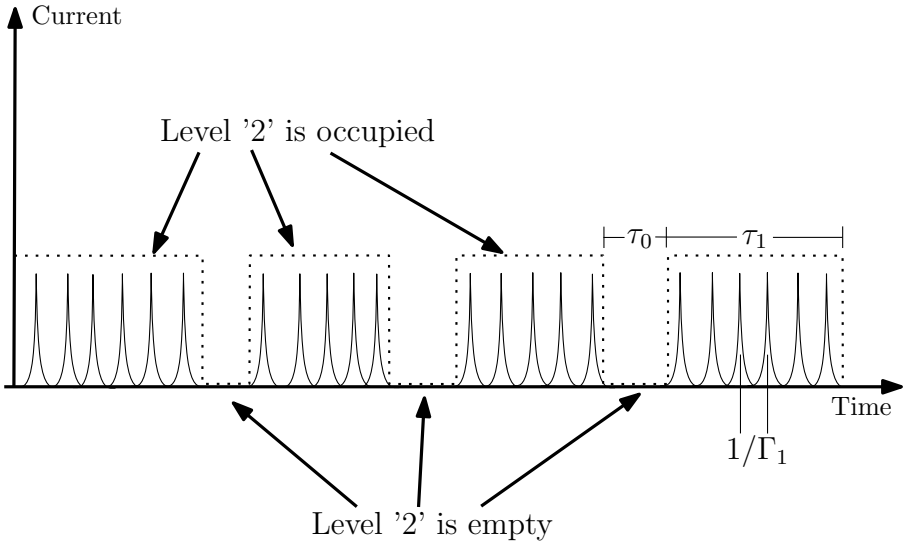

Figure 2.4: A qualitative description of the transport through the two level system in the region $\mu^R < E_1+U < \mu^L$. Electrons are tunneling through level 1 until the electron in level 2 tunnels out and then the current is blocked. The tunneling events through level 1 resume when another electron tunnels into level 2. The current behaves as a multiplication of two signals: A sequence of current pulses through level 1 and a telegraphic signal, the occupation of level 2. Γ_1 is the average rate of tunneling events through level 1, τ_0 is the average time duration until level 2 is filled, and τ_1 is the average time duration until level 2 gets empty.

The noise is related to the auto-correlation function of the total current via Wiener-Khinchin theorem

$$\begin{aligned} S(\omega) &= 2\int_{-\infty}^{\infty} d\tau e^{i\omega\tau}(\langle I(t+\tau)I(t)\rangle - \langle I\rangle^2) \qquad (2.65)\\ &= \langle I_{\text{shot}}\rangle^2 S_{\text{telegraph}}(\omega) + \langle C_{\text{telegraph}}\rangle^2 S_{\text{shot}}(\omega) + \frac{1}{\pi} S_{\text{shot}}(\omega) * S_{\text{telegraph}}(\omega). \end{aligned}$$

Using the known results for the shot noise and the telegraph noise [119] we get

$$S(\omega) = 2e^2\Gamma_1 \frac{\tau_1}{\tau_1+\tau_0} + \frac{4e^2\Gamma_1^2}{(\tau_1+\tau_0)((1/\tau_1+1/\tau_0)^2+\omega^2)}\,. \qquad (2.66)$$

Fano factor and asymmetry dependence

Before we study the Fano factor and its left-right asymmetry dependence, it seems necessary to inquire about the linear dependence of the noise on the current as the second term in (2.66) is quadratic in Γ_1. Since the rates $1/\tau_1$ and $1/\tau_0$ are the rates of tunneling out of and into level 2, they depend, up to a symmetry factor, linearly on γ_2 that was defined in Eq. (2.62). Similarly, Γ_1 is linear in γ_1. Therefore, under the reasonable assumption that γ_1/γ_2 is independent of the left-right asymmetry (that is, the couplings of the levels to the leads cannot be changed independently), $1/\tau_1$ and $1/\tau_0$ are linear in Γ_1. Hence, the zero-frequency noise, $S(0)$, depends linearly on Γ_1 and therefore depends linearly on the current.

The probability of finding level 2 occupied, which is the probability of finding $C_{\text{telegraph}} = 1$, is $P_{\text{f}} = \frac{\tau_1}{\tau_0+\tau_1}$. Similarly, the probability of finding level 2 empty, which at zero temperature is the probability of finding *only* level 1 occupied is $P_{\text{e}} = \frac{\tau_0}{\tau_0+\tau_1}$. The Fano factor is

$$F = \frac{S(0)}{2e\langle I\rangle} = 1 + \frac{2\tau_0^2\tau_1\Gamma_1}{(\tau_0+\tau_1)^2} = 1 + \Gamma_1\tau_1 2P_{\text{e}}^2 \,. \tag{2.67}$$

Notice that $\Gamma_1\tau_1$ is the average number of tunneling events during a $C_{\text{telegraph}} = 1$ stage, which is the average number of tunneling events through level 1 before a tunneling event out of level 2 takes place. At zero temperature it can be estimated as $|t_1^R|^2/|t_2^R|^2$, or, assuming the same left-right asymmetry for the two levels, $\Gamma_1\tau_1 = \gamma_1/\gamma_2$. The Fano factor (2.67) becomes

$$F = 1 + 2\frac{\gamma_1}{\gamma_2}P_{\text{e}}^2 \,. \tag{2.68}$$

The probability P_{e} depends on the asymmetry between the coupling to the left and the right leads, *i.e.* on the ratio $|t_i^L|^2/|t_i^R|^2$. To see this consider the simple case of zero temperature and large U. For $\mu^L > \mu^R$ (see Fig. 2.3), the rate of tunneling out of level 2 is, according to Fermi's golden rule, $\Gamma_{\text{f}\to\text{e}} = \frac{2\pi}{\hbar}|t_2^R|^2$. Similarly, the rate of tunneling into level 2 is $\Gamma_{\text{e}\to\text{f}} = \frac{2\pi}{\hbar}|t_2^L|^2$. If we neglect cotunneling effects there are no direct tunneling processes from level 1 to level 2, so the steady state probabilities satisfy

$$P_{\text{e}}\Gamma_{\text{e}\to\text{f}} = P_{\text{f}}\Gamma_{\text{f}\to\text{e}} \,. \tag{2.69}$$

P_{f} is the probability of finding both level 1 and level 2 occupied. In the limit $|E_1 - E_2| \ll V_{\text{bias}}$, the probability of finding only level 1 occupied, P_{e}, equals the probability of finding only level 2 occupied. In the limit of large U, the

probability of finding both level 1 and level 2 empty (for $\mu^R < E_1 + U < \mu^L$) is zero. Thus, $P_\mathrm{f} + 2P_\mathrm{e} = 1$. The steady state solution (2.69) becomes

$$P_\mathrm{e} = \frac{\Gamma_{\mathrm{f}\to\mathrm{e}}}{\Gamma_{\mathrm{e}\to\mathrm{f}} + 2\Gamma_{\mathrm{f}\to\mathrm{e}}} = \frac{1}{|t_i^L|^2/|t_i^R|^2 + 2} \,. \tag{2.70}$$

By increasing $|t_i^L|^2/|t_i^R|^2$, we decrease P_e. In the limit $|t_i^L|^2/|t_i^R|^2 \to \infty$, $P_\mathrm{e} \to 0$ so the Fano factor (2.68) $F \to 1$. By decreasing $|t_i^L|^2/|t_i^R|^2$ we increase P_e and in the limit $|t_i^L|^2/|t_i^R|^2 \to 0$ it gets its maximal value $P_\mathrm{e} = 1/2$ and the Fano factor is maximal, $F = 1 + \frac{\gamma_1}{2\gamma_2} \approx \frac{\gamma_1}{2\gamma_2}$.

Finite temperature

At zero temperature, the only possible tunneling event that follows a tunneling event from the system to the right lead, is from the left lead into the empty level. Therefore, changing the value of $C_\mathrm{telegraph}$ from one to zero in the simplified model, corresponds to a tunneling event from level 2 to the right. In addition, every tunneling event from level 1 to the right, corresponds to a current-pulse in the simplified model. Hence, we can estimate the number of tunneling events during a $C_\mathrm{telegraph} = 1$ stage as $\Gamma_1\tau_1 \approx |t_1^R|^2/|t_2^R|^2$. At finite temperature, there is also a finite probability that a tunneling event from the system to the right will be followed by a tunneling event from the right lead back to the empty level. In the limit $|t_i^L|^2/|t_i^R|^2 \to 0$ the probability of tunneling from right to left may become important. If the couplings to the right are much stronger than the couplings to the left, electrons may tunnel many times back and forth between the right lead and the system before a tunneling event from the left lead to the system takes place. The time scales τ_1 and τ_0 in this case, become smaller than $1/\Gamma_1$, and the value of $\Gamma_1\tau_1$ goes to zero. Therefore, we expect that at finite temperature the Fano factor will have the value one in the limit $|t_i^L|^2/|t_i^R|^2 \to 0$. To conclude, as we decrease $|t_i^L|^2/|t_i^R|^2$ the Fano factor (2.67) gets larger, but at finite temperature, at some point, if we decrease $|t_i^L|^2/|t_i^R|^2$ even further, the Fano factor will start to decrease toward the value one at $|t_i^L|^2/|t_i^R|^2 \to 0$.

Cotunneling effects

Similar to finite temperature, cotunneling processes may suppress the Fano factor at $|t_i^L|^2/|t_i^R|^2 \to 0$. Consider the limit $|t_i^L|^2 \ll |t_i^R|^2$. Without cotunneling, if level 2 is empty, the electron in level 1 need to wait a long time before it can tunnel out to the right lead since such a tunneling event must follows a tunneling event into level 2 which, at zero temperature, is possible

only from the left lead. Cotunneling processes, however, allow the two processes at once; occupying level 2 and evacuating level 1 in a single quantum process. In particular, the electron in level 1 can virtually tunnel out to the right lead while another electron is virtually tunnel from the right lead into level 2 (we use the term virtually to emphasize the fact that the intermediate state does not conserve energy). In the limit $|t_i^L|^2/|t_i^R|^2 \to 0$ the total rate of such processes may become larger than the rate of sequential tunneling from the left lead into level 1. Thus the occupation of level 2 and therefore the telegraphic signal, $C_{\text{telegraph}}(t)$, fluctuates much faster than the pulses' rate $1/\Gamma_1$, and the value of $\Gamma_1\tau_1$ goes to zero. Therefore we expect a suppression of the Fano factor due to the cotunneling processes toward the value one in the limit $|t_i^L|^2/|t_i^R|^2 \to 0$.

Weak interactions

Up to this point, we have assumed strong interactions, namely, a very large U. If U is not large compared to the bias voltage, $U < eV_{\text{bias}}$, changing the occupation of level 2 doesn't block completely the current through level 1 since electrons can tunnel through level 1 in both cases; while level 2 is empty or occupied. Yet, we can still use the intuitive picture of a sequence of current pulses through level 1 and a random telegraph signal describing the occupation of level 2. The rate of the pulses depends on the occupation of level 2 and we consider two different rates: Γ_1 describes the tunneling rate through level 1 while level 2 is full and $\tilde{\Gamma}_1$ describes the tunneling rate through level 1 while level 2 is empty (previously $\tilde{\Gamma}_1$ was zero). Similar to Eq. (2.63), we consider the current

$$I(t) = I_{\text{shot}}(t) \times C_{\text{telegraph}}(t) + \tilde{I}_{\text{shot}}(t) \times [1 - C_{\text{telegraph}}(t)] \,, \tag{2.71}$$

where I_{shot} ($\tilde{I}_{\text{shot}}$) is a sequence of current pulses with a characteristic rate Γ_1 ($\tilde{\Gamma}_1$). The Fano factor is

$$F = 1 + \frac{2(\Gamma_1 - \tilde{\Gamma}_1)^2\tau_0^2\tau_1^2}{(\tau_0 + \tau_1)^2(\tau_1\Gamma_1 + \tau_0\tilde{\Gamma}_1)} \,, \tag{2.72}$$

where τ_1 is the average time duration in which level 2 is occupied and electrons tunnel through level 1 with an average rate Γ_1, and τ_0 is the average time duration in which level 2 is empty and electrons tunnel through level 1 with an average rate $\tilde{\Gamma}_1$.

At low temperatures, $K_BT \ll eV_{\text{bias}}$, if $\mu^R < E_1 < \mu^L$ and $\mu^R < E_1 + U < \mu^L$, the tunneling rate through level 1 barely depends on the occupation of

level 2, *i.e.* $\Gamma_1 \approx \tilde{\Gamma}_1$. We can approximate (2.72) by

$$F \approx 1 + \frac{2(\Delta\Gamma_1)^2}{\Gamma_1\Gamma_2} P_{\rm e}^2 (1 - P_{\rm e})^2 \ , \tag{2.73}$$

where $\Delta\Gamma_1 \equiv \tilde{\Gamma}_1 - \Gamma_1$ and $\Gamma_2 = (\tau_0 + \tau_1)^{-1}$ (at low temperatures this is the tunneling rate through level 2). Notice that $P_{\rm e} = \frac{\tau_0}{\tau_0+\tau_1}$, which is the probability of finding level 2 empty, is different from the probability of finding only level 1 occupied, since now the two levels can be empty simultaneously.

2.5.2 The Anderson model- tunneling rates

We now go back to the Anderson model for the two interacting levels (2.61). We want to analyze the system with rate equations, so we describe it using the four states, $|n_1, n_2\rangle$, where n_1 and n_2 label the occupation of the two levels. The system dynamics is driven by transitions between states that are caused by tunneling processes. For example: Transition from the state $|0,0\rangle$ to the state $|1,0\rangle$ happens when an electron is tunneling from the left lead or the right lead into level 1 while level 2 is empty. The term $H_{\rm t}$ in the Hamiltonian (2.61) allows tunneling processes and the rates of the transitions are derived perturbatively in $H_{\rm t}$.

Sequential tunneling rates

To the lowest order in $H_{\rm t}$ the transition rates can be calculated using Fermi's golden rule. We use the notation $\omega^{\rightarrow}_{i,j}$ for the rate of a tunneling process that changes the system's state from 'i' to 'j' by tunneling an electron from the left to the right direction (and similarly $\omega^{\leftarrow}_{i,j}$ for electron that moves from right to left). For example, $\omega^{\rightarrow}_{00,10} = \Gamma_1^L F_{FD}(E_1 - \mu^L)$ is the rate of tunneling from the left lead into level 1 while level 2 is empty, where we have defined

$$\Gamma_i^L \equiv \nu \frac{2\pi}{\hbar} |t_i^L|^2, \quad \Gamma_i^R \equiv \nu \frac{2\pi}{\hbar} |t_i^R|^2, \tag{2.74}$$

and the Fermi's function $F_{FD}(x) = (1 + e^{\beta x})^{-1}$ gives the probability for the availability of an electron for the tunneling process. In Fig. 2.5 we depict the lowest order tunneling processes, to which we refer as *sequential tunneling* processes. The rates of all the sequential tunneling processes are listed in Appendix B.

Cotunneling rates

The next leading order perturbation in H_t generates cotunneling processes with intermediate virtual states. Usually, when the tunneling coefficients are

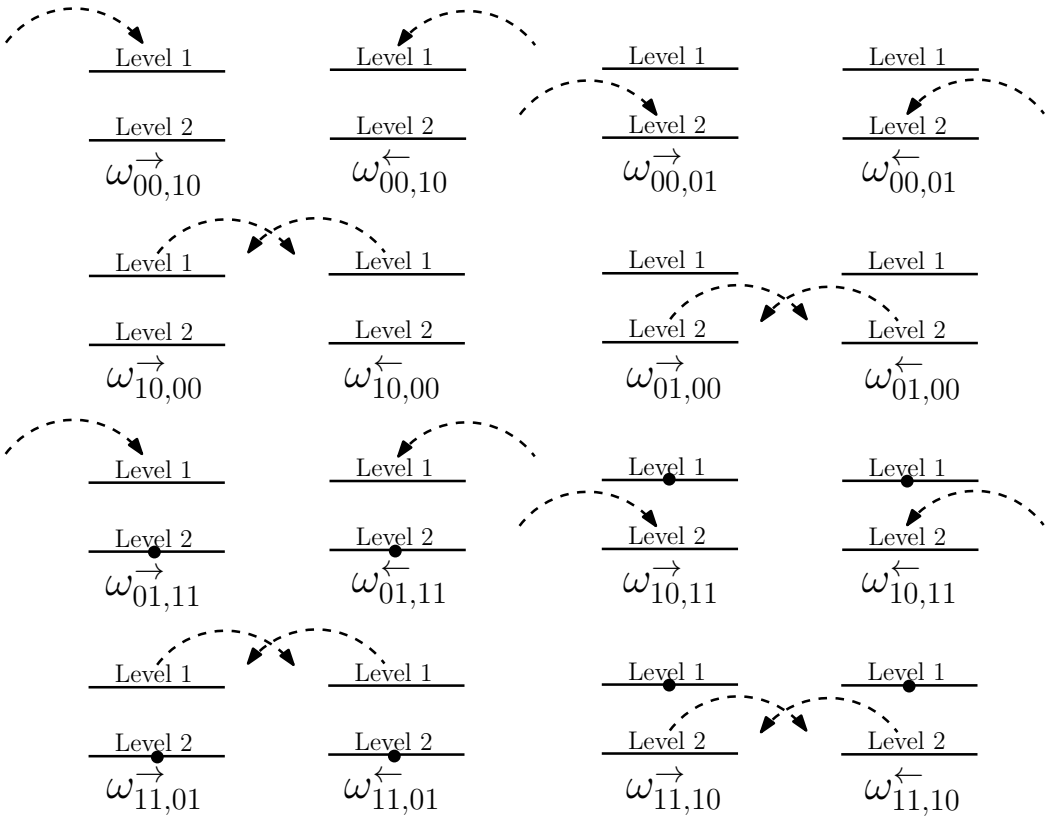

Figure 2.5: A schematic picture of the lowest order in H_{t} transitions (the sequential tunneling processes) and their notations.

small [$\gamma_{1,2}$ of Eq. (2.62) are much smaller than the temperature or bias voltage] the higher order perturbation theory is not crucial as it barely improves the approximation. However, this is not always true. Consider, for example, the limit $t_i^R \ll t_i^L$; in this case, a cotunneling process, which takes an electron out of level 2 into the left lead and takes another electron from the left lead into level 1, can become more likely to happen than a sequential tunneling from level 2 to the right lead. In other words, a second leading order perturbation in t_i^L can be more important that a first leading order perturbation in t_i^R. We discuss later the importance of the cotunneling processes in the two level model and at the moment we emphasize that this is more than a small improvement of the approximation. We discuss two types of cotunneling processes: elastic-cotunneling, namely, processes that contribute current but don't change the state of the two level system, and inelastic-cotunneling, namely, processes that change the state of the two level system (and might not contribute to the current through it).

Elastic-cotunneling rates. Figure 2.6 depicts schematically the elastic-cotunneling processes that we take into account in the transport calculations of the two level system. Each process has two possible intermediate states. For example, electron can tunnel through an empty system via level 1 or 2, thus, cotunneling processes of the form $|0,0\rangle \longrightarrow |0,0\rangle$ have two possible intermediate states: $|1,0\rangle$ and $|0,1\rangle$. The two possible paths interfere and we need to sum the amplitudes of the two possibilities rather than their probabilities. If there is a quantum number that distinguish the two levels (*e.g.*, if the system is a single spinful level with spin-dependent couplings to the leads) the two path do not interfere, and we simply sum their rates. We use the notation $\omega_{i,i}^{\rightarrow}$ ($\omega_{i,i}^{\leftarrow}$) for elastic-cotunneling processes in which an electron is tunneling to the right (left) direction (see Fig. 2.6). Elastic-cotunneling processes in which an electron tunnels back and forth between one of the levels and one of the leads don't change the state of the system and don't contribute any current, and therefore don't appear directly in the transport calculations. The total elastic-cotunneling rates are the sum of the rates of all the possible processes, namely, integration over all incoming electron's energies. For example,

$$\omega_{00,00}^{\rightarrow} = \frac{2\pi\nu^2}{\hbar}\int d\epsilon F_{FD}\left(\epsilon-\mu^L\right)\left[1-F_{FD}\left(\epsilon-\mu^R\right)\right]\left|\frac{t_1^L t_1^R}{\epsilon-E_1}+\frac{t_2^L t_2^R}{\epsilon-E_2}\right|^2 . \tag{2.75}$$

The rates of all the elastic-cotunneling processes are listed in Appendix B. Equation (2.75) is a formal expression and the actual rate, which we use in the rate equations, cannot be directly calculated from it. The reason is the

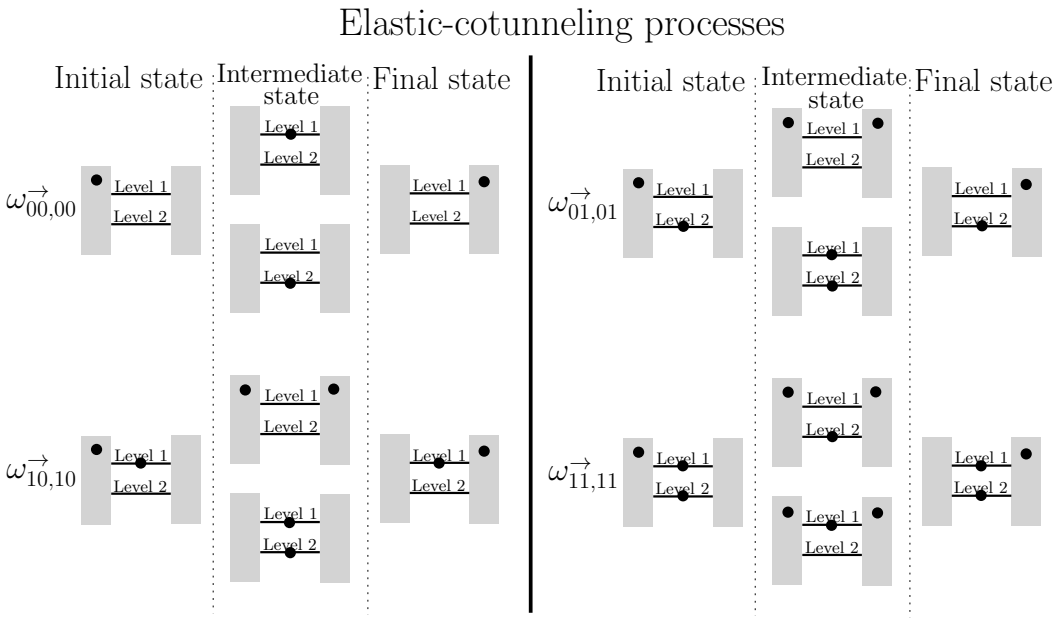

Figure 2.6: A schematic picture of the elastic cotunneling processes and their notations. Each process has two possible virtual intermediate states. The rate is the sum of the amplitudes of the two possible paths (rather than the sum of their probabilities). The processes $\omega^{\leftarrow}_{i,i}$ are the same as $\omega^{\rightarrow}_{i,i}$ after exchanging the final states with the initial states.

divergence of the integral due to the finite widths of the two levels (which we treat as two delta functions in energy). This divergence was already discussed before [120, 121], and a regularization scheme for the calculation of the cotunneling rates was developed. We summarize the regularization scheme in Appendix C. It is worth noting that one can avoid the necessity of regularization by using the diagrammatic technique that was developed in Refs. [122, 123, 124]. We find that additional correction due to levels shifts and broadening captured by this approach [125] are irrelevant in the large bias limit ($\gamma_i \ll eV_{\rm bias}$) that we consider. Calculation procedure of the average current and current noise using this technique was developed in Ref. [126] and gives the same results in the $\gamma_i \ll eV_{\rm bias}$ limit.

Inelastic-cotunneling rates. In Fig. 2.7, we depict the cotunneling processes that change the state of the two level system, *i.e.* the inelastic-cotunneling processes. To this order in H_t, the inelastic-cotunneling processes change the system's state between the following states: $|1,0\rangle \longleftrightarrow |0,1\rangle$, $|0,0\rangle \longleftrightarrow |1,1\rangle$. The latter are somewhat more complex than the other cotunneling processes as they have four possible intermediate states (see

Fig. 2.7). We use the notation $\omega^{\rightleftarrows}_{i,j}$ for the rate of processes in which the system changes its state from $|i\rangle$ to $|j\rangle$ in the following way: the electron that enters or leaves level 1 tunnels to the right direction, while the electron that enters or leaves level 2 tunnels to the left, and similarly we define $\omega^{\leftrightarrows}_{i,j}, \omega^{\rightrightarrows}_{i,j}, \omega^{\leftleftarrows}_{i,j}$. We use the notation $\omega^{\leftrightarrow}_{00,11}$, $\omega^{\leftrightarrow}_{11,00}$ for processes in which the two electrons enter or leave the two levels by tunneling one to the right and the other to the left. The rates of all the inelastic-cotunneling processes are listed in Appendix B.

Beyond the cotunneling approximation. The rate equations based calculation is valid as long as the tunneling coefficients are small enough as we insert the tunneling processes only up to second order in the perturbation H_t. Practically, it means that either $\gamma_i/eV_{\rm bias}$ or γ_i/K_BT need to be small numbers. Yet, the next leading order in H_t generates logarithmic contributions that diverge at low temperatures and bias voltages [5]. Hence, for bias voltages smaller than a characteristic energy scale, the Kondo temperature, the perturbative approach fails. The Kondo temperature in our case is $T_K \sim \sqrt{\gamma_1 U} e^{-U/2\gamma_1}$ and in all cases in this work we consider much larger bias voltages. We also want to note that small corrections due to the renormalization of the energy levels and broadening play very minor role in the large bias case that we consider. They at most slightly modify the quantitative results with no important effect on the qualitative behavior.

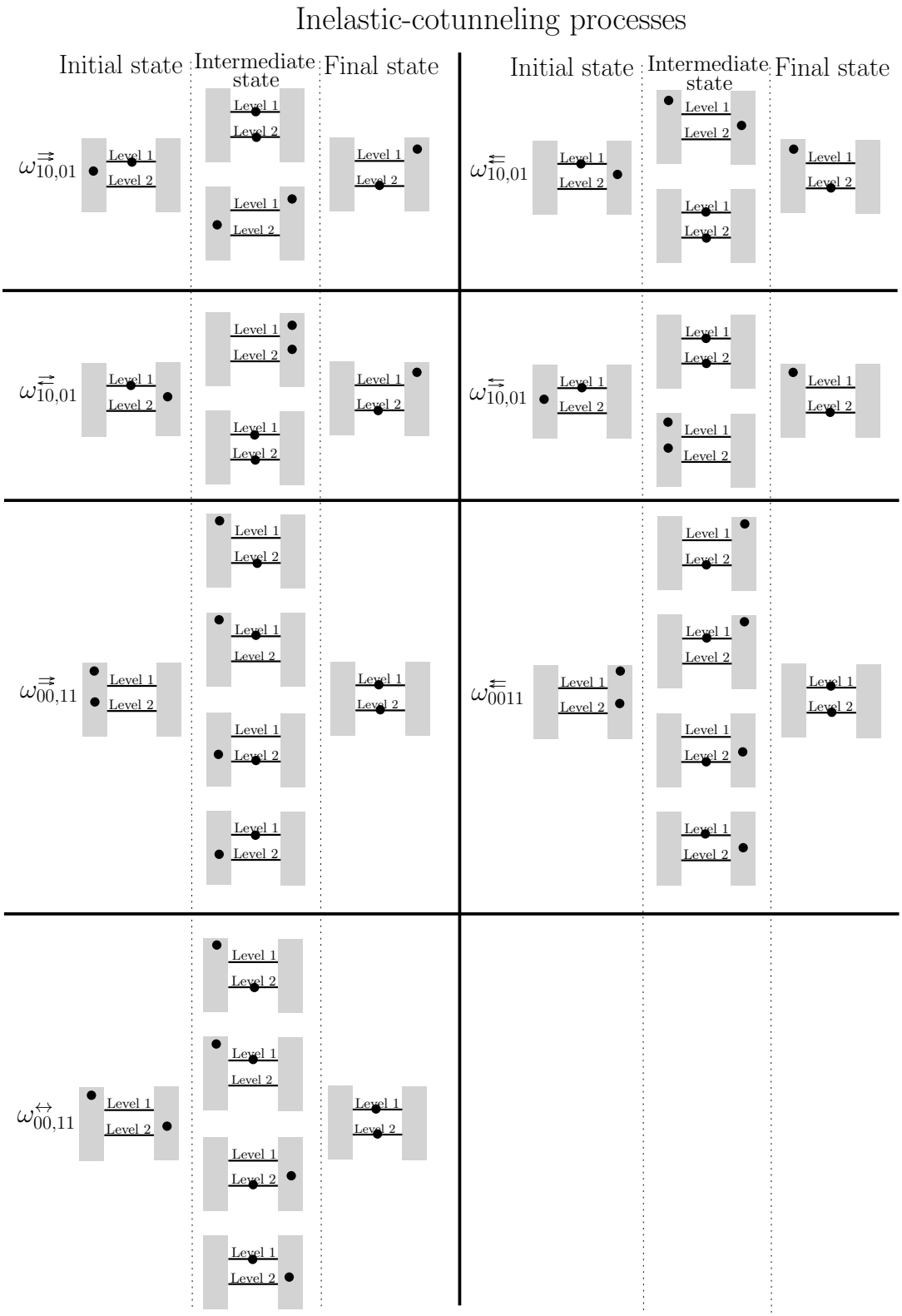

Figure 2.7: A schematic picture of the inelastic cotunneling processes and their notations. The processes $\omega_{01,10}$ are the same as $\omega_{10,01}$ after exchanging the two levels. The processes $\omega_{11,00}$ are the same as $\omega_{00,11}$ after exchanging the final states with the initial states.

Chapter 3

Results

In this chapter we present the main results for three projects: First, we present the analysis of the $SU(2)$ and $SU(3)$ systems that we suggest. Second, we present our results about the coherence properties of transmission through Kondo impurities. Last, we present our analysis of the shot noise and Fano factor of asymmetric two-level systems.

3.1 Realization of $SU(2)$ and $SU(3)$ Kondo

We first look at the UV limit (high temperature or bias voltage) and later discuss the Kondo physics at the IR. Special attention is given to the measurement of each pseudo-spin/flavor independently. In order to measure transport properties in one flavor we split an edge into two different edges which are coupled to the same dot, as drawn in Fig. 2.1(d). In equilibrium, one linear combination of the two edge states is decoupled from the upper dot and the orthogonal linear combination plays the role of a single edge state that is coupled to the upper dot. Transport is measured by applying a voltage difference between the two edges allowing measurements of average current $\langle I \rangle$, zero frequency shot noise S_{shot}, and the Fano factor $F = \frac{S_{\text{shot}}}{2e\langle I \rangle}$ of each flavor separately. Measuring correlations between two flavors can be carried out by splitting two edges as drawn in Fig. 2.1(b), where we can apply different bias voltages on different flavors.

3.1.1 UV description

We assume a constant density of states ν in the edges and a very weak coupling between the dots and the edge states ($\nu|W|^2 \ll T$, or $\nu|W|^2 \ll V_{\text{bias}}$), and use the rate equations method [117] to calculate the conductivity and the current noise.

Figs. 3.1(a) and 3.1(c) plot the Coulomb peaks structures of the $SU(2)$ and $SU(3)$ systems. Contrary to naive expectations, at finite temperature the outer peaks are not centered around ϵ_F, $\epsilon_F - U$, in the N=2 case, or around ϵ_F, $\epsilon_F - 2U$ in the N=3 case. Due to the asymmetry between occupied and empty states near the outer peaks, the peaks are shifted by $T\ln(N)/2$. We discuss this point in Appendix D.

The Fano factor of a single spinful quantum dot which is attached to two spinful leads is 5/9 at the Coulomb peaks. In the system of Fig. 2.1(b) it corresponds to applying the same bias voltage on the two pseudo spins and measuring the total current $(I_\uparrow + I_\downarrow)$. However, in the systems of Figs. 2.1(b) and 2.1(d), we can apply distinct bias voltages and measure distinct currents for the different pseudo spins or flavors. The Fano factors that we obtain are:

$$F_2 = 7/9 \ , \quad F_3^o = 7/8 \ , \quad F_3^c = 11/18 \ ,$$

where F_2 is the Fano factor near the N=2 Coulomb peaks, and F_3^o (F_3^c) is the Fano factor near a outer (central) peak of the N=3 case. The Fano factor is related to the effective charge of the current pulses that cross the dots, it is therefore counter-intuitive to find different Fano factors in the total and single flavor currents. The difference is a result of the zero frequency cross-correlations between the different flavors. Using rate equations we find in the $N = 2$ case:

$$\begin{aligned} S_{\uparrow\downarrow}(0) &\equiv \lim_{\omega\to 0}\int dt e^{i\omega t} 2\left[\langle I_\uparrow(t) I_\downarrow(0)\rangle - \langle I_\uparrow\rangle \langle I_\downarrow\rangle\right] \\ &= -\frac{2\pi\nu|W|^2e^2}{\hbar}\frac{4}{27}\tanh\frac{eV_\uparrow}{4T}\tanh\frac{eV_\downarrow}{4T} \ , \end{aligned} \tag{3.1}$$

where $V_{\uparrow,\downarrow}$ are the pseudo-spin bias voltages. Similarly, in the N=3 case, for $\alpha \neq \beta$:

$$S^{(i)}_{\alpha\beta}(0) = -\frac{2\pi\nu|W|^2e^2}{\hbar}R^{(i)}\tanh\frac{eV_\alpha}{4T}\tanh\frac{eV_\beta}{4T} \ , \tag{3.2}$$

where the index $i = o, c$ labels a central (outer) peak, and $R^o = 1/16$, $R^c = 1/27$.

3.1.2 The IR Kondo fixed point

In Figs. 3.1(b) and 3.1(d) we depict the zero temperature conductance of a single pseudo spin/flavor in the $N = 2, 3$ cases. The conductance was calculated using self consistent Hartree approximation. We average over the solutions of the self consistent equations for the average occupations of the levels [127] $n_\alpha = \frac{1}{2} - \frac{1}{\pi}\tan^{-1}\frac{E_d + U(\sum_{\beta\neq\alpha} n_\beta)}{\gamma}$, where γ represents the identical width of the levels. The Friedel sum rule and spin/flavor symmetry are then used to determine the phase shift $\delta_\alpha = \delta = \pi\sum_{\alpha=1}^N n_\alpha/N$ and the conductance $\sin^2(\delta)$. Let us focus on the N=3 case [Fig. 3.1(d)]. When the gate voltage is tuned to have only a single electron or a single hole in the three dots, the conductance is enhanced due to the flavor-interaction and the Coulomb valleys disappear. An unusual plateau is created instead of the

three peaks of the UV limit. As long as the dots are occupied by a single electron or a single hole we find the conductivity

$$G_{SU(3)-\text{Kondo}} = \frac{3}{4}\frac{e^2}{h} \,. \tag{3.3}$$

At the exact particle hole symmetric point, $\epsilon_g = \epsilon_F - U$, we find a full e^2/h conductivity and a sharp peak is formed, indicating the larger symmetry.

3.1.3 Edge states cross-correlations in the Kondo limit

We now discuss the finite frequency flavors correlations in the IR limit. The cross-flavors correlations is a new observable made available by our realization, whereas it is not experimentally accessible in most existing realizations of Kondo effect. This cross-flavors correlations is of order ω/T_K relative to the familiar large thermal noise in the total flavor. For $\omega = 100$MHz and $T_K \sim 1$K, $\omega/T_k \sim 1\%$ which, being the only contribution in the cross channel, can be readily observed.

Formally, we define $J_i(x) =: \psi_i^\dagger(x)\psi_i(x):$ and

$$J_c(x) = \sum_{i=1}^{N} J_i(x), \quad \vec{J}_{(N)}(x) = \sum_{ij=1}^{N} :\psi_i^\dagger(x)\vec{T}_{ij}^{(N)}\psi_j(x): \,,$$

where $N = 2, 3$, $\vec{T}^{(2)}$ are the three Pauli matrices, and $\vec{T}^{(3)}$ are the eight Gell-Mann matrices. The effective Hamiltonians of the two systems are [51, 8, 9]:

$$H_2 = \frac{1}{8\pi}\int dx \left[J_c^2(x) + \frac{1}{3}\vec{J}_{(2)}^2(x) + \lambda_2 \vec{J}_{(2)}^2(x)\delta(x)\right], \tag{3.4}$$

$$H_3 = \frac{1}{8\pi}\int dx \left[J_c^2(x) + \frac{3}{8}\vec{J}_{(3)}^2(x) + \lambda_3 \vec{J}_{(3)}^2(x)\delta(x)\right], \tag{3.5}$$

with $\lambda_N \sim 1/T_k$. We calculate the noise functions

$$S_{ij}(\omega; x, x') = \int e^{i\omega t} \left\langle \{J_i(x,t), J_j(x',t')\} \right\rangle, \tag{3.6}$$

and we find that they receive $\mathcal{O}(\omega/T_k)$ correction ($i \neq j$):

$$\begin{aligned} S_{ii}^{(N)}(\omega; x, x') &= e^{-i\omega(x-x')}\frac{\omega}{\pi}\coth\frac{\beta\omega}{2}\left(1 - i\widetilde{\lambda}_N \frac{\omega}{\pi}F_{xx'}\right), \\ S_{ij}^{(N)}(\omega; x, x') &= \frac{i\widetilde{\lambda}_N}{N-1}e^{-i\omega(x-x')}\left(\frac{\omega}{\pi}\right)^2 \coth\frac{\beta\omega}{2}F_{xx'} \,, \end{aligned} \tag{3.7}$$

with $F_{xx'} = \theta(x) - \theta(x')$, $N = 2, 3$, $\widetilde{\lambda}_2 = 6\lambda_2$ and $\widetilde{\lambda}_3 = \frac{32}{3}\lambda_3$. Due to $F_{xx'}$, S_{ij} receive correction only if the two currents are measured at two different sides of the dots.

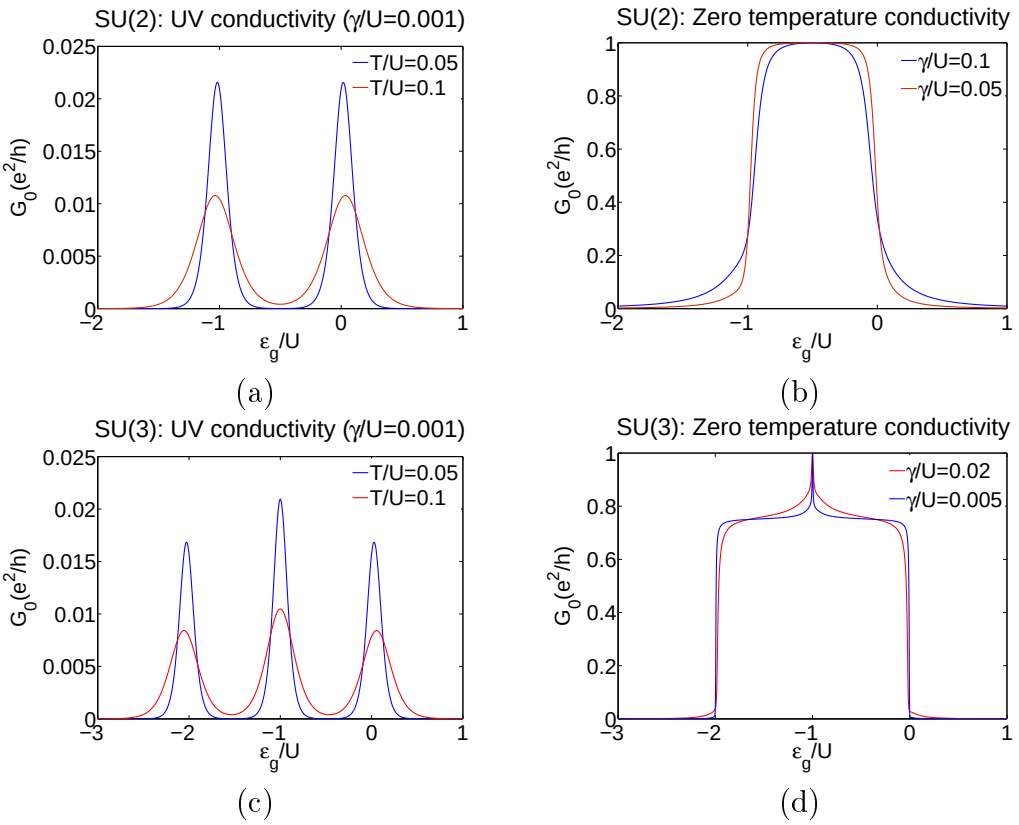

Figure 3.1: *SU*(2) *system*: **(a)** The conductivity of a single pseudo spin at high temperature ($T \gg \gamma$) for two different T/U ratios. We choose the Fermi energies of the leads to be zero. The Coulomb peaks are not exactly centered around 0, $-U$ due to the asymmetry between empty/occupied states near the peaks. **(b)** Self consistent Hartree solution of the zero temperature conductivity of a single pseudo spin for two different γ/U ratios. *SU*(3) *system*: **(c)** The conductivity of a single flavor at high temperature ($T \gg \gamma$) for two different T/U ratios choosing the Fermi energy to be zero. The outer peaks are not exactly centered around 0, $-2U$ due to the asymmetry between empty/occupied states near the peaks. **(d)** Self consistent Hartree solution of the zero temperature conductivity of a single flavor for two different γ/U ratios.

3.2 Transmission properties of Kondo impurities

In this section, we present the results of the transmission phase φ_t, and normalized visibility η of Kondo impurities [both were defined in Eq. (1.9)]. We focus on the 1CK impurity and the 2CK impurity, since there are concrete realizations of such impurities with quantum dots, and only quote the results for the general k-channel Kondo. In the 2CK case, we consider both its non-Fermi liquid fixed point, and its Fermi liquid fixed points, reached by turning on a finite magnetic field or a finite channel anisotropy.

3.2.1 Single channel Kondo

In the 1CK case, the $\mathcal{T}_{s,\psi\psi}$ matrix element, up to second order in $1/T_K$, is [40]

$$\mathcal{T}_{s,\psi\psi}(\epsilon) = i\left[2 + i\frac{2\epsilon}{T_K} - 3\left(\frac{\epsilon}{T_K}\right)^2 - \left(\frac{\pi T}{T_K}\right)^2\right] . \tag{3.8}$$

Since $\int \epsilon d\epsilon \left(-\frac{\partial f}{\partial \epsilon}\right) = 0$, then $\int d\epsilon \left(-\frac{\partial f}{\partial \epsilon}\right) \mathcal{T}_{s,\psi\psi}(\epsilon)$ is purely imaginary, therefore the transmission phase is

$$\varphi_t = \frac{\pi}{2} + \mathcal{O}\left(T/T_K\right)^3 . \tag{3.9}$$

The transmission phase matches the scattering phase shift of the 1CK (up to T/T_K corrections) when potential scattering is neglected. The normalized visibility

$$\eta = 1 - \left(\frac{\pi T}{T_K}\right)^2 + \mathcal{O}\left(T/T_K\right)^3 . \tag{3.10}$$

Two mechanisms reduce the nonzero-temperature normalized visibility, elastic scattering with energy-dependent phase shift, $\delta_\psi(\epsilon) = \pi/2 + \epsilon/T_K$, and the appearance of inelastic scattering. Both are allowed by the dominant irrelevant operator near the 1CK fixed point [40].

Finite magnetic field

At zero magnetic field, the $\mathcal{T}$-matrix is independent of spin (*i.e.*, $\mathcal{T}_{\uparrow,\psi\psi} = \mathcal{T}_{\downarrow,\psi\psi}$), because of the symmetry between the two spins. Therefore, the transmission phase and the normalized visibility of the spin-summed conductance, are the same as the transmission phase and the normalized visibility of each spin separately. However, when a magnetic field is applied, the $\mathcal{T}$-matrix

becomes spin-dependent. Hence, the transmission phase and the normalized visibility of each spin are, in general, different from each other and from the measured (spin-summed) quantities.

Consider, for example, the zero temperature case, where, as long as $B \ll T_K$, the system is described by a Fermi liquid theory, so [116] $\mathcal{T}_{s,\psi\psi} = i(1 - e^{2i\delta_{\psi s}})$. As we discussed in Sec. 2.3, the particle hole symmetry $\psi_{ks} \to \psi^\dagger_{-k,-s}$, enforces $\delta_{\psi\uparrow}(\epsilon) = -\delta_{\psi\downarrow}(-\epsilon)$. In this case,

$$\delta_{\psi s}(0) = \left(\frac{\pi}{2} - \alpha_s \frac{B}{T_K}\right) , \tag{3.11}$$

where $\alpha_\uparrow = 1$, and $\alpha_\downarrow = -1$. Notice that since $\delta_{\psi s}$ is *half* of the phase of $\mathcal{S}_{\psi\psi}$, it is defined up to $\pm\pi$. As we measure the conductance of the two spins together, the total transmission phase $\varphi_t = \pi/2$ independent of B [see Eq. (2.50)], and the normalized visibility is less than one, $\eta = \sin^2(\frac{\pi}{2} - \frac{B}{T_K}) \approx 1 - (\frac{B}{T_K})^2$ [see Eq. (2.51)], even though all the scattering processes are single-particle to single-particle scattering.

A possible way to overcome this $\pi/2$ phase-lock of the transmission phase, is to measure the conductance of a distinct spin [49]. The distinct spin transmission phase at zero temperature would simply be $\delta_{\psi s}$, and there is a $\frac{2B}{T_K}$ difference between the spin up and spin down phases. The normalized visibility of each distinct spin would be $\eta = 1$, as we expect for a Fermi liquid fixed point.

3.2.2 Two channel Kondo

In the 2CK case, two disconnected channels interact with the impurity. We consider a case where we can measure the transport in one of the channels, and there is no charge transfer between the different channels (this was the case, for example, in the experimental setup of Ref. [39]). Notice that in this case, the index i in the states $|n_L, n_R, i\rangle$ [see, for example, equation (2.7)], labels states with different particle-hole excitations in the leads and also states with different excitations in the other channel.

If the two channels are equally coupled to the impurity, then the system flows to a non-Fermi liquid fixed point. In this case, up to first order in $1/\sqrt{T_K}$, the matrix element $\mathcal{T}_{s,\psi\psi}$ is [40]

$$\mathcal{T}_{s,\psi\psi}(\epsilon) = i\left(1 - 3\lambda\sqrt{\pi T} I(\epsilon)\right) , \tag{3.12}$$

where

$$I(\epsilon) = \int_0^1 du \left(u^{-\frac{i\epsilon}{2\pi T}} F_{21}(u) \sqrt{\frac{1-u}{u}} - \frac{4}{\pi} \frac{1}{\sqrt{u}(1-u)^{\frac{3}{2}}} \right) . \tag{3.13}$$

$\lambda \sim 1/\sqrt{T_K}$ is the strength of the leading irrelevant operator near the 2CK fixed point, and $F_{21}(u)$ is the hypergeometric function $F_{21}(u) \equiv \frac{1}{2\pi}\int_o^{2\pi} \frac{d\theta}{\left(u+1-2\sqrt{u}\cos\theta\right)^{\frac{3}{2}}}$.

The thermally averaged value of $\mathcal{T}_{s,\psi\psi}$ is

$$\int d\epsilon \left(-\frac{\partial f}{\partial \epsilon}\right) \mathcal{T}_{s,\psi\psi}(\epsilon) = i\left(1 + 4\lambda\sqrt{\pi T}\right). \tag{3.14}$$

Since $\int d\epsilon \left(-\frac{\partial f}{\partial \epsilon}\right) \mathcal{T}_{s,\psi\psi}(\epsilon)$ is purely imaginary, the transmission phase is

$$\varphi_t = \frac{\pi}{2} + \mathcal{O}\left(T/T_K\right) \ . \tag{3.15}$$

The normalized visibility is

$$\eta = \frac{1}{2}\left(1 + 4\lambda\sqrt{\pi T}\right) + \mathcal{O}\left(T/T_K\right) \ . \tag{3.16}$$

These results are not surprising, since at zero temperature, there are no single ψ-particle to single ψ-particle scattering processes at the non-Fermi liquid fixed point. Thus, $\mathcal{S}_{\psi\psi} = 0$ for both spins, and hence $\varphi_t = \pi/2$ [see Eq. (2.44)]. Since in this case $\mathcal{T}_{\psi\psi} = i$, we find a normalized visibility $\eta = 1/2$, indicating that half of the conductance is carried by elastic single-particle scattering [55, 56].

The sign of λ depends on the initial strength of the Kondo coupling. λ is positive for strong coupling, and negative for weak coupling [40]. The normalized visibility can, in principle, be *enhanced* by nonzero temperature, unlike the usual case where the temperature reduces interference effects. The enhancement of the normalized visibility is due to the fact that the nonzero temperature allows single ψ-particles scattering off the impurity ($s_{\psi\psi} \neq 0$).

Finite magnetic field and finite channel anisotropy

The non-Fermi liquid fixed point is unstable, since finite magnetic field and finite channel anisotropy turn on relevant perturbations near the non-Fermi liquid fixed point [128]. In the presence of such perturbations, the system flows under renormalization group to a Fermi liquid fixed point, at zero temperature, rather than the non-Fermi liquid one. In the case of channel anisotropy, the channel which is coupled more strongly to the dot flows to the 1CK-like fixed point, and the other channel flows to a free-electrons-like fixed point. Under a finite magnetic field, the system flows to a Fermi liquid fixed point which is different from the 1CK fixed point.

In this subsection we study the 2CK case under these two possible perturbations. At zero temperature, $\mathcal{T}_{s,\psi\psi}$ is given by [129, 130]

$$\mathcal{T}_{s,\psi\psi}(\epsilon) = i\left[1 - \frac{-(\nu\Delta\sqrt{T_K}) + i\alpha_s(\frac{c_B B_z}{\sqrt{T_K}})}{\sqrt{(\nu\Delta\sqrt{T_K})^2 + (\frac{c_B B_z}{\sqrt{T_K}})^2}}\mathcal{G}(\epsilon/T^*)\right], \tag{3.17}$$

where Δ is the difference between the coupling strengths of the two channels, and c_B is a dimensionless number of order one. $T^* \sim T_K(\nu\Delta)^2 + (c_B B)^2/T_K$ is an energy scale that characterizes the flow away from the non-Fermi liquid fixed point. $\mathcal{G}(x) = \frac{2}{\pi}K(ix)$, where $K(x)$ is the complete elliptic integral of the first kind. $\alpha_\uparrow = 1$, $\alpha_\downarrow = -1$, and we have assumed $\vec{B} = B_z$. At zero temperature, the averaged value of $\mathcal{T}_{\psi\psi}$ is

$$\frac{1}{2}\sum_s \mathcal{T}_{s,\psi\psi} = i\left[1 - \frac{-(\nu\Delta\sqrt{T_K})}{\sqrt{(\nu\Delta\sqrt{T_K})^2 + (\frac{c_B B_z}{\sqrt{T_K}})^2}}\right] . \tag{3.18}$$

Thus, for $\Delta = 0$, $\langle\mathcal{T}_{\psi\psi}\rangle = i$. Hence, the transmission phase is $\varphi_t = \pi/2$ and the normalized visibility is $\eta = 1/2$ even for $B \neq 0$, where all the electrons are elastically scattered with a phase $\delta_{\psi,s} = \alpha_s\pi/4$. A spin-resolved measurement, however, would lead to $\varphi_t = \alpha_s\pi/4$ and $\eta = 1$, since for $\Delta = 0$

$$\int d\epsilon \left(-\frac{\partial f}{\partial\epsilon}\right)\mathcal{T}_{s,\psi\psi} = i\left(1 - i\alpha_s\right) . \tag{3.19}$$

In Table 3.1, we summarize the results for the zero temperature normalized visibility and transmission phase for the various relevant perturbations, where we define

$$\cos(\gamma) \equiv \frac{\nu|\Delta|\sqrt{T_K}}{\sqrt{(\nu\Delta\sqrt{T_K})^2 + (\frac{c_B B_z}{\sqrt{T_K}})^2}} , \tag{3.20}$$

$$\sin(\gamma) \equiv \frac{c_B B_z/\sqrt{T_K}}{\sqrt{(\nu\Delta\sqrt{T_K})^2 + (\frac{c_B B_z}{\sqrt{T_K}})^2}} . \tag{3.21}$$

Channel anisotropy. Recall that we are measuring the conductance through one of the channels. At zero magnetic field, if $\Delta > 0$, the ψ-particles form together with the impurity a singlet, while the electrons in the other channel are simply free. Thus, η and φ_t are the same as in the 1CK case. On the other hand, if $\Delta < 0$, the electrons in the other channel form a singlet with the impurity, and the ψ-particles are free. Therefore at zero temperature

the conductance through the impurity, the dot, is zero. In this case there is no interference, and hence, $\eta = 0$ and φ_t is not defined. Although this is a Fermi liquid, $\eta < 1$ near this fixed point since most of the charge is reflected. To explain it we now discuss the nonzero-temperature case.

At nonzero temperature, the $\Delta < 0$ case should be treated more delicately. Up to second order in $1/T^*$, $\mathcal{T}_{s,\psi\psi}$ is [130]

$$\mathcal{T}_{s,\psi\psi}(\epsilon) = \frac{\epsilon}{4T^*} + i\frac{9}{64}\left(\frac{\epsilon}{T^*}\right)^2 + i\frac{7}{64}\left(\frac{\pi T}{T^*}\right)^2 . \tag{3.22}$$

Most of the charge is reflected and only a small amount of charge can be transmitted, either elastically or inelastically. This is similar to the 1CK case, where at nonzero temperature most of the charge is transmitted, and only a small part is reflected either elastically or inelastically. Up to second order in $1/T^*$, the portion of elastic transmission through the impurity out of all scattering events of incoming particles with energy ϵ is

$$\frac{|\mathcal{T}_{s,\psi\psi}(\epsilon)|^2}{2Im\left\{\mathcal{T}_{s,\psi\psi}(\epsilon)\right\}} = \frac{2/9}{1+\frac{7}{9}\left(\frac{\pi T}{\epsilon}\right)^2} . \tag{3.23}$$

In the $\epsilon \gg T$ limit, 2/9 of the charge is transmitted elastically. The phase that the particles accumulate in this limit is proportional to ϵ, $\varphi_t(\epsilon) \approx \frac{9\epsilon}{16T^*}$. The thermal averaging, however, has a crucial effect in this limit. The thermally-averaged $\mathcal{T}$-matrix ,$\langle\mathcal{T}_{\psi\psi}\rangle = i\frac{5}{32}\left(\frac{\pi T}{T^*}\right)^2$, is purely imaginary and proportional to T^2, and therefore

$$\eta(T) = 5\left(\frac{\pi T}{8T^*}\right)^2 , \qquad \varphi_t = \pi/2 . \tag{3.24}$$

Finite magnetic field. At finite magnetic field, we see that in order to access the phase shift of the ψ-particles, $\delta_{\psi s}$, one needs to measure each spin separately. Notice that at $\Delta \to 0$ ($\gamma \to \pi/2$), the spin-averaged normalized visibility and the transmission phase are the same as in the non-Fermi liquid fixed point ($B = 0, \Delta = 0$): $\eta = 1/2$ and $\varphi_t = \pi/2$. In order to distinguish the Fermi-liquid fixed points from the non-Fermi liquid fixed point, one can measure the temperature dependence of the conductance through the impurity. Non trivial $\sqrt{T}$-dependence indicates a non-Fermi liquid fixed point. Alternatively, as we already mentioned, spin dependent measurements of η_s and φ_{ts} give different results for the Fermi liquid and the non-Fermi liquid fixed points.

Table 3.1: Zero temperature normalized visibility and transmission phase for various relevant perturbations.

	η_s	φ_{ts}	η	φ_t
$B=0,\Delta=0$	$1/2$	$\pi/2$	$1/2$	$\pi/2$
$B=0,\Delta>0$	1	$\pi/2$	1	$\pi/2$
$B=0,\Delta<0$	0	-	0	-
$B\neq 0,\Delta=0$	1	$\alpha_s\pi/4$	$1/2$	$\pi/2$
$B\neq 0,\Delta>0$	1	$\alpha_s(\pi/2-\gamma/2)$	$\cos^2(\gamma/2)$	$\pi/2$
$B\neq 0,\Delta<0$	1	$\alpha_s\gamma/2$	$\sin^2(\gamma/2)$	$\pi/2$

Generalization to k-channels

We have focused on the 1CK and the 2CK impurities, since there are concrete realizations of these impurities with quantum dots. Yet, it is worthwhile to study the more general k-channel Kondo case. In the Fermi liquid fixed points at zero temperature, all the ψ-particles are scattered into ψ-particles, namely, $|\mathcal{S}_{\psi\psi}|=1$. In the non-Fermi liquid 2CK fixed point, none of the ψ-particles are scattered into ψ-particles, namely, $|\mathcal{S}_{\psi\psi}|=0$. In the more general k-channel Kondo case, however, where $\mathrm{k}>1$ channels screen the impurity, a finite part of the ψ-particles are elastically scattered off the impurity. At zero temperature, the single ψ-particle element of the $\mathcal{S}$-matrix is [40]

$$S_{\psi\psi}^{\mathrm{kCK}}=\frac{\cos\left(\frac{2\pi}{2+\mathrm{k}}\right)}{\cos\left(\frac{\pi}{2+\mathrm{k}}\right)}\ . \tag{3.25}$$

The conductance, up to $\mathcal{O}\left(T/T_K\right)^{\frac{4}{2+\mathrm{k}}}$, is [40]

$$G_{\mathrm{d}}=\frac{e^2}{h}\sin^2(2\alpha)\left[1-\frac{\cos\left(\frac{2\pi}{2+\mathrm{k}}\right)}{\cos\left(\frac{\pi}{2+\mathrm{k}}\right)}+c_K\left(\frac{T}{T_K}\right)^{\frac{2}{2+\mathrm{k}}}\right]\ , \tag{3.26}$$

where the factor c_K can be calculated numerically [40]. The normalized visibility is

$$\eta=\frac{1}{2}\left[1-\frac{\cos\left(\frac{2\pi}{2+\mathrm{k}}\right)}{\cos\left(\frac{\pi}{2+\mathrm{k}}\right)}+c_K\left(\frac{T}{T_K}\right)^{\frac{2}{2+\mathrm{k}}}\right]+\mathcal{O}\left(T/T_K\right)^{\frac{4}{2+\mathrm{k}}}\ , \tag{3.27}$$

and since $\mathcal{S}_{\psi\psi}^{\mathrm{kCK}}$ is real, the transmission phase is

$$\varphi_t=\frac{\pi}{2}+\mathcal{O}\left(T/T_K\right)^{\frac{4}{2+\mathrm{k}}}\ . \tag{3.28}$$

3.2.3 External dephasing

In Sec. 2.2 of Chapter 2, we defined the normalized visibility η, which is the amplitude of the AB oscillations, normalized in a certain way. In Sec. 2.3, we showed that η has a physical meaning, and that it is related to the proportion of the total conductance carried by single-particle scattering. In this subsection we want to comment about the feasibility of η-measurements.

So far, we have discussed three mechanisms that reduce the normalized visibility: the possibility of non-coherent charge transfer through the dot into many-body states, thermal averaging over a transmission with energy-dependent phase, and averaging over spin-dependent transmission phase. AB oscillations in a real-life experimental setup can also be suppressed by other mechanisms that are not related to the physical properties of the examined impurity. A real experimental two-path setup is usually coupled to a complicated environment. For example, in an open AB ring setup the shapes of the two paths, the quantum dot(s), the tunnel barriers, and many other components of the setup are all defined by applying voltages to nearby nano-patterned electrodes. Therefore, each component of the system is coupled to an environment (metal electrodes, semiconducting leads) with associated noise and degrees of freedom.

An electron that propagates through the two paths leaves a trace in the environment; equivalently, a propagating electron that interacts with the environment, accumulates a *random* phase [131], φ. As a result, the amplitude of the AB oscillations is multiplied by the averaged value $\langle e^{i\varphi}\rangle$. The normalized visibility in the presence of the environment is therefore [60]

$$\sqrt{\eta} = \langle e^{i\varphi}\rangle \frac{\left|\int d\epsilon \left(-\frac{\partial f}{\partial \epsilon}\right) \mathcal{T}_{\psi\psi}\right|}{\sqrt{\int d\epsilon \left(-\frac{\partial f}{\partial \epsilon}\right) 2Im\left\{\mathcal{T}_{\psi\psi}\right\}}} \approx \left[1 - \frac{1}{2}\langle \delta\varphi^2\rangle\right] \frac{\left|\int d\epsilon \left(-\frac{\partial f}{\partial \epsilon}\right) \mathcal{T}_{\psi\psi}\right|}{\sqrt{\int d\epsilon \left(-\frac{\partial f}{\partial \epsilon}\right) 2Im\left\{\mathcal{T}_{\psi\psi}\right\}}} \,. \tag{3.29}$$

The details of the coupling to the environment depend on the details of a specific experimental setup. Yet, we can roughly estimate the external dephasing by assuming that the phase-randomness originates mostly from the thermal fluctuations of the environment. At nonzero temperature T, the electrodes in the environment suffer from Nyquist noise, and we can estimate $\langle \delta\varphi^2\rangle \sim T$. Hence, dephasing by the environment can reduce the normalized visibility linearly in the temperature. In the Fermi liquid fixed points, η has T^2 corrections without external dephasing. This means that at low temperatures the dominant suppression of η would be due to external dephasing. In the non-Fermi liquid fixed point of the 2CK, η has a $\sqrt{T}$ dependence in the absence of external dephasing. Thus, at low temperatures the change in η

(enhancement for $\lambda > 0$ and reduction for $\lambda < 0$), is expected to be stronger than its suppression due to external dephasing. The relation between the system and the environment is outside the scope of this work. In particular, we do not get into specific models for the environment. We want to note that there are models that treat rigorously the effect of a specific environment on the interference in AB rings (for example, a quantum-point-contact that is coupled to an embedded quantum dot [132, 133]; or a fluctuating magnetic flux [134]).

In the 2CK non-Fermi liquid case, a noisy environment can, in principle, turn on relevant operators. Thus, a noisy environment with strong effect on the system would make the observation of the non-Fermi liquid behavior difficult. Hence, if a non-Fermi liquid behavior is indeed observed in an experimental system, it indicates a relatively weak external dephasing.

3.3 Enhanced shot noise in asymmetric interacting two-level systems

In this section we present the main results for the shot noise and the current through interacting two-level system that is modeled by Eq. (2.61). The calculations are based on the rate equations method which we presented in Chapter 2 [Sec. 2.4]. The results are explained using the approximated intuitive approach of signal analysis that we developed in Sec. 2.5.1.

3.3.1 Strong interactions

Current

In Fig. 3.2(a), we plot the symmetric current ($\Gamma_i^L = \Gamma_i^R$) through the two level system as a function of E_1 at large U ($U > eV_{\text{bias}}$) with the following parameters ($\Gamma \equiv \Gamma_1^R + \Gamma_1^L + \Gamma_2^R + \Gamma_2^L$): $K_BT = \hbar\Gamma$, $eV_{\text{bias}} = 10\hbar\Gamma$, $E_1 - E_2 = \hbar\Gamma$, $U = 100\hbar\Gamma$ and $\Gamma_1^{R,L} = 10\Gamma_2^{R,L}$. Two Coulomb peaks with a width $\sim eV_{\text{bias}}$ appear in the current: at $E_1 \approx 0$ (the right peak), where the two levels are between the leads' chemical potentials, μ^L and μ^R (similar to the schematic picture in Fig. 2.3), and at $E_1 \approx -U$, where one of the levels is occupied so the other level is effectively shifted and placed between μ^L and μ^R. The right peak is a bit lower than the left peak because of the small energy difference between the two levels ($E_1 > E_2$). At finite temperature, this small energy difference makes the probability of finding level 2 occupied a bit larger than the probability of finding level 1 occupied. While near the right peak the

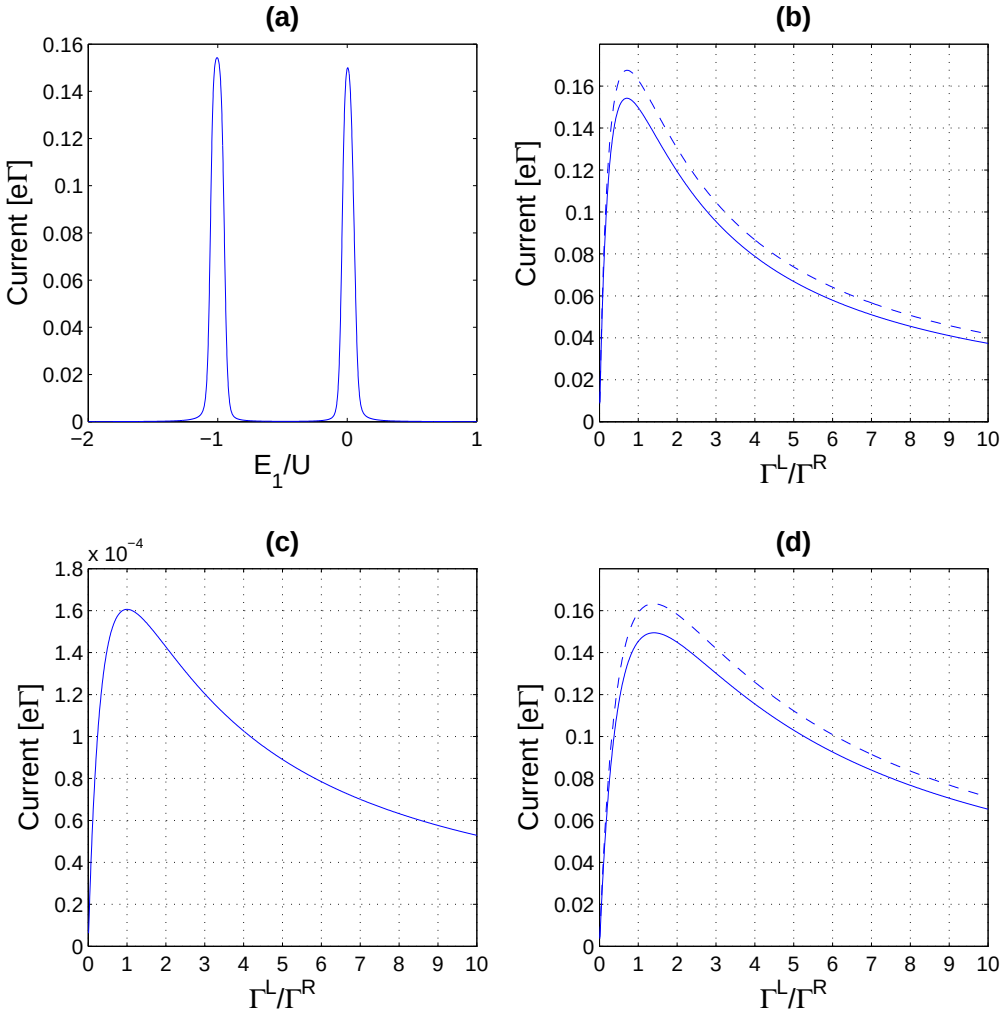

Figure 3.2: The current through the two level system with the following parameters ($\Gamma \equiv \Gamma_1^R+\Gamma_1^L+\Gamma_2^R+\Gamma_2^L$): $K_BT = \hbar\Gamma$, $eV_{\rm bias} = 10\hbar\Gamma$, $E_1-E_2 = \hbar\Gamma$, $U = 100\hbar\Gamma$ and $\Gamma_1^{R,L} = 10\Gamma_2^{R,L}$. We assume the same left-right asymmetry for the two levels: $\Gamma_1^L/\Gamma_1^R = \Gamma_2^L/\Gamma_2^R \equiv \Gamma^L/\Gamma^R$. **(a)** The symmetric ($\Gamma^L/\Gamma^R = 1$) current as a function of E_1. **(b)** The current at the right peak, $E_1 = 0$, as a function of the left-right asymmetry. The dashed line is the sequential tunneling current, and the solid line is the current including both sequential and cotunneling processes. **(c)** The (cotunneling) current at the valley, $E_1 = -U/2$, as a function of the left-right asymmetry. The sequential tunneling current is practically zero at the valley. **(d)** The current at the left peak, $E_1 = -U$, as a function of the left-right asymmetry. The dashed line is the sequential tunneling current, and the solid line is the current including both sequential and cotunneling processes.

current through the strongly coupled level- level 1- is blocked by the occupation of level 2, near the left peak the occupation of level 2 allows it, and therefore the left peak is a bit higher. If the sign of the energy difference was the opposite ($E_1 < E_2$) the right peak was higher than the left peak.

In Figs. 3.2(b) and 3.2(d) we plot the left-right asymmetry dependence of the current at the right and left peaks respectively. We assume the same left-right asymmetry for the two levels, $\Gamma_1^L/\Gamma_1^R = \Gamma_2^L/\Gamma_2^R \equiv \Gamma^L/\Gamma^R$. Due to the lack of a particle-hole symmetry at the peaks the current is not maximal when the system is symmetrically coupled to the leads. To understand this consider the current at the left peak in the simple case of zero temperature and no cotunneling processes. The right lead current (2.55) in this case is simply $\langle I\rangle = P_{11}(\Gamma_1^R+\Gamma_2^R) \approx P_{11}\Gamma_1^R$ where P_{11} is the probability of finding the system doubly occupied. The probability P_{11} can be easily calculated since the probability of finding the system empty in this case (zero temperature and $E_1 = -U$) is zero. Also, in the limit $|E_1 - E_2| \ll V_{\rm bias}$ the probability of finding only level 1 occupied, P_{10}, and the probability of finding only level 2 occupied P_{01} are identical and given by $P_{\rm e}$ of Eq. (2.70). The probability of finding the system doubly occupied is therefore $P_{11} = 1 - 2P_{\rm e}$. The average current is $\langle I\rangle = \Gamma_1^R(1-2P_{\rm e}) = (\Gamma_1^L+\Gamma_1^R)\frac{1}{\Gamma^L/\Gamma^R+1}(1-\frac{2}{\Gamma^L/\Gamma^R+2})$, and it is maximal, for a fixed $\Gamma_1^L+\Gamma_1^R$, at $\Gamma^L/\Gamma^R = \sqrt{2}$. Indeed, the current in Fig. 3.2(d) is maximal at $\Gamma^L/\Gamma^R \approx \sqrt{2}$ (the calculation is done at finite temperature and includes cotunneling therefore $\sqrt{2}$ is only an approximation). Similarly, the maximum of the right peak is at $\Gamma^L/\Gamma^R \approx 1/\sqrt{2}$. The current at the valley $E_1 = -U/2$, depicted in Fig. 3.2(c), carried by cotunneling processes, is maximal where the two levels are symmetrically coupled to the leads, $\Gamma^L = \Gamma^R$.

Fano factor

The current is carried by tunneling of electrons, namely current pulses of charge 'e', resulting in a shot noise. On top of the tunneling events, as we discussed in Sec. 2.5.1, there is also a telegraph noise; by tunneling into or out of level 2, we change the tunneling rate through level 1. Since most of the current is carried by tunneling through level 1 the current alternates between two different average values. For example, if we focus on the left peak of the current, $E_1 = -U$ [see Fig. 3.2(a)], most of the tunneling events are via level 1 while level 2 is occupied. However, because of the strong interactions, each time the electron leaves the narrow level, level 2, the current drops dramatically and resumes only when a new electron enters level 2.

In Fig. 3.3, we depict the Fano factor at the left peak ($E_1 = -U$) of the current through the two level system with the following parameters: $eV_{\rm bias} =$

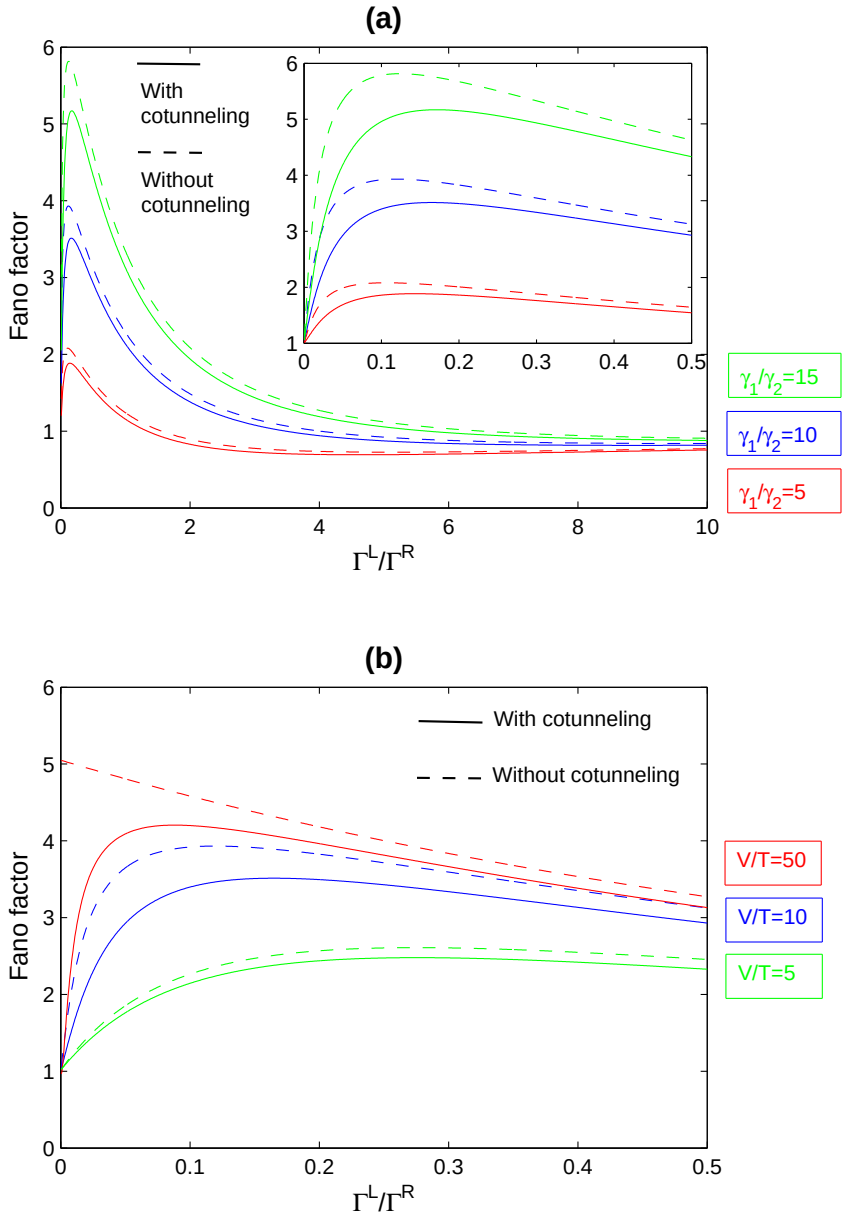

Figure 3.3: The Fano factor, $F = \frac{S}{2e\langle I\rangle}$ at $E_1 = -U$ (the left peak of the current) as a function of the left-right asymmetry with the following parameters: $eV_{\rm bias} = 0.1U$, $E_1 - E_2 = 0.01U$ and $\hbar\Gamma_1^L + \hbar\Gamma_1^R + \hbar\Gamma_2^L + \hbar\Gamma_2^R = 0.01U$. We assume that the two levels have the same left-right asymmetry, Γ^L/Γ^R. When we change Γ^L/Γ^R we keep the total width of each level fixed. **(a)** The Fano factor for different ratios of the two levels' widths ($\gamma_i = \hbar(\Gamma_i^R + \Gamma_i^L)/2$) with $K_BT = 0.01U$ and $eV_{\rm bias} = 0.1U$. The dashed lines are the sequential tunneling Fano factors and the solid lines are the calculated Fano factors including cotunneling processes. In the inside box in the upper right corner we zoom in on the small values of Γ^L/Γ^R. The Fano factor is larger than one (super-Poissonian noise) and maximal in asymmetric coupling. **(b)** The Fano factor as a function of the left-right asymmetry for different values of $eV_{\rm bias}/T$. The ratio between the levels' widths is $\Gamma_1^{R,L} = 10\Gamma_2^{R,L}$. The dashed lines are the sequential tunneling Fano factors and the solid lines are the calculated Fano factors including cotunneling processes. The cotunneling processes dramatically decrease the Fano factor for large $eV_{\rm bias}/T$.

$0.1U$, $E_1 - E_2 = 0.01U$, and $\hbar\Gamma_1^L + \hbar\Gamma_1^R + \hbar\Gamma_2^L + \hbar\Gamma_2^R = 0.01U$. By increasing γ_1/γ_2, we increase the average number of electrons that tunnel through level 1 while level 2 is occupied [the quantity $\Gamma_1\tau_1$ in Eq. (2.67)]. Indeed, similar to what we expect for the simplified model of Sec. 2.5.1 [Eqs. (2.67) and (2.68)], the noise is larger for large γ_1/γ_2 as one can see from Fig. 3.3(a).

In Fig. 3.3, we plot the left-right asymmetry dependence of the Fano factor. Similar to the simplified case of Sec. 2.5.1, we find the following asymmetry dependence of the Fano factor: for large Γ^L/Γ^R, the Fano factor is $F = 1$, and as we decrease Γ^L/Γ^R, we see enhancement of the the Fano factor. Also, as we discussed in Sec.2.5.1, the finite temperature suppresses the Fano factor below some $\Gamma^L/\Gamma^R \ll 1$ toward the value $F = 1$ in the limit $\Gamma^L/\Gamma^R \to 0$. The most interesting feature in Fig. 3.3 is the unexpected influence that the cotunneling processes have on the Fano factor. At low temperatures ($K_BT \ll eV_{\rm bias}$), the cotunneling processes suppress the Fano factor significantly in the asymmetric coupling regime $\Gamma^L \ll \Gamma^R$ (the dashed lines in Fig. 3.3 represent calculations without cotunneling processes).

The physics behind the reduction of the Fano factor in the $\Gamma^L/\Gamma^R \ll 1$ limit can be explained by the simplified picture of Sec. 2.5.1. At zero temperature and taking into account sequential tunneling only, as we reduce Γ^L/Γ^R the Fano factor is enhanced toward the value $F \approx \frac{\gamma_1}{2\gamma_2}$ in the limit $\Gamma^L/\Gamma^R \to 0$ [see Eqs. (2.68) and (2.70)]. This suits the upper (red) dashed line in Fig. 3.3. Finite temperature allows backward tunneling- opposite to the voltage bias direction, which reduces the number of current pulses through level 1 each time level 2 is occupied. The reason is that for $\Gamma^L \ll \Gamma^R$ electrons tunnel many times back and forth between the right lead and the system before a tunneling event from the left lead to the system takes place. Thus, the quantity $\Gamma_1\tau_1$ in Eq. (2.67) (see also Fig. 2.4) is reduced and the Fano factor is suppressed.

Cotunneling processes, similar to the finite temperature, allow backward tunneling. Virtual tunneling to the left is possible as a part of a full two particle cotunneling process. The important cotunneling processes which suppress the Fano factor in the asymmetric limit are the inelastic processes than change the system's state between the states $|1,0\rangle \longleftrightarrow |0,1\rangle$. In the asymmetric limit, the total rate of these processes becomes larger than the rate of sequential tunneling from the left lead into level 1. As a result, the occupation of level 2 changes faster than the time delay between consecutive current pulses through level 1. The quantity $\Gamma_1\tau_1$ is reduced and the Fano factor is suppressed toward the value $F = 1$ in the extremely asymmetric limit $\Gamma^L/\Gamma^R \to 0$.

We want to mention the experimental work that was reported in Ref. [64],

where a super-Poisson noise with a strong asymmetry dependence was measured in quantum dot that was attached to two leads at strong magnetic field. One of the suggested explanations for the enhancement of the noise in this system was an additional level that is weakly coupled to the leads. Indeed, the strong dependence of the Fano factor on the asymmetry of the dot-leads coupling, which is very similar to the asymmetry dependence of the Fano factor we have in Fig. 3.3, indicates a possible two level system. We must emphasize that although our results fits qualitatively the experimental measurements, the rate equations formalism is not suitable for quantitative analysis of the experimental results since the quantum dot was attached relatively strong to the leads, a situation that makes the rate equations approach invalid. Nevertheless, qualitatively, we believe that the significant asymmetry dependence of the Fano factor is a strong evidence for the presence of a second interacting level that was weakly attached to the leads in the experimental setup.

Spinful electrons

In order to avoid unnecessary complexities, we have assumed that the electrons are spinless. Physically, this situation can be realized by two-level quantum dot at strong magnetic field or two single level quantum dots at strong magnetic field. The spin degree of freedom can be added to the problem in two ways: single spinful level with spin dependent couplings to the leads or two spinful levels with different couplings to the leads. The single spinful level case is very similar to the system that we analyze, the only difference is the fact that processes with different spins cannot interfere. Therefore some of the cotunneling rates are slightly different (*e.g.*, cotunneling of electron through an empty level). Nevertheless, we want to stress that the most important cotunneling processes in the more physical situation of relatively strong interactions, which are the inelastic processes $|1,0\rangle \leftrightarrow |0,1\rangle$ (or $|\uparrow\rangle \leftrightarrow |\downarrow\rangle$), have exactly the same rates as in our model. Moreover, and this is the important point, the physics behind the noise enhancement in the spinful case and in the spinless case, is the same. The noise is enhanced because of the blocking effect which is a result of the Coulomb interactions. Therefore, the same qualitative dependence on the asymmetry is expected. This is true also in the two spinful levels case, and in fact also in multi-level systems with interactions. If the blocking effect enhances the noise, we expect similar dependence of the Fano factor on Γ^L/Γ^R with similar suppression due to finite temperature and cotunneling.

3.3.2 Weak interactions

While U is large, say $U > eV_{\rm bias}$, the current at the left (right) peak, $E_1 \approx -U$ ($E_1 \approx 0$) is changed dramatically when an electron is tunneling into or out of level 2, since the strong interaction blocks the tunneling through level 1. This is not the case for small U. If U is small compared to $V_{\rm bias}$ the current alternates between two relatively close values, and the effect on the noise is smaller. Yet, if the ratio between the levels' widths, γ_1/γ_2 is large enough, the enhancement of the noise can be important. In Fig. 3.4 we depict the current and the Fano factor for relatively small U ($U = eV_{\rm bias}/5$) with the following parameters ($\Gamma \equiv \Gamma_1^R + \Gamma_1^L + \Gamma_2^R + \Gamma_2^L$): $U = 2\hbar\Gamma$, $eV_{\rm bias} = 10\hbar\Gamma$, $K_BT = \hbar\Gamma$, $E_1 - E_2 = 0.5\hbar\Gamma$ and $\gamma_1 = 10000\gamma_2$. We see again that the cotunneling processes are important as they enhance the Fano factor significantly (the cotunneling processes contribute less than 20% of the current but almost double the Fano factor). Notice also that unlike the Fano factor of the strong U case, the Fano factor is maximal when the system is symmetrically coupled to the leads, $\Gamma^L = \Gamma^R$.

To explain the enhancement of the noise in the small U case, we use the intuitive picture that we studied in Sec. 2.5.1; a sequence of current pulses through level 1 and a random telegraph signal describing the occupation of level 2. The rate of the pulses depends on the occupation of level 2 and we consider two different rates: Γ_1 describes the tunneling rate through level 1 while level 2 is full and $\tilde{\Gamma}_1$ describes the tunneling rate while level 2 is empty. The Fano factor is given by (2.73)

$$F \approx 1 + \frac{2(\Delta\Gamma_1)^2}{\Gamma_1\Gamma_2} P_{\rm e}^2 (1 - P_{\rm e})^2, \tag{3.30}$$

where the rate $\Gamma_2 = (\tau_0 + \tau_1)^{-1}$ is the tunneling rate through level 2, $\Delta\Gamma_1 \equiv \tilde{\Gamma}_1 - \Gamma_1$, $P_{\rm e} = \frac{\tau_0}{\tau_0+\tau_1}$, and we have used the fact that $\tilde{\Gamma}_1 = \Gamma_1 + \Delta\Gamma_1 \approx \Gamma_1$ for $U < eV_{\rm bias}$. We see that although the Fano factor is usually reduced to one for $\frac{\Delta\Gamma_1}{\Gamma_1} \ll 1$, in the extreme case of $\frac{\Gamma_2}{\Gamma_1} < \left(\frac{\Delta\Gamma_1}{\Gamma_1}\right)^2$ the Fano factor can be enhanced.

We can now understand why the Fano factor is enhanced noticeably due to the cotunneling processes. For $U < eV_{\rm bias}$, the rate of the sequential tunneling through level 1 barely depends on the occupation of level 2 since the energies E_1 and $E_1 + U$ are close to each other compared to $V_{\rm bias}$. The cotunneling processes however, are much more sensitive to U. In Fig. 3.5 we illustrate this point by comparing the dependence of the sequential tunneling and the cotunneling rates through level 1 on the occupation of level 2, with the same parameters of Fig. 3.4(b). In Fig. 3.5(a), we plot the sequential

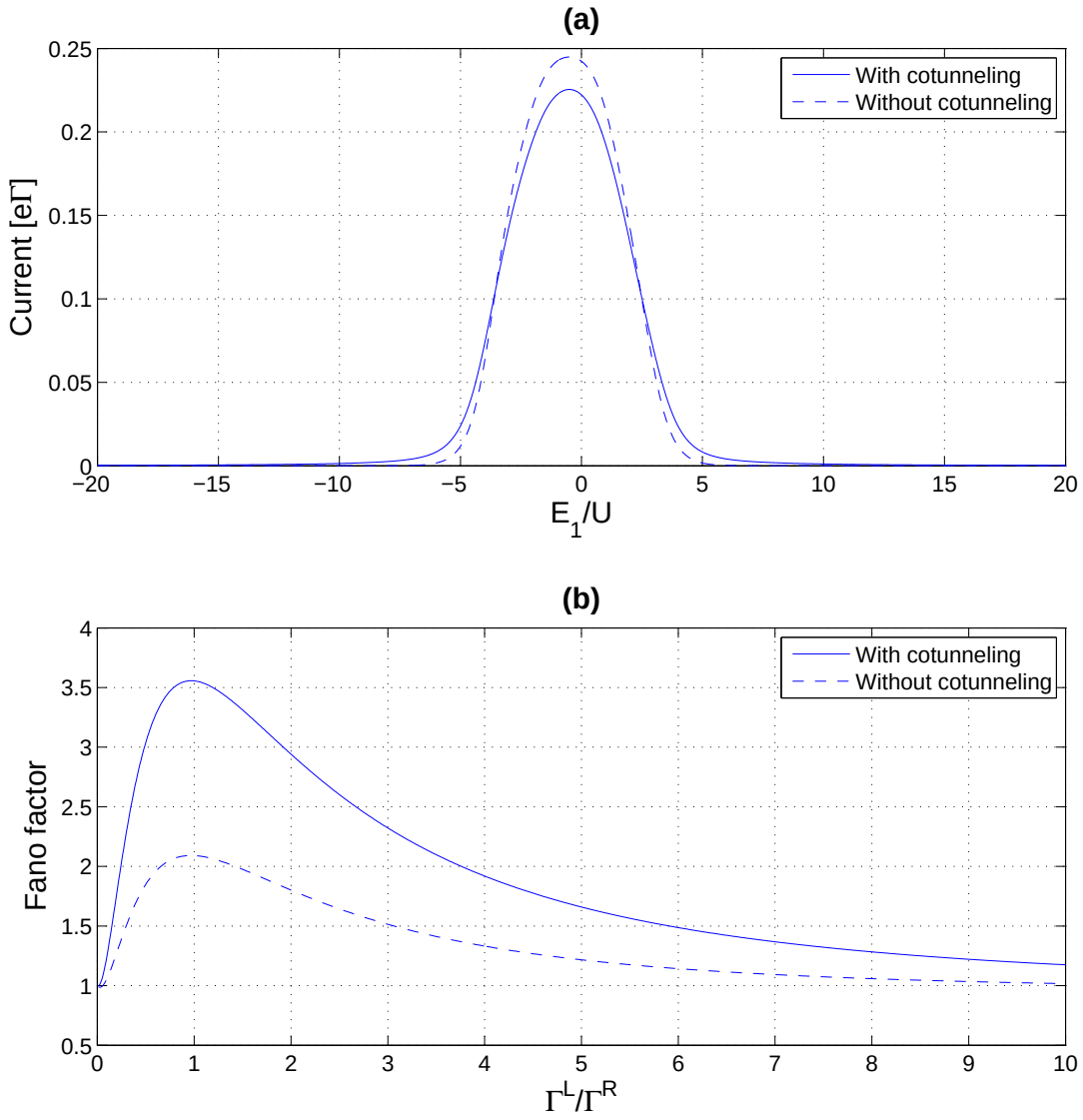

Figure 3.4: The current and the Fano factor in the small U ($U < eV_{\rm bias}$) region with the following parameters ($\Gamma \equiv \Gamma_1^R + \Gamma_1^L + \Gamma_2^R + \Gamma_2^L$): $U = 2\hbar\Gamma$, $eV_{\rm bias} = 10\hbar\Gamma$, $K_BT = \hbar\Gamma$, $E_1 - E_2 = 0.5\hbar\Gamma$ and $\gamma_1 = 10000\gamma_2$. **(a)** The current as a function of E_1 at the symmetric point, $\Gamma^L = \Gamma^R$. The dashed line is the current including sequential tunneling only, and the solid line is the current including also cotunneling processes. **(b)** The Fano factor at $E_1 = 0$ as a function of the left-right asymmetry. The dashed line is the sequential tunneling Fano factor and the solid line is the Fano factor including cotunneling processes. The cotunneling processes enhance the Fano factor significantly.

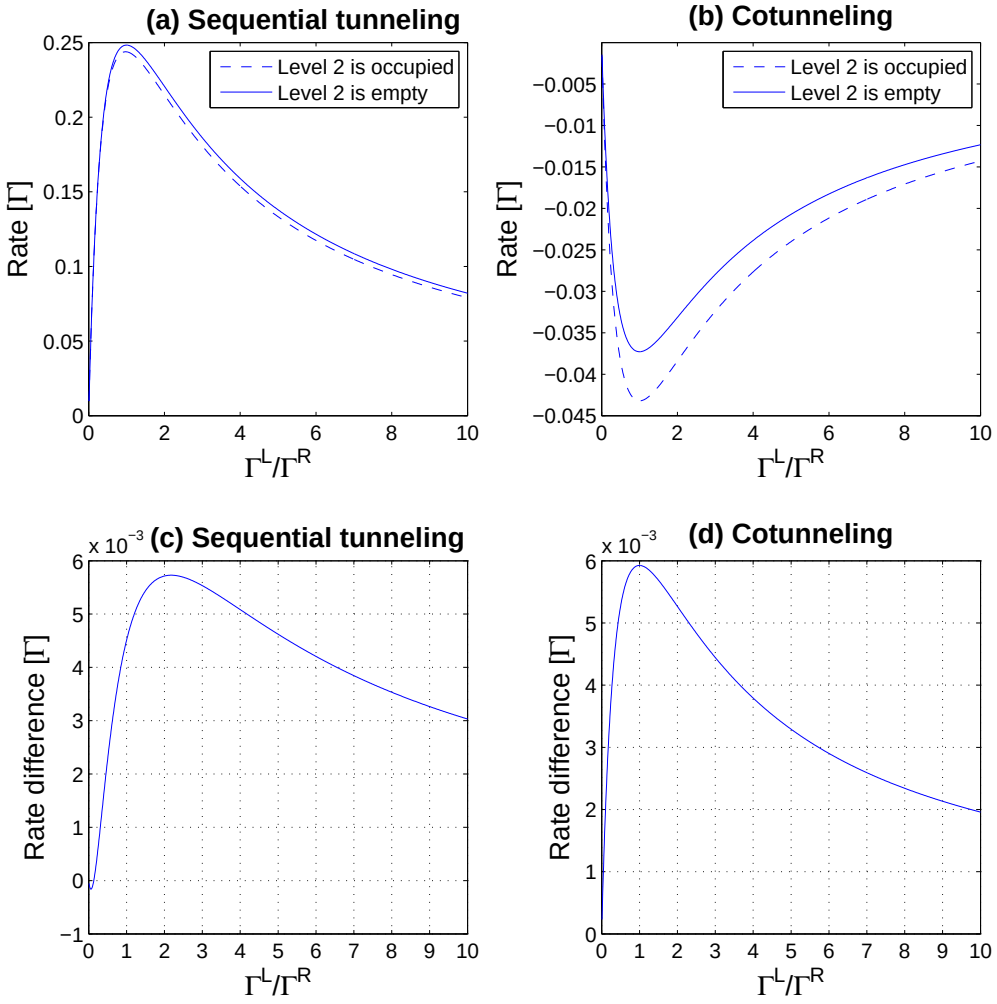

Figure 3.5: The dependence of the tunneling rates through level 1 on the occupation of level 2 in the small U ($U < eV_{\text{bias}}$) region with the following parameters ($\Gamma \equiv \Gamma_1^R + \Gamma_1^L + \Gamma_2^R + \Gamma_2^L$): $U = 2\hbar\Gamma$, $V_{\text{bias}} = 10\hbar\Gamma$, $K_BT = \hbar\Gamma$, $E_1 = 0$, $E_2 = -0.5\hbar\Gamma$ and $\gamma_1 = 10000\gamma_2$. Negative cotunneling rates mean that the cotunneling processes decrease the current (see for example Ref. [[118]]). **(a)** The sequential tunneling rate from the left lead through level 1 to the right lead $(((\omega^{\rightarrow}_{11,01})^{-1} + (\omega^{\rightarrow}_{01,11})^{-1})^{-1}$ when level 2 is occupied and $((\omega^{\rightarrow}_{10,00})^{-1} + (\omega^{\rightarrow}_{00,10})^{-1})^{-1}$ when level 2 is empty). **(b)** The cotunneling rates from the left lead through level 1 to the right lead ($\omega^{\rightarrow}_{11,11} + \omega^{\rightarrow}_{01,01}$ when level 2 is occupied and $\omega^{\rightarrow}_{10,10} + \omega^{\rightarrow}_{00,00}$ when level 2 is empty). **(c)** The difference between the sequential tunneling rates of the two stages (level 2 is empty and full). **(d)** The difference between the cotunneling rates of the two stages (level 2 is empty and full).

tunneling rates from the left lead through level 1 to the right lead when level 2 is empty- $[(\omega^{\rightarrow}_{10,00})^{-1}+(\omega^{\rightarrow}_{00,10})^{-1}]^{-1}$, and full- $[(\omega^{\rightarrow}_{11,01})^{-1}+(\omega^{\rightarrow}_{01,11})^{-1}]^{-1}$ (expressions for the rates are given in Appendix B, see Fig. 2.5 to clarify the notations). In Fig. 3.5(b) we plot the cotunneling rates from the left lead through level 1 when level 2 is empty- $\omega^{\rightarrow}_{10,10}+\omega^{\rightarrow}_{00,00}$, and full- $\omega^{\rightarrow}_{11,11}+\omega^{\rightarrow}_{01,01}$ (expressions for the rates are given in Appendix B, see Fig. 2.6 to clarify the notations). In Figs. 3.5(c) and 3.5(d) we plot the difference between the values of the tunneling rates through level 1 when level 2 is empty and the values of the tunneling rates when level 2 is full [in Fig. 3.5(c) the sequential tunneling rate and 3.5(d) the cotunneling rate]. We see that although the sequential tunneling rate is order of magnitude larger than the cotunneling rate, the cotunneling processes are much more sensitive to the occupation of level 2, making the difference between the two values of the cotunneling rate on the same order of the difference between the two values of the sequential tunneling rate. Thus, even though the cotunneling processes have a small contribution to the current, they contribute the same as the sequential tunneling to $\Delta\Gamma_1$ and therefore have an important contribution to the Fano factor. We want to emphasize that the Fano factor is enhanced in the weak interactions regime only if level 2 is coupled to the leads extremely weaker than level 1, as we require $\frac{\Gamma_2}{\Gamma_1}<\left(\frac{\Delta\Gamma_1}{\Gamma_1}\right)^2$ where $\left(\frac{\Delta\Gamma_1}{\Gamma_1}\right)^2$ is a very small number.

Since (2.73) depends quadratically on the multiplication of the probabilities of finding level 2 empty and full, $P_{\rm e}(1-P_{\rm e})$, the enhancement of the Fano factor due to $\Delta\Gamma_1$ is maximal where $P_{\rm e}(1-P_{\rm e})$ is maximal. In the limit of small U, the energy of the system, wether it is empty, singly occupied or doubly occupies, is more or less the same for $E_1=0$, therefore $P_{\rm e}(1-P_{\rm e})$ is maximal where the system is symmetrically coupled to the leads.

Chapter 4

Conclusions

In the following, we summarize the main ideas that this thesis expresses. We mention the novelties, compared to existing works, and provide an outlook for possible further studies.

In this thesis, we have presented our suggested **realization of SU(N)-Kondo** impurities with quantum dots structures. The physics of the familiar Kondo effect is the low energy fixed point of a $SU(2)$ symmetric system with an impurity. Although the generalization of this problem to $SU(N)$ symmetric system was discussed, physical realizations of $SU(N > 2)$ Kondo models are rare, usually complex and limited to $N = 4$. In this work we suggest a realization of Kondo effect using edge states of the quantum Hall effect that interact with multiple quantum dot structure. This realization is naturally generalized to $SU(N)$ Kondo.

We have analyzed the transport properties of the suggested $SU(2)$ and $SU(3)$ systems in the two fixed points: The high energy fixed point and the low energy one. We showed new features of the pseudo-spin-resolved current: The spin-spin correlations (or more generally the flavor-flavor correlations) and the different Fano factor of a single pseudo spin current. The ability of measuring a distinct pseudo spin current in the suggested systems makes these features experimentally accessible. Following our suggestion, an experimental realization of $SU(2)$-Kondo with access to each spin separately was built and measured [50], and a spin-resolved spectroscopy of the Kondo effect was made. We also present explicitly the conductance of the $SU(3)$ system in the Kondo regime where it has an unusual fractional value 3/4.

Besides the ability of realizing $SU(N)$ Kondo, the systems that we suggest have four more advantages: First, as our realization is based on edge states it can be easily integrated into electronic Mach-Zehnder interferometer, allowing accurate phase shift measurements. Second, our realization allows measurements of a single pseudo-spin [or generally a single flavor for $SU(N > 2)$] transport. Third, breaking of the $SU(N)$ symmetry can be brought under a good experimental control, potentially allowing a non Fermi liquid behavior such as in the two impurity Kondo model and its generalizations. Fourth, it paves the way to possible generalization to fractional quantum Hall edges which may show richer structure.

We also presented, in this thesis, our work on **transmission phase shift and normalized visibility of Kondo impurities**. We explore interference (and hence coherence) in transport through both Fermi liquid (conventional

Kondo) and non-Fermi liquid (e.g., two-channel Kondo) states. It is not obvious that there should even be coherent transport through a non-Fermi liquid, since quasi-particles need to convert to more exotic excitations, and then back to quasi-particles. But we find that substantial coherence does remain even in this case.

We provide a novel many body scattering theory which enables a theoretical analysis of the coherence of the transport. In addition to the commonly measured quantity in two-paths experiments, the transmission phase shift, we discuss the visibility- the ratio between the flux-dependent part of the conductance and the average conductance. We show that if the visibility is normalized properly, then the normalized visibility is related to the portion of the coherent part of the transport. Our many body scattering approach enables us to calculate the conductance through the dot, the transmission phase shift and the normalized visibility. In Fermi liquids at zero temperature, the transmission phase shift is identical to the scattering phase shift of the quantum dot, and the normalized visibility is one. We give the temperature correction for these results, and the generalization to non-Fermi liquid cases. In particular, we show that in the non-Fermi liquid fixed point of the two-channel-Kondo, the normalized visibility at zero temperature is half, indicating that exactly half of the conductance is carried by coherent transport. In this case, we find that the transmission phase shift is $\pi/2$ even though a scattering phase shift is not defined for such an impurity.

The conductance of a two-path setup with a penetrating magnetic flux depends on the magnetic flux because of the Aharonov-Bohm effect. Measurements of the flux-dependent conductance give access to information about the coherent nature of the transport. Manipulations on quantum dots allow the realization of various types of Kondo fixed points. Hence, we discuss a two-paths setup with an embedded quantum dot as a tool for studying the coherent properties of transmission through Kondo impurities. In particular we discuss the special non-Fermi liquid fixed point of the two-channel-Kondo impurity. We show that regular measurements of the conductance of the two spins together, are not sufficient in the absence of spin-symmetry. Special particle-hole symmetry locks the phase shift at $\pi/2$, independent of the actual phase that electrons accumulate when they are transmitted through the impurity. A way to overcome this phase-lock is to perform a spin-resolved measurement.

In this thesis, we also study the **shot noise enhancement in asymmetric interacting two-level systems**. Measurements of the shot noise, S, provide additional information about the system, which is not accessible from measurements of the average current, $\langle I \rangle$. In several situations,the Fano factor $F = S/2\langle I \rangle$ gives the effective charge of the current carriers and

therefore it is crucial to understand it thoroughly. We present a detailed study of the Fano factor for interacting two-level systems and its dependence on various parameters. In most cases, Coulomb interactions reduce S. However, several theoretical and experimental works have showed that Coulomb interactions may also enhance S, resulting in a Fano factor $F \geq 1$. In this work, we study in detail a model of two-level system coupled to two electronic leads where the coupling of one level is stronger than the other. There are many physical realizations of two level systems, such as one spin-full level in a quantum dot with a spin dependent coupling or two levels in a quantum dot subjected to a strong magnetic field. In the absence of Coulomb interactions, the expected Fano factor of such systems is $\frac{1}{2} \leq F \leq 1$. We show that strong interactions enhance the Fano factor significantly in such systems, and that the enhancement depends very strongly on the asymmetry between the couplings to the two different leads. Our results are relevant to large variety of experimental situations and explain in detail and in a simple intuitive way the dependence of the Fano factor F on various parameters of the system.

In particular, the dependence of the Fano factor on the asymmetry of the couplings to the leads was hardly discussed before, and a clear picture of this dependence and its origin was missing. We calculate the current and the shot noise using rate equations formalism and show that while at zero temperature the Fano factor is a monotonic function of the asymmetry of the couplings to the leads, at finite temperature it has a maximum. In our calculations we include both sequential tunneling processes and the more complex cotunneling processes, and we show that the cotunneling processes play a crucial role in such systems. There is a range of parameters in which the cotunneling processes affect the noise significantly, even though most of the current is carried by sequential tunneling processes. In particular, the cotunneling processes change the dependence of the Fano factor on the asymmetry of the coupling to the leads. Even if the interactions are relatively weak, if the coupling of one level is much stronger than the other the shot noise can still be enhanced. Significant part of this enhancement is due to the rarer cotunneling processes.

Also, we develop a simple intuitive picture of the current through the two levels as a multiplication of two signals: A sequence of current pulses and a telegraphic signal. This simplified picture capture, at least qualitatively, most of the results that we achieve through the rigorous rate equations based calculations and can be used to gain an intuitive understanding of the transport through the system. We believe that our results can be used to identify two level systems and to explain existing and possible future experiments, where the shot noise is enhanced due to additional weakly coupled states.

Appendix A

Model for a quantum dot impurity embedded into an open AB ring

In this appendix, we present a model for a possible setup of a quantum dot that is embedded into an open AB ring. Setups of this kind, can be used to study the transmission through 1CK and 2CK impurities.

Consider the open AB ring setup that is depicted in Fig. A.1. The system contains two external leads (source and drain) and two internal paths. The external leads are coupled to the two paths by four transmission coefficients ($t_s^{\rm ref}$, $t_d^{\rm ref}$, t_s^L, t_d^R) which are assumed to be very small. The two possible paths are either through the quantum dot (the lower arm in Fig. A.1) or through the reference arm (the upper arm in Fig. A.1). When an electron is propagating along the lower arm, it has a finite probability to leak outside the system. However, once it gets close enough to the dot we assume that it can only scattered (forward or backward) off the dot. We refer to the area near the dot from the left (right) as left (right) lead (not to be confused with the external leads, source and drain). The Hamiltonian of the system is

$$H = H_{\rm external} + H_{\rm ref} + H_{\rm system} + H_t \ , \tag{A.1}$$

where each of the three first elements on the right hand side of (A.1) describes one part of the system. $H_{\rm external}$ describes the external leads

$$H_{\rm external} = \sum_{r=S,D} \sum_{k,s} \epsilon_k c_{rks}^\dagger c_{rks} \ , \tag{A.2}$$

where c_{rks} are the annihilation operators of electrons with spin s in external lead r. $H_{\rm ref}$ describes the free electrons in the reference arm. The lower arm is described by the Hamiltonian

$$H_{\rm system} = \sum_{i=L,R} \sum_{k,s} \epsilon_k c_{iks}^\dagger c_{iks} + H_{\rm dot} + \sum_{i=L,R} \sum_{ks} \left(t_i c_{iks}^\dagger d_s + h.c. \right) , \tag{A.3}$$

where c_{rks} are the annihilation operators of electrons with spin s in the internal lead i, and d_s annihilates an electron with spin s in the dot. $H_{\rm dot}$ describes the quantum dot itself and any other system that might interact with it but do not interact directly with the other part of the setup (*e.g.* a capacitively coupled gate electrode, other dots etc.). The different parts of

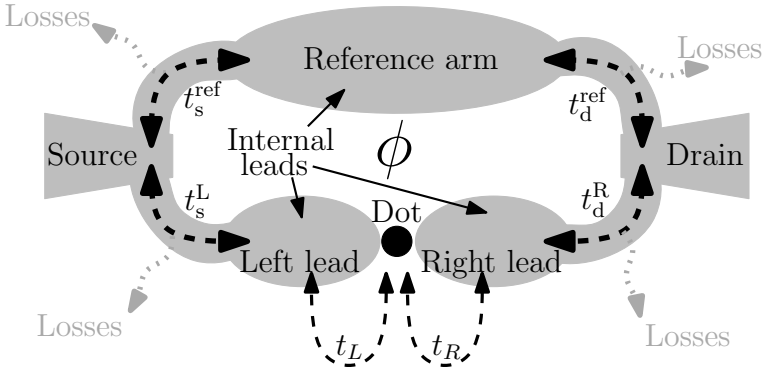

Figure A.1: Schematic model of a quantum dot embedded into an open AB ring. The four transmission coefficients between the two paths and the external leads ($t_{\rm s}^{\rm ref}$, $t_{\rm d}^{\rm ref}$,$t_{\rm s}^{\rm L}$,$t_{\rm d}^{\rm R}$), are very small. To the lowest order in the external transmission coefficients the propagations along the arms are independent of each other. Because of the losses, time reversal symmetry is broken. We encode the losses in the transmission coefficients.

the setup are connected via H_t

$$H_t = \sum_{ks}\sum_{r} t_r^{\rm ref} c_{rks}^\dagger c_{{\rm ref},ks} + \sum_{ks} t_s^L c_{Sks}^\dagger c_{Lks} + \sum_{ks} t_d^R c_{Dks}^\dagger c_{Rks} + h.c.\,. \quad \text{(A.4)}$$

We don't get into the details of how the setup is coupled to other side leads.

To the lowest order in the external transmission coefficients, H_t, the two paths are independent of each other. Therefore, using the definitions of φ_t and η [see Eq. (1.9)], the conductance can be written in the form

$$G_{\rm sd} = G_{\rm d} + G_{\rm ref} + 2\sqrt{\eta}\sqrt{G_{\rm d}G_{\rm ref}}\cos\left(\frac{e\phi}{\hbar c} + \varphi_t\right),$$

where $G_{\rm ref}$ is the conductance through the reference arm, and $G_{\rm d}$ is the conductance through the dot. There is a linear combination of the internal leads, $\xi = -\sin(\alpha)c_L + \cos(\alpha)c_R$, where $\alpha = \arctan(t_R/t_L)$, which is decoupled both from the dot and from the orthogonal combination of the leads, $\psi = \cos(\alpha)c_L + \sin(\alpha)c_R$. Following the discussion on Chapter 2 [Sec. 2.3] the transmission through the dot is proportional to the $\mathcal{T}$-matrix of the ψ-particles.

So far, we haven't specified what is the Hamiltonian of the dot, $H_{\rm dot}$. In other words, we haven't specified other systems that interact with the dot (and do not interact directly with the ring). In the following two subsections, we discuss two specific cases: a 1CK case, where the dot is attached to a gate electrode and tuned to form a 1CK impurity, and a 2CK case, where another

large dot is coupled to the small dot with appropriate gate electrodes to form a 2CK impurity [37].

A.1 Single-channel Kondo

The dot is capacitively coupled to a gate electrode. If a gate voltage is applied, then at low enough energies, by tuning the gate voltage and the tunneling barriers between the dot and the ring ($t_{L,R}$), one can bring the Hamiltonian (A.3) to the form of Kondo Hamiltonian [135]

$$H_{\text{system}} = \sum_{k,s} \epsilon_k \psi^\dagger_{ks} \psi_{ks} + \sum_{k,s} \epsilon_k \xi^\dagger_{ks} \xi_{ks} + J \sum_{k,s} \sum_{k',s'} \psi^\dagger_{ks} \vec{\sigma}_{ss'} \psi_{k's'} \cdot \vec{S} \,, \qquad \text{(A.5)}$$

where $\xi = -\sin(\alpha) c_L + \cos(\alpha) c_R$, and $\psi = \cos(\alpha) c_L + \sin(\alpha) c_R$. J is the Kondo interaction strength, $\vec{\sigma}$ are the three Pauli matrices, and $\vec{S}$ is the total spin of the dot. Up to second order in $1/T_K$ the $\mathcal{T}_{s,\psi\psi}$-matrix is [40]

$$\mathcal{T}_{s,\psi\psi}(\epsilon) = i \left[2 + i \frac{2\epsilon}{T_K} - 3 \left(\frac{\epsilon}{T_K} \right)^2 - \left(\frac{\pi T}{T_K} \right)^2 \right] . \qquad \text{(A.6)}$$

A.2 Two-channel Kondo

We can tune the part of the system that is described by H_{dot} to form a 2CK impurity (*e.g.*, by adding another relatively large quantum dot, and couple it to the small dot [37]). The Hamiltonian (A.3) becomes [37, 136]

$$\begin{aligned} H_{\text{system}} = & \sum_{k,s} \epsilon_k \psi^\dagger_{ks} \psi_{ks} + \sum_{k,s} \epsilon_k \xi^\dagger_{ks} \xi_{ks} + \sum_{k,s} \epsilon_k D^\dagger_{ks} D_{ks} \\ & + \sum_{k,s} \sum_{k',s'} \left(J_\psi \psi^\dagger_{ks} \vec{\sigma}_{ss'} \psi_{k's'} + J_D D^\dagger_{ks} \vec{\sigma}_{ss'} D_{k's'} \right) \cdot \vec{S} \,, \end{aligned} \qquad \text{(A.7)}$$

where D_{ks} are the annihilation operators of the large dot, and J_D (J_ψ) is the strength of the interaction between the spin of the electrons in the large dot (in the ψ lead) and the total spin of the small dot. By tuning the parameters properly, we can bring the system to the symmetric point $J_\psi \approx J_D$, where it displays a non Fermi liquid behavior [37]. In this case, up to order $1/\sqrt{T_K}$, the $\mathcal{T}_{s,\psi\psi}$-matrix is [40]

$$\mathcal{T}_{s,\psi\psi}(\epsilon) = i \left(1 - 3\lambda \sqrt{\pi T} I(\epsilon) \right) \,,$$

where $I(\epsilon)$ was defined in Eq. (3.13).

Appendix B

List of tunneling rates

In this appendix we give the expressions for all the tunneling rates that enter the rate equations calculation for the two interacting levels.

B.1 Sequential tunneling rates

To the lowest order in $H_{\rm t}$ the transition rates can be calculated using Fermi's golden rule. We use the notation $\omega^{\rightarrow}_{i,j}$ for the rate of a tunneling process that changes the system's state from 'i' to 'j' by tunneling an electron from the left to the right direction (and similarly $\omega^{\leftarrow}_{i,j}$ for electron that moves from right to left). For example $\omega^{\rightarrow}_{00,10}$ is the rate of tunneling from the left lead into level 1 while level 2 is empty. The rates of the sequential tunneling processes are

$$\omega^{\rightarrow}_{00,10} = \Gamma^L_1 F_{FD}(E_1 - \mu^L) \,, \tag{B.1}$$
$$\omega^{\rightarrow}_{00,01} = \Gamma^L_2 F_{FD}(E_2 - \mu^L) \,, \tag{B.2}$$
$$\omega^{\rightarrow}_{10,00} = \Gamma^R_1 F_{FD}(\mu^R - E_1) \,, \tag{B.3}$$
$$\omega^{\rightarrow}_{01,00} = \Gamma^R_2 F_{FD}(\mu^R - E_2) \,, \tag{B.4}$$
$$\omega^{\rightarrow}_{01,11} = \Gamma^L_1 F_{FD}(E_1 + U - \mu^L) \,, \tag{B.5}$$
$$\omega^{\rightarrow}_{10,11} = \Gamma^L_2 F_{FD}(E_2 + U - \mu^L) \,, \tag{B.6}$$
$$\omega^{\rightarrow}_{11,01} = \Gamma^R_1 F_{FD}(\mu^R - E_1 - U) \,, \tag{B.7}$$
$$\omega^{\rightarrow}_{11,10} = \Gamma^R_2 F_{FD}(\mu^R - E_2 - U) \,. \tag{B.8}$$

We have defined

$$\Gamma^L_i \equiv \nu \frac{2\pi}{\hbar} |t^L_i|^2, \quad \Gamma^R_i \equiv \nu \frac{2\pi}{\hbar} |t^R_i|^2, \tag{B.9}$$

and the Fermi's function $F_{FD}(x) = (1 + e^{\beta x})^{-1}$ gives the probability for the availability of an electron or a hole for the tunneling process. The left moving rates, $\omega^{\leftarrow}_{i,j}$, have similar expressions with $\mu^L \leftrightarrow \mu^R$ and $\Gamma^L_{1,2} \leftrightarrow \Gamma^R_{1,2}$.

B.2 Elastic-cotunneling rates

Each elastic cotunneling process has two possible intermediate states. For example, electron can tunnel through an empty system via level 1 or 2,

thus, cotunneling processes of the form $|0,0\rangle \longrightarrow |0,0\rangle$ have two possible intermediate states: $|1,0\rangle$ and $|0,1\rangle$. The two possible paths interfere and we need to sum the amplitudes of the two possibilities rather than their probabilities. We use the notation $\omega^{\rightarrow}_{i,i}$ ($\omega^{\leftarrow}_{i,i}$) for elastic-cotunneling processes in which the electron tunnels to the right (left) direction. The total elastic-cotunneling rates are the sum of the rates of all the possible processes, namely integrating over all incoming electron's energies.

$$\omega^{\rightarrow}_{00,00} = \frac{2\pi\nu^2}{\hbar}\int d\epsilon F_{FD}\left(\epsilon-\mu^L\right)\left[1-F_{FD}\left(\epsilon-\mu^R\right)\right]\left|\frac{t_1^L t_1^R}{\epsilon-E_1}+\frac{t_2^L t_2^R}{\epsilon-E_2}\right|^2 , \tag{B.10}$$

$$\omega^{\rightarrow}_{10,10} = \frac{2\pi\nu^2}{\hbar}\int d\epsilon F_{FD}\left(\epsilon-\mu^L\right)\left[1-F_{FD}\left(\epsilon-\mu^R\right)\right]\left|\frac{t_1^L t_1^R}{\epsilon-E_1}+\frac{t_2^L t_2^R}{\epsilon-E_2-U}\right|^2 , \tag{B.11}$$

$$\omega^{\rightarrow}_{01,01} = \frac{2\pi\nu^2}{\hbar}\int d\epsilon F_{FD}\left(\epsilon-\mu^L\right)\left[1-F_{FD}\left(\epsilon-\mu^R\right)\right]\left|\frac{t_1^L t_1^R}{\epsilon-E_1-U}+\frac{t_2^L t_2^R}{\epsilon-E_2}\right|^2 , \tag{B.12}$$

$$\omega^{\rightarrow}_{11,11} = \frac{2\pi\nu^2}{\hbar}\int d\epsilon F_{FD}\left(\epsilon-\mu^L\right)\left[1-F_{FD}\left(\epsilon-\mu^R\right)\right]\left|\frac{t_1^L t_1^R}{\epsilon-E_1-U}+\frac{t_2^L t_2^R}{\epsilon-E_2-U}\right|^2 . \tag{B.13}$$

The left moving elastic-cotunneling rates, $\omega^{\leftarrow}_{i,i}$, have similar expressions with $\mu^L \leftrightarrow \mu^R$. Equations (B.10)-(B.13) are formal expressions, and the rates which we use as input for the rate equations, cannot be directly calculated from these integrals. The reason is the divergence of these expressions due to the finite widths of the two levels (which we treat as two delta functions in energy). We use a regularization scheme [120, 121] for the calculation of the cotunneling rates. The regularization scheme is summarized in Appendix C.

B.3 Inelastic-cotunneling rates

We consider the inelastic-cotunneling processes that change the system's state between $|1,0\rangle \longleftrightarrow |0,1\rangle$ and $|0,0\rangle \longleftrightarrow |1,1\rangle$. We begin with the former; we use the notation $\omega^{\rightleftarrows}_{i,j}$ for the rate of processes in which the system changes its state from $|i\rangle$ to $|j\rangle$ in the following way: the electron that enters or leaves level 1 tunnels to the right direction, while the electron that enters or leaves level 2 tunnels to the left, and similarly, we define $\omega^{\leftrightarrows}_{i,j}, \omega^{\rightrightarrows}_{i,j}, \omega^{\leftleftarrows}_{i,j}$. For example, if the system's initial state is $|1,0\rangle$ and the electron in level 1 tunnels to the right lead, while another electron from the right lead tunnels

to level 2, we denote the rate of this process by $\omega^{\rightleftarrows}_{10,01}$. Again, there are two possible intermediate states for the processes $|1,0\rangle \longleftrightarrow |0,1\rangle$, and we need to sum them properly. The formal expression for these rates are

$$\omega^{\rightrightarrows}_{10,01} = \frac{2\pi\nu^2}{\hbar}\int d\epsilon F_{FD}\left(\epsilon-\mu^L\right)\left[1-F_{FD}\left(\epsilon+E_1-E_2-\mu^R\right)\right]\left|\frac{t_1^R t_2^L}{\epsilon-E_2}-\frac{t_1^R t_2^L}{\epsilon-E_2-U}\right|^2, \tag{B.14}$$

$$\omega^{\leftleftarrows}_{10,01} = \frac{2\pi\nu^2}{\hbar}\int d\epsilon F_{FD}\left(\epsilon-\mu^R\right)\left[1-F_{FD}\left(\epsilon+E_1-E_2-\mu^L\right)\right]\left|\frac{t_1^L t_2^R}{\epsilon-E_2}-\frac{t_1^L t_2^R}{\epsilon-E_2-U}\right|^2, \tag{B.15}$$

$$\omega^{\rightleftarrows}_{10,01} = \frac{2\pi\nu^2}{\hbar}\int d\epsilon F_{FD}\left(\epsilon-\mu^R\right)\left[1-F_{FD}\left(\epsilon+E_1-E_2-\mu^R\right)\right]\left|\frac{t_1^R t_2^R}{\epsilon-E_2}-\frac{t_1^R t_2^R}{\epsilon-E_2-U}\right|^2, \tag{B.16}$$

$$\omega^{\leftrightarrows}_{10,01} = \frac{2\pi\nu^2}{\hbar}\int d\epsilon F_{FD}\left(\epsilon-\mu^L\right)\left[1-F_{FD}\left(\epsilon+E_1-E_2-\mu^L\right)\right]\left|\frac{t_1^L t_2^L}{\epsilon-E_2}-\frac{t_1^L t_2^L}{\epsilon-E_2-U}\right|^2. \tag{B.17}$$

To get these integrals we used the energy conservation: if the incoming electron (that enters level 2) has the energy ϵ, the outgoing electron (that leaves level 1) must have the energy $\epsilon + E_1 - E_2$. To get the rates: $\omega^{\rightrightarrows}_{01,10}$, $\omega^{\leftleftarrows}_{01,10}$, $\omega^{\rightleftarrows}_{01,10}$ and $\omega^{\leftrightarrows}_{01,10}$, we may write integrals like (B.14)-(B.17) and exchange $t_1^{L,R} \leftrightarrow t_2^{L,R}$ and $E_1 \leftrightarrow E_2$. Once again, the formal expressions (B.14)-(B.17) need to be regularized in order to extract the input terms for the rate equations calculation (see Appendix C).

The last rates that we discuss are the inelastic $|0,0\rangle \longleftrightarrow |1,1\rangle$ processes' rates. These processes are somewhat more complex than the other cotunneling processes as they have four possible intermediate states. We use the notation $\omega^{\rightrightarrows}_{00,11}$ ($\omega^{\leftleftarrows}_{00,11}$) and $\omega^{\rightrightarrows}_{11,00}$ ($\omega^{\leftleftarrows}_{11,00}$) for processes in which two electrons enter or leave the two levels by tunneling to the right (left). We use the notation $\omega^{\leftrightarrows}_{00,11}$, $\omega^{\leftrightarrows}_{11,00}$ for processes in which the two electrons enter or leave the two levels by tunneling one to the right and the other to the left. The

rates for the $|0,0\rangle \longleftrightarrow |1,1\rangle$ inelastic cotunneling processes are

$$\omega^{\rightrightarrows}_{00,11} = \frac{2\pi\nu^2}{\hbar}\int d\epsilon \frac{1}{2} F_{FD}\left(\epsilon-\mu^L\right) F_{FD}\left([-\epsilon+E_1+E_2+U]-\mu^L\right)\times \left|\frac{t_1^L t_2^L}{\epsilon-E_1}-\frac{t_1^L t_2^L}{\epsilon-E_1-U}-\frac{t_1^L t_2^L}{\epsilon-E_2}+\frac{t_1^L t_2^L}{\epsilon-E_2-U}\right|^2, \tag{B.18}$$

$$\omega^{\leftleftarrows}_{00,11} = \frac{2\pi\nu^2}{\hbar}\int d\epsilon \frac{1}{2} F_{FD}\left(\epsilon-\mu^R\right) F_{FD}\left([-\epsilon+E_1+E_2+U]-\mu^R\right)\times \left|\frac{t_1^R t_2^R}{\epsilon-E_1}-\frac{t_1^R t_2^R}{\epsilon-E_1-U}-\frac{t_1^R t_2^R}{\epsilon-E_2}+\frac{t_1^R t_2^R}{\epsilon-E_2-U}\right|^2, \tag{B.19}$$

$$\omega^{\leftrightarrows}_{00,11} = \frac{2\pi\nu^2}{\hbar}\int d\epsilon F_{FD}\left(\epsilon-\mu^L\right) F_{FD}\left([-\epsilon+E_1+E_2+U]-\mu^R\right)\times \left|\frac{t_1^L t_2^R}{\epsilon-E_1}-\frac{t_1^L t_2^R}{\epsilon-E_1-U}-\frac{t_1^R t_2^L}{\epsilon-E_2}+\frac{t_1^R t_2^L}{\epsilon-E_2-U}\right|^2, \tag{B.20}$$

$$\omega^{\rightrightarrows}_{11,00} = \frac{2\pi\nu^2}{\hbar}\int d\epsilon \frac{1}{2} F_{FD}\left(\mu^L-\epsilon\right) F_{FD}\left(\mu^L-[-\epsilon+E_1+E_2+U]\right)\times \left|\frac{t_1^L t_2^L}{\epsilon-E_1}-\frac{t_1^L t_2^L}{\epsilon-E_1-U}-\frac{t_1^L t_2^L}{\epsilon-E_2}+\frac{t_1^L t_2^L}{\epsilon-E_2-U}\right|^2, \tag{B.21}$$

$$\omega^{\leftleftarrows}_{11,00} = \frac{2\pi\nu^2}{\hbar}\int d\epsilon \frac{1}{2} F_{FD}\left(\mu^R-\epsilon\right) F_{FD}\left(\mu^R-[-\epsilon+E_1+E_2+U]\right)\times \left|\frac{t_1^R t_2^R}{\epsilon-E_1}-\frac{t_1^R t_2^R}{\epsilon-E_1-U}-\frac{t_1^R t_2^R}{\epsilon-E_2}+\frac{t_1^R t_2^R}{\epsilon-E_2-U}\right|^2, \tag{B.22}$$

$$\omega^{\leftrightarrows}_{11,00} = \frac{2\pi\nu^2}{\hbar}\int d\epsilon F_{FD}\left(\mu^L-\epsilon\right) F_{FD}\left(\mu^R-[-\epsilon+E_1+E_2+U]\right)\times \left|\frac{t_1^L t_2^R}{\epsilon-E_1}-\frac{t_1^L t_2^R}{\epsilon-E_1-U}-\frac{t_1^R t_2^L}{\epsilon-E_2}+\frac{t_1^R t_2^L}{\epsilon-E_2-U}\right|^2. \tag{B.23}$$

The factor $1/2$ that appears in Eqs. (B.18), (B.19), (B.21) and (B.22) is due to the double counting of processes: by integrating over ϵ we sum both $\epsilon=\epsilon'$ and $\epsilon=-\epsilon'+E_1+E_2+U$, however these two processes are identical since in both cases when the two levels are empty the two electrons are in the same lead with energies ϵ' and $-\epsilon'+E_1+E_2+U$. Hence, as we double count each process we insert a factor of $1/2$. Notice also that for $\omega^{\rightrightarrows}_{00,11}$, $\omega^{\leftleftarrows}_{00,11}$, $\omega^{\rightrightarrows}_{11,00}$ and $\omega^{\leftleftarrows}_{11,00}$, by including the point $\epsilon=\frac{E_1+E_2+U}{2}$ in the integral, we include an impossible process, as the two electrons in the lead have the same energy ($\frac{E_1+E_2+U}{2}$). Nevertheless, this point contribute zero to the integrals, and therefore we have no problems with the formal expressions (B.18), (B.19), (B.21) and (B.22). The integrals in (B.18)-(B.23) need a regularization in

order to extract the rates that we use in the rate equations, the regularization scheme appears in Appendix C.

Appendix C

Regularization scheme

In this appendix we summarize the regularization procedure for the cotunneling rates [120, 121]. All the cotunneling rates that appear in Appendix B, excluding the $|0,0\rangle \longleftrightarrow |1,1\rangle$ rates, can be brought to the form

$$I(A,B,E_a,E_b,\mu_1,\mu_2) = \frac{2\pi\nu^2}{\hbar}\int d\epsilon F_{FD}(\epsilon-\mu_1)\left[1-F_{FD}(\epsilon-\mu_2)\right]\left|\frac{A}{\epsilon-E_a}+\frac{B}{\epsilon-E_b}\right|^2 , \tag{C.1}$$

where the amplitudes A, B are multiplications of two tunneling coefficients, and one might need to use the relation $F_{FD}(-\epsilon) = 1 - F_{FD}(\epsilon)$ in order to bring the expression of a specific cotunneling rate to this form. The integral (C.1) diverges due to the finite widths of the energy levels [120, 121]. We first add by hand a width to the levels

$$\begin{aligned} &I(A,B,E_a,E_b,\mu_1,\mu_2) = \frac{2\pi\nu^2}{\hbar}\times \\ &\int d\epsilon F_{FD}(\epsilon-\mu_1)\left[1-F_{FD}(\epsilon-\mu_2)\right]\left|\frac{A}{\epsilon-E_a+i\gamma}+\frac{B}{\epsilon-E_b+i\gamma}\right|^2 . \end{aligned} \tag{C.2}$$

Next, we solve the integral (C.2) and write the solution as a power series in γ. We extract the cotunneling rate by subtracting the $1/\gamma$ term and taking the limit $\gamma \to 0$. We should emphasize that in general each level has its own width and the sign $\pm i\gamma$ depends on the process; we associate different signs for incoming and outgoing electrons. If one adds the widths properly, the divergent term $(1/\gamma)$ has a physical meaning, and one can read the sequential tunneling rates from it. Nevertheless, these details are not important for the regularization procedure, and the finite values of the cotunneling rates are independent of the details of the regulator γ. We can write (C.2) as

$$\begin{aligned} &I(A,B,E_a,E_b,\mu_1,\mu_2) = \frac{2\pi\nu^2}{\hbar}\times \\ &\left[I1(A,E_a,\mu_1,\mu_2)+I1(B,E_b,\mu_1,\mu_2)+I2(A,B,E_a,E_b,\mu_1,\mu_2)\right], \end{aligned}$$

where

$$I1(A,E_a,\mu_1,\mu_2)=\int d\epsilon F_{FD}(\epsilon-\mu_1)\left[1-F_{FD}(\epsilon-\mu_2)\right]\left|\frac{A}{\epsilon-E_a+i\gamma}\right|^2,$$

$$I2(A,B,E_a,E_b,\mu_1,\mu_2)=\int d\epsilon F_{FD}(\epsilon-\mu_1)\left[1-F_{FD}(\epsilon-\mu_2)\right]\times 2Re\left\{\frac{A}{\epsilon-E_a+i\gamma}\frac{B}{\epsilon-E_b-i\gamma}\right\}.$$

The solutions of $I1$ and $I2$ can be written using digamma functions with complex variables ($\psi(z)$). $I1$ contains a divergent part

$$I1(A,E_a,\mu_1,\mu_2)=\frac{|A|^2N_B(\mu_2-\mu_1)}{\gamma}\times Im\left\{\psi\left[\frac{1}{2}+\frac{\beta\gamma}{2\pi}+\frac{i\beta}{2\pi}(\mu_2-E_a)\right]-\psi\left[\frac{1}{2}+\frac{\beta\gamma}{2\pi}+\frac{i\beta}{2\pi}(\mu_1-E_a)\right]\right\}, \tag{C.3}$$

where $\beta=1/(K_BT)$ and $N_B(\mu_2-\mu_1)=[e^{\beta(\mu_2-\mu_1)}-1]^{-1}$. After the subtraction of the $1/\gamma$ term and taking the limit $\gamma\to 0$:

$$I1(A,E_a,\mu_1,\mu_2)=|A|^2N_B(\mu_2-\mu_1)\frac{\beta}{2\pi}\times Im\left\{\psi'\left[\frac{1}{2}+\frac{i\beta}{2\pi}(\mu_2-E_a)\right]-\psi'\left[\frac{1}{2}+\frac{i\beta}{2\pi}(\mu_1-E_a)\right]\right\}. \tag{C.4}$$

There is no divergence in $I2$, therefore we simply solve it and take the limit $\gamma\to 0$

$$I2(A,B,E_a,E_b,\mu_1,\mu_2)=AB\frac{N_B(\mu_2-\mu_1)}{E_a-E_b}Re\left\{\psi\left[\frac{1}{2}+\frac{i\beta}{2\pi}(E_a-\mu_2)\right]\right. \tag{C.5}$$
$$\left.-\psi\left[\frac{1}{2}+\frac{i\beta}{2\pi}(E_b-\mu_2)\right]-\psi\left[\frac{1}{2}+\frac{i\beta}{2\pi}(E_a-\mu_1)\right]+\psi\left[\frac{1}{2}+\frac{i\beta}{2\pi}(E_b-\mu_1)\right]\right\}.$$

We can use the solution of (C.1) to solve the rates of the processes $|0,0\rangle\longleftrightarrow|1,1\rangle$. Notice that the formal expressions for these rates [Eqs. (B.18)-(B.23)] contain four terms inside the absolute value. We may use the trivial identity

$$|a+b+c+d|^2=|a+b|^2+|a+c|^2-|a-d|^2-|b-c|^2+|b+d|^2+|c+d|^2,$$

to write Eqs. (B.18)-(B.23) as sums of six terms of the form of (C.1).

Appendix D

Coulomb peaks structure of the conductivity at finite temperature

Figs. 3.1(a) and 3.1(c) plot the Coulomb peaks structures of the conductivity of the $SU(2)$ and $SU(3)$ systems. Contrary to naive expectations, at finite temperature the outer peaks are not centered around ϵ_F, $\epsilon_F - U$, in the N=2 case, or around ϵ_F, $\epsilon_F - 2U$ in the N=3 case ($\epsilon_F = 0$ in the plots). Focusing on the right most peak, the conductivity through a dot α is proportional to:

$$G_\alpha \sim [P_0(\epsilon_g) + P_\alpha(\epsilon_g)] f(\epsilon_g)[1 - f(\epsilon_g)], \tag{D.1}$$

where $P_0 = \left(1 + Ne^{-\epsilon_g/T}\right)^{-1}$ is the probability of finding all the dots empty, $P_\alpha = (1 - P_0)/N$ is the probability of finding an electron in the dot α (for $T \ll U$) and $f(\epsilon)$ is the Fermi Dirac distribution function of electrons in the edges. The term $[P_0(\epsilon_g) + P_\alpha(\epsilon_g)]$ does not have a particle hole symmetry at finite temperature, therefore the peak is shifted from ϵ_F, in this case by $T \ln(N)/2$. In the $SU(3)$ system the point $\epsilon_g = \epsilon_F - U$ is a half-filling point; the three dots are occupied on average by 3/2 electrons. Due to particle hole symmetry, the Coulomb peaks structure is symmetric around $\epsilon_g = \epsilon_F - U$ and the central peak is pinned at this half-filling point.

Bibliography

[1] L. D. Landau. Theory of fermi-liquids. *Sov. Phys. JETP*, 3:920, 1957.

[2] L. D. Landau. Oscillations in a fermi-liquid. *Sov. Phys. JETP*, 5:101, 1957.

[3] L. D. Landau. On the theory of the fermi-liquid. *Sov. Phys. JETP*, 8:70, 1957.

[4] J. Kondo. Resistance minimum in dilute magnetic alloys. *Prog. Theor. Phys.*, 32(1):37, 1964.

[5] A. C. Hewson. *The kondo problem to heavy fermions*. Cambridge University Press, 1997.

[6] W.J. de Haas, J. de Boer, and G.J. van den Berg. The electrical resistance of gold, copper and lead at low temperatures. *Physica*, 1:1115, 1934.

[7] P. Nozieres and A. Blandin. Kondo effect in real metals. *J. physique (paris)*, 41:193, 1980.

[8] I. Affleck. A current algebra approach to the kondo effect. *Nuclear Physics B*, 336:517, 1990.

[9] Christophe Mora. Fermi-liquid theory for SU(n) kondo model. *Phys. Rev. B*, 80:125304, 2009.

[10] Christophe Mora, Pavel Vitushinsky, Xavier Leyronas, Aashish A. Clerk, and Karyn Le Hur. Theory of nonequilibrium transport in the SU(n) kondo regime. *Phys. Rev. B*, 80:155322, 2009.

[11] M. A. Kastner. The single-electron transistor. *Rev. Mod. Phys.*, 64:849, 1992.

[12] U. Meirav and E. B. Foxman. Single-electron phenomena in semiconductors. *Semicond. Sci. Technol.*, 11:255, 1996.

[13] L. P. Kouwenhoven and C. M. Markus. Quantum dots. *Physics World*, 11:35, 1998.

[14] L. P. Kouwenhoven, C. M. Markus, P. L. McEuen, S. Tarucha, R. M. Westervelt, and N. S. Wingreen. Electron transport in quantum dots. In L. L. Sohn, L. P. Kouwenhoven, and G. Schön, editors, *Mesoscopic Electron Transport*, page 105. Kluwer Academic Publishers, Dordrecht, Boston, London, 1997.

[15] L. I. Glazman and M. E. Raikh. Resonant kondo transparency of a barrier with quasilocal impurity states. *JETP Lett.*, 47:452, 1988.

[16] D. Goldhaber-Gordon, H. Shtrikman, D. Mahalu, D. Abusch-Magder, and U. M. A. Meirav. Kondo effect in a single-electron transistor. *Nature*, 391:156, 1998.

[17] S. M. Cronenwett, T. H. Oosterkamp, and L. P. Kouwenhoven. A tunable kondo effect in quantum dots. *Science*, 281:540, 1998.

[18] P. W. Anderson. Localized magnetic states in metals. *Phys. Rev.*, 124:41, Oct 1961.

[19] I. L. Kurland, I. L. Aleiner, and B. L. Altshuler. Mesoscopic magnetization fluctuations for metallic grains close to the stoner instability. *Phys. Rev. B*, 62:14886, 2000.

[20] I. L. Aleiner, P. W. Brouwer, and L. I. Glazman. Quantum effects in coulomb blockade. *Physics Reports*, 358:309, 2002.

[21] J. R. Schrieffer and P. A. Wolff. Relation between the anderson and kondo hamiltonians. *Phys. Rev.*, 149:491, 1966.

[22] D. L. Cox. Quadrupolar kondo effect in uranium heavy-electron materials? *Phys. Rev. Lett.*, 59:1240, 1987.

[23] M.J. Besnus, M. Benakki, A. Braghta, H. Danan, G. Fischer, J.P. Kappler, A. Meyer, and P. Panissod. Specific heat and nmr of the kondo system $ybpd_2si_2$. *Journal of Magnetism and Magnetic Materials*, 76:471, 1988.

[24] C. L. Seaman, M. B. Maple, B. W. Lee, S. Ghamaty, M. S. Torikachvili, J. S. Kang, L. Z. Liu, J. W. Allen, and D. L. Cox. Evidence for non-fermi liquid behavior in the kondo alloy $y_{1-x}u_xpd_3$. *Phys. Rev. Lett.*, 67:2882, 1991.

[25] Sheng-Shiuan Yeh and Juhn-Jong Lin. Two-channel kondo effects in $Al/alo_x/Sc$ planar tunnel junctions. *Phys. Rev. B*, 79:012411, 2009.

[26] A. Zawadowski. Kondo-like state in a simple model for metallic glasses. *Phys. Rev. Lett.*, 45:211, 1980.

[27] D. C. Ralph and R. A. Buhrman. Observations of kondo scattering without magnetic impurities: A point contact study of two-level tunneling systems in metals. *Phys. Rev. Lett.*, 69:2118, 1992.

[28] D. C. Ralph, A. W. W. Ludwig, Jan von Delft, and R. A. Buhrman. 2-channel kondo scaling in conductance signals from 2 level tunneling systems. *Phys. Rev. Lett.*, 72:1064, 1994.

[29] T. Cichorek, A. Sanchez, P. Gegenwart, F. Weickert, A. Wojakowski, Z. Henkie, G. Auffermann, S. Paschen, R. Kniep, and F. Steglich. Two-channel kondo effect in glasslike thasse. *Phys. Rev. Lett.*, 94:236603, 2005.

[30] Tomasz Cichorek, Lukasz Bochenek, Rainer Niewa, Marcus Schmidt, Andreas Schlechte, Rudiger Kniep, and Frank Steglich. Electron scattering off structural two-level systems in $zras_{1.595}se_{0.393}$. *Journal of Physics: Conference Series*, 200:012021, 2010.

[31] K. Sengupta and G. Baskaran. Tuning kondo physics in graphene with gate voltage. *Phys. Rev. B*, 77:045417, 2008.

[32] Laila Souza. *Correlated electrons probed by scanning tunneling microscopy.* PhD thesis, Stanford university, 2009.

[33] Zhen-Gang Zhu, Kai-He Ding, and Jamal Berakdar. Single- or multi-flavor kondo effect in graphene. *EPL (Europhysics Letters)*, 90:67001, 2010.

[34] K. A. Matveev. Coulomb blockade at almost perfect transmission. *Phys. Rev. B*, 51:1743, 1995.

[35] M. Fabrizio and A. O. Gogolin. Interacting one-dimensional electron gas with open boundaries. *Phys. Rev. B*, 51:17827, 1995.

[36] Eran Lebanon, Avraham Schiller, and Frithjof B. Anders. Coulomb blockade in quantum boxes. *Phys. Rev. B*, 68:041311, 2003.

[37] Y. Oreg and D. Goldhaber-Gordon. Two-channel kondo effect in a modified single electron transistor. *Phys. Rev. Lett.*, 90:136602, 2003.

[38] H. E. Kim, G. Sierra, and C. Kallin. Observing 2-channel kondo physics in a carbon nanotube single-electron transistor. *J. Phys.: Condens. Matter*, 16:749, 2004.

[39] R. M. Potok, I. G. Rau, H. Shtrikman, Y. Oreg, and D. Goldhaber-Gorden. Observation of the two-channel kondo effect. *Nature*, 446:167, 2007.

[40] I. Affleck and Andreas W. W. Ludwig. Exact conformal-field-theory results on the multichannel kondo effect: Single-fermion green's function, self-energy, and resistivity. *Phys. Rev. B*, 48:7297, 1993.

[41] László Borda, Gergely Zaránd, Walter Hofstetter, B. I. Halperin, and Jan von Delft. Su(4) fermi liquid state and spin filtering in a double quantum dot system. *Phys. Rev. Lett.*, 90:026602, 2003.

[42] Karyn Le Hur, Pascal Simon, and László Borda. Maximized orbital and spin kondo effects in a single-electron transistor. *Phys. Rev. B*, 69:045326, 2004.

[43] Rosa López, David Sánchez, Minchul Lee, Mahn-Soo Choi, Pascal Simon, and Karyn Le Hur. Probing spin and orbital kondo effects with a mesoscopic interferometer. *Phys. Rev. B*, 71:115312, 2005.

[44] S. Sasaki, S. Amaha, N. Asakawa, M. Eto, and S. Tarucha. Enhanced kondo effect via tuned orbital degeneracy in a spin 1/2 artificial atom. *Phys. Rev. Lett.*, 93:017205, 2004.

[45] Takahide Numata, Yunori Nisikawa, Akira Oguri, and Alex C. Hewson. Kondo effects in a triangular triple quantum dot: Numerical renormalization group study in the whole region of the electron filling. *Phys. Rev. B*, 80:155330, 2009.

[46] Manh-Soo Choi, Rosa López, and Ramón Aguado. Su(4) kondo effect in carbon nanotubes. *Phys. Rev. Lett.*, 95:067204, 2005.

[47] J. Jarillo-Herrero, J. Kong, H. S. J. Van der Zant, C. Dekker, L. P. Kouwenhoven, and S. De Franceschi. Orbital kondo effect in carbon nanotubes. *Nature*, 434:484, 2005.

[48] Jong Soo Lim, Mahn-Soo Choi, M. Y. Choi, Rosa López, and Ramón Aguado. Kondo effects in carbon nanotubes: From su(4) to su(2) symmetry. *Phys. Rev. B*, 74:205119, 2006.

[49] Assaf Carmi, Yuval Oreg, and Micha Berkooz. Realization of the SU(n) kondo effect in a strong magnetic field. *Phys. Rev. Lett.*, 106:106401, 2011.

[50] S. Amasha, A. J. Keller, I. G. Rau, A. Carmi, J. A. Katine, H. Shtrikman, Y. Oreg, and D. Goldhaber-Gordon. Pseudospin-resolved transport spectroscopy of the kondo effect in a double quantum dot. *Cond-mat:1207.0526v1*, 2012.

[51] P. Nozieres. A "fermi-liquid" description of the kondo problem at low temperatures. *J. Low Temp. Phys.*, 17:31, 1974.

[52] Ulrich Gerland, Jan von Delft, T. A. Costi, and Yuval Oreg. Transmission phase shift of a quantum dot with kondo correlations. *Phys. Rev. Lett.*, 84:3710, 2000.

[53] V. J. Emery and S. Kivelson. Mapping of the two-channel kondo problem to a resonant-level model. *Phys. Rev. B*, 46:10812, 1992.

[54] Assaf Carmi, Yuval Oreg, Micha Berkooz, and David Goldhaber-Gordon. Transmission phase shifts of kondo impurities. *arXiv:1207.2258v1*, 2012.

[55] Gergely Zaránd, László Borda, Jan von Delft, and Natan Andrei. Theory of inelastic scattering from magnetic impurities. *Phys. Rev. Lett.*, 93:107204, 2004.

[56] László Borda, Lars Fritz, Natan Andrei, and Gergely Zaránd. Theory of inelastic scattering from quantum impurities. *Phys. Rev. B*, 75:235112, 2007.

[57] R. Landauer. Spatial variation of currents and fields due to localized scatterers in metallic conduction. *IBM Journal of Research and Development*, 1:223, 1957.

[58] M. Büttiker, Y. Imry, R. Landauer, and S. Pinhas. Generalized many-channel conductance formula with application to small rings. *Phys. Rev. B*, 31:6207, 1985.

[59] M. Büttiker. Four-terminal phase-coherent conductance. *Phys. Rev. Lett.*, 57:1761, 1986.

[60] Y. Imry. *Introduction to mesoscopic physics*. Mesoscopic physics and nanotechnology. Oxford University Press, 2002.

[61] M. Zaffalon, A. Bid, M. Heiblum, D. Mahalu, and V. Umansky. Transmission phase of a singly occupied quantum dot in the kondo regime. *Phys. Rev. Lett.*, 100:226601, 2008.

[62] Assaf Carmi and Yuval Oreg. Enhanced shot noise in asymmetric interacting two-level systems. *Phys. Rev. B*, 85:045325, 2012.

[63] Assaf Carmi. Super poisson shot noise in quantum dots. Master's thesis, Weizmann Institute of Science, 2008.

[64] O. Zarchin, Y. C. Chung, M. Heiblum, D. Rohrlich, and V. Umansky. Electron bunching in transport through quantum dots in a high magnetic field. *Phys. Rev. Lett.*, 98:066801, 2007.

[65] Ya M. Blanter and M. Buttiker. Shot noise in mesoscopic conductors. *Physics Reports*, 336:1, 2000.

[66] L. Y. Chen and C. S. Ting. Noise characteristics of sequential tunneling through double-barrier junctions. *Phys. Rev. B*, 46:4714, 1992.

[67] Selman Hershfield, John H. Davies, Per Hyldgaard, Christopher J. Stanton, and John W. Wilkins. Zero-frequency current noise for the double-tunnel-junction coulomb blockade. *Phys. Rev. B*, 47:1967, 1993.

[68] Ulrik Hanke, Yu. M. Galperin, K. A. Chao, and Nanzhi Zou. Finite-frequency shot noise in a correlated tunneling current. *Phys. Rev. B*, 48:17209, 1993.

[69] Eugene V. Sukhorukov, Guido Burkard, and Daniel Loss. Noise of a quantum dot system in the cotunneling regime. *Phys. Rev. B*, 63:125315, 2001.

[70] M. Reznikov, M. Heiblum, Hadas Shtrikman, and D. Mahalu. Temporal correlation of electrons: Suppression of shot noise in a ballistic quantum point contact. *Phys. Rev. Lett.*, 75:3340, 1995.

[71] B. R. Bułka, J. Martinek, G. Michałek, and J. Barnaś. Shot noise in ferromagnetic single-electron tunneling devices. *Phys. Rev. B*, 60:12246, 1999.

[72] Bogdan R. Bułka. Current and power spectrum in a magnetic tunnel device with an atomic-size spacer. *Phys. Rev. B*, 62:1186, 2000.

[73] I. Weymann, J. Barnaś, and S. Krompiewski. Theory of shot noise in single-walled metallic carbon nanotubes weakly coupled to nonmagnetic and ferromagnetic leads. *Phys. Rev. B*, 76:155408, 2007.

[74] I Weymann and J Barnas. Transport through two-level quantum dots weakly coupled to ferromagnetic leads. *Journal of Physics: Condensed Matter*, 19:096208, 2007.

[75] Axel Thielmann, Matthias H. Hettler, Jürgen König, and Gerd Schön. Super-poissonian noise, negative differential conductance, and relaxation effects in transport through molecules, quantum dots, and nanotubes. *Phys. Rev. B*, 71:045341, 2005.

[76] W. Belzig. Full counting statistics of super-poissonian shot noise in multilevel quantum dots. *Phys. Rev. B*, 71:161301, 2005.

[77] Ivana Djuric, Bing Dong, and H. L. Cui. Super-poissonian shot noise in the resonant tunneling due to coupling with a localized level. *Appl. Phys. Lett.*, 87:032105, 2005.

[78] Jasmin Aghassi, Axel Thielmann, Matthias H. Hettler, and Gerd Schön. Strongly enhanced shot noise in chains of quantum dots. *Appl. Phys. Lett.*, 89:052101, 2006.

[79] G. Kießlich, E. Schöll, T. Brandes, F. Hohls, and R. J. Haug. Noise enhancement due to quantum coherence in coupled quantum dots. *Phys. Rev. Lett.*, 99:206602, 2007.

[80] F. Bodoky, W. Belzig, and C. Bruder. Connection between noise and quantum correlations in a double quantum dot. *Phys. Rev. B*, 77:035302, 2008.

[81] Rafael Sánchez, Sigmund Kohler, Peter Hänggi, and Gloria Platero. Electron bunching in stacks of coupled quantum dots. *Phys. Rev. B*, 77:035409, 2008.

[82] Rafael Sánchez, Gloria Platero, and Tobias Brandes. Resonance fluorescence in driven quantum dots: Electron and photon correlations. *Phys. Rev. B*, 78:125308, 2008.

[83] A. Cottet, W. Belzig, and C. Bruder. Positive cross correlations in a three-terminal quantum dot with ferromagnetic contacts. *Phys. Rev. Lett.*, 92:206801, 2004.

[84] A. Cottet and W. Belzig. Dynamical spin-blockade in a quantum dot with paramagnetic leads. *Europhysics Letters*, 66:405, 2004.

[85] A. Cottet, W. Belzig, and C. Bruder. Positive cross-correlations due to dynamical channel blockade in a three-terminal quantum dot. *Phys. Rev. B*, 70:115315, 2004.

[86] S. S. Safonov, A. K. Savchenko, D. A. Bagrets, O. N. Jouravlev, Y. V. Nazarov, E. H. Linfield, and D. A. Ritchie. Enhanced shot noise in resonant tunneling via interacting localized states. *Phys. Rev. Lett.*, 91:136801, 2003.

[87] Yuanzhen Chen and Richard A. Webb. Full shot noise in mesoscopic tunnel barriers. *Phys. Rev. B*, 73:035424, 2006.

[88] S. Gustavsson, R. Leturcq, B. Simovič, R. Schleser, P. Studerus, T. Ihn, K. Ensslin, D. C. Driscoll, and A. C. Gossard. Counting statistics and super-poissonian noise in a quantum dot: Time-resolved measurements of electron transport. *Phys. Rev. B*, 74:195305, 2006.

[89] P. Barthold, F. Hohls, N. Maire, K. Pierz, and R. J. Haug. Enhanced shot noise in tunneling through a stack of coupled quantum dots. *Phys. Rev. Lett.*, 96:246804, 2006.

[90] D. M. Schröer, A. K. Hüttel, K. Eberl, S. Ludwig, M. N. Kiselev, and B. L. Altshuler. Kondo effect in a one-electron double quantum dot: Oscillations of the kondo current in a weak magnetic field. *Phys. Rev. B*, 74(23):233301, 2006.

[91] D. T. McClure, L. DiCarlo, Y. Zhang, H. A. Engel, C. M. Marcus, M. P. Hanson, and A. C. Gossard. Tunable noise cross correlations in a double quantum dot. *Phys. Rev. Lett.*, 98(5):056801, 2007.

[92] A. Hübel, J. Weis, W. Dietsche, and K. v. Klitzing. Two laterally arranged quantum dot systems with strong capacitive interdot coupling. *Applied Physics Letters*, 91(10):102101, 2007.

[93] A. Hübel, K. Held, J. Weis, and K. v. Klitzing. Correlated electron tunneling through two separate quantum dot systems with strong capacitive interdot coupling. *Phys. Rev. Lett.*, 101:186804, 2008.

[94] D. Schröer, A. D. Greentree, L. Gaudreau, K. Eberl, L. C. L. Hollenberg, J. P. Kotthaus, and S. Ludwig. Electrostatically defined serial triple quantum dot charged with few electrons. *Phys. Rev. B*, 76(7):075306, 2007.

[95] L. Gaudreau, A. Kam, G. Granger, S. A. Studenikin, P. Zawadzki, and A. S. Sachrajda. A tunable few electron triple quantum dot. *Applied Physics Letters*, 95:193101, 2009.

[96] Jürgen König and Yuval Gefen. Aharonov-bohm interferometry with interacting quantum dots: Spin configurations, asymmetric interference patterns, bias-voltage-induced aharonov-bohm oscillations, and symmetries of transport coefficients. *Phys. Rev. B*, 65:045316, 2002.

[97] E. J. Heller, K. E. Aidala, B. J. LeRoy, A. C. Bleszynski, A. Kalben, R. M. Westervelt, K. D. Maranowski, and A. C. Gossard. Thermal averages in a quantum point contact with a single coherent wave packet. *Nano Letters*, 5:1285, 2005.

[98] M. P. Jura, M. A. Topinka, M. Grobis, L. N. Pfeiffer, K. W. West, and D. Goldhaber-Gordon. Electron interferometer formed with a scanning probe tip and quantum point contact. *Phys. Rev. B*, 80:041303, 2009.

[99] Van Der Pauw. A method of measuring specific resistivity and hall effect of discs of arbitrary shape. *Philips Research Reports*, 13:1, 1958.

[100] A. Yacoby, M. Heiblum, D. Mahalu, and H. Shtrikman. Coherence and phase sensitive measurements in a quantum dot. *Phys. Rev. Lett.*, 74(20):4047, 1995.

[101] R. Schuster, E. Buks, M. Heiblum, D. Mahalu, V. Umansky, and H. Shtrikman. Phase measurement in a quantum dot via a double-slit interference experiment. *Nature*, 385:417, 1997.

[102] Y. Ji, M. Heiblum, D. Sprinzak, D. Mahalu, and H. Shtrikman. Phase evolution in a kondo-correlated system. *Science*, 290:779, 2000.

[103] Y. Ji, M. Heiblum, and H. Shtrikman. Transmission phase of a quantum dot with kondo correlation near the unitary limit. *Phys. Rev. Lett.*, 88(7):076601, 2002.

[104] M. Avinun-Kalish, M. Heiblum, O. Zarchin, D. Mahalu, and V. Umansky. Crossover from 'mesoscopic' to 'universal' phase for electron transmission in quantum dots. *Nature*, 436:529, 2005.

[105] A. Aharony, O. Entin-Wohlman, B. I. Halperin, and Y. Imry. Phase measurement in the mesoscopic aharonov-bohm interferometer. *Phys. Rev. B*, 66:115311, 2002.

[106] Maria A. Davidovich, E. V. Anda, J. R. Iglesias, and G. Chiappe. Bohm-aharonov and kondo effects on tunneling currents in a mesoscopic ring. *Phys. Rev. B*, 55:R7335, 1997.

[107] Walter Hofstetter, Jürgen König, and Herbert Schoeller. Kondo correlations and the fano effect in closed aharonov-bohm interferometers. *Phys. Rev. Lett.*, 87:156803, 2001.

[108] Tae-Suk Kim and S. Hershfield. Thermopower of an aharonov-bohm interferometer: Theoretical studies of quantum dots in the kondo regime. *Phys. Rev. Lett.*, 88:136601, 2002.

[109] Amnon Aharony and Ora Entin-Wohlman. Measuring the kondo effect in the aharonov-bohm interferometer. *Phys. Rev. B*, 72:073311, 2005.

[110] Pascal Simon, O. Entin-Wohlman, and A. Aharony. Flux-dependent kondo temperature in an aharonov-bohm interferometer with an in-line quantum dot. *Phys. Rev. B*, 72:245313, 2005.

[111] Ryosuke Yoshii and Mikio Eto. Scaling analysis for kondo effect in quantum dot embedded in aharonov-bohm ring. *Journal of the Physical Society of Japan*, 77:123714, 2008.

[112] Justin Malecki and Ian Affleck. Influence of interference on the kondo effect in a quantum dot. *Phys. Rev. B*, 82:165426, 2010.

[113] M. Pustilnik and L. I. Glazman. Kondo effect induced by a magnetic field. *Phys. Rev. B*, 64:045328, 2001.

[114] Yuval Oreg and David Goldhaber-Gordon. The two channel kondo effect in quantum dots. In Sachindra Nath Karmakar, Santanu Kumar Maiti, and Jayeeta Chowdhury, editors, *Physics of Zero- and One-Dimensional Nanoscopic Systems*, volume 156 of *Springer Series in Solid-State Sciences*, page 27. Springer Berlin Heidelberg, 2007.

[115] Ileana Rau, Sami Amasha, Yuval Oreg, and David Goldhaber-Gordon. Quantum phase transitions in quantum dots. In L. Carr and L.D. Carr, editors, *Understanding Quantum Phase Transitions*, page 341. Taylor and Francis, 2010.

[116] Michael Pustilnik and Leonid Glazman. Kondo effect in quantum dots. *Journal of Physics: Condensed Matter*, 16:R513, 2004.

[117] A. N. Korotkov. Intrinsic noise of the single-electron transistor. *Phys. Rev. B*, 49:10381, 1994.

[118] Jens Koch, Felix von Oppen, and A. V. Andreev. Theory of the franck-condon blockade regime. *Phys. Rev. B*, 74:205438, 2006.

[119] Noise in semiconductors: Spectrum of a two-parameter random signal.

[120] D. V. Averin. Periodic conductance oscillations in the single-electron tunneling transistor. *Physica B*, 194:979, 1994.

[121] M. Turek and K. A. Matveev. Cotunneling thermopower of single electron transistors. *Phys. Rev. B*, 65:115332, 2002.

[122] Jürgen König, Herbert Schoeller, and Gerd Schön. Zero-bias anomalies and boson-assisted tunneling through quantum dots. *Phys. Rev. Lett.*, 76:1715, 1996.

[123] Jürgen König, Herbert Schoeller, and Gerd Schön. Cotunneling at resonance for the single-electron transistor. *Phys. Rev. Lett.*, 78:4482, 1997.

[124] Jürgen König, Jörg Schmid, Herbert Schoeller, and Gerd Schön. Resonant tunneling through ultrasmall quantum dots: Zero-bias anomalies, magnetic-field dependence, and boson-assisted transport. *Phys. Rev. B*, 54:16820, 1996.

[125] Jürgen König, Herbert Schoeller, and Gerd Schön. Cotunneling and renormalization effects for the single-electron transistor. *Phys. Rev. B*, 58:7882, 1998.

[126] Axel Thielmann, Matthias H. Hettler, Jürgen König, and Gerd Schön. Shot noise in tunneling transport through molecules and quantum dots. *Phys. Rev. B*, 68:115105, 2003.

[127] Michael Sindel, Alessandro Silva, Yuval Oreg, and Jan von Delft. Charge oscillations in quantum dots: Renormalization group and hartree method calculations. *Phys. Rev. B*, 72:125316, 2005.

[128] Ian Affleck, Andreas W. W. Ludwig, H. B. Pang, and D. L. Cox. Relevance of anisotropy in the multichannel kondo effect: Comparison of conformal field theory and numerical renormalization-group results. *Phys. Rev. B*, 45:7918, 1992.

[129] Eran Sela, Andrew K. Mitchell, and Lars Fritz. Exact crossover green function in the two-channel and two-impurity kondo models. *Phys. Rev. Lett.*, 106:147202, 2011.

[130] Andrew K. Mitchell and Eran Sela. Universal low-temperature crossover in two-channel kondo models. *Phys. Rev. B*, 85:235127, 2012.

[131] Ady Stern, Yakir Aharonov, and Yoseph Imry. Phase uncertainty and loss of interference: A general picture. *Phys. Rev. A*, 41:3436, 1990.

[132] Y. Levinson. Dephasing in a quantum dot due to coupling with a quantum point contact. *EPL (Europhysics Letters)*, 39:299, 1997.

[133] I. L. Aleiner, Ned S. Wingreen, and Yigal Meir. Dephasing and the orthogonality catastrophe in tunneling through a quantum dot: The "which path?" interferometer. *Phys. Rev. Lett.*, 79:3740, 1997.

[134] Florian Marquardt and C. Bruder. Aharonov-bohm ring with fluctuating flux. *Phys. Rev. B*, 65:125315, 2002.

[135] M. Pustilnik and L. I. Glazman. Kondo effect in real quantum dots. *Phys. Rev. Lett.*, 87:216601, 2001.

[136] M. Pustilnik, L. Borda, L. I. Glazman, and J. von Delft. Quantum phase transition in a two-channel-kondo quantum dot device. *Phys. Rev. B*, 69:115316, 2004.